12

MICROSTRUCTURE AND NONLINEAR VISCOELASTICITY IN ORIENTED POLYPROPYLENE

Jeanne L. Courter
David K. Roylance

January 1981

Final Report
Contract Number N00014-76-C-0846

DEPARTMENT
OF
MATERIALS SCIENCE
AND
ENGINEERING

SCHOOL OF ENGINEERING
MASSACHUSETTS INSTITUTE OF TECHNOLOGY
Cambridge, Massachusetts 02139

prepared for

Office of Naval Research
Arlington, VA 22217

81

(12)

(6) MICROSTRUCTURE AND
NONLINEAR VISCOELASTICITY IN
ORIENTED POLYPROPYLENE.

(10) Jeanne L. Courter
David K. Roylance

(11) January 1981

(12) 177 C

(9) Final Report.

Contract Number N00014-76-C-0846

(15)

prepared for

Office of Naval Research
Arlington, VA 22217

409463

ABSTRACT

Oriented semicrystalline polymers do not show linear viscoelastic mechanical behavior in useful ranges of strain. The relationship of the nonlinear viscoelasticity of the stress relaxation modulus to microstructural features, including crystallinity, crystalline orientation and amorphous orientation, was examined using oriented polypropylene film. The microstructure was altered by annealing in such a way that crystallinity and crystalline orientation were kept constant. Birefringence and sonic modulus were used to measure amorphous orientation. The strain dependence of the isochronal stress relaxation modulus and the amorphous orientation were then compared for unannealed and annealed films.

Upon annealing no change was found in the nonlinear strain dependence of stress relaxation modulus even though the overall level of modulus decreased. The stress relaxation modulus was found to be a more sensitive indicator of structural changes than the orientation functions. Also, structural changes large enough to decrease the stress relaxation modulus did not alter the nonlinear strain dependence of the modulus. By controlling crystallinity and crystalline orientation, structural changes required to cause changes in nonlinear behavior may have been prevented. The structural change caused by annealing was not a simple retraction of amorphous material, as evidenced by an increase in amorphous orientation. It is proposed that, upon annealing, microfibrillar motion and increased lamellar perfection cause a reduction in crystal-crystal connections and an increase in crystal-amorphous connections along the draw direction, thereby decreasing the modulus.

In addition, the strain dependence of the stress relaxation modulus was modeled using the multiple integral representation. At least four terms in the series were needed to fit the data. Problems of series convergence are discussed.

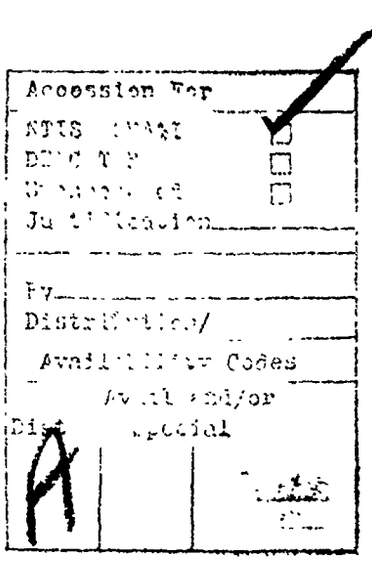

TABLE OF CONTENTS

LIST OF FIGURES

LIST OF TABLES

ACKNOWLDEGEMENTS

The authors wish to thank the many helpful contributions made to this work by Dr. Rakesh Popli, Prof. Ioannis Yannas, and Prof. Frederick McGarry. We are also most grateful for the financial support and technical advice made available by the Office of Naval Research under Contract N00014-76-C-0846.

INTRODUCTION

Isotropic semicrystalline polymers have advantages for several applications, including those where toughness and chemical stability are required. However, their use has been limited because their stiffnesses are rather low compared to metals or ceramics, and even to glassy polymers. One approach to stiffening these and other polymers has been to use them in composite form, reinforcing them with various stiff fibers and particulate fillers. However, another approach which is possible with the higher crystallinity polymers is a form of "self-reinforcing" which can be achieved by orientation. For example, these polymers are drawn uniaxially or biaxially and the crystals are aligned in one or two dimensions, giving a "microcomposite" effect. Such films are then stiffer and stronger in the draw direction and may be useful for products requiring those properties.

An example of such an end-use is the subject of this work. Highly oriented polypropylene films were formed by uniaxial drawing, resulting in a high stiffness film. These films were laminated together into $\pm$ 45° plates having around eighty film layers. These laminates are being tested by the Army Materials and Mechanics Research Center in Worcester, MA for protection of radar systems against ballistic impact. They were an interesting case of the use of self-reinforcing polymers. They provided a chance to examine a system all the way from the microstructure of the individual films through the film's mechanical properties, and finally to the laminate properties. This thesis will deal with the first part of this work: the relationship between the microstructural features of the films and their stiffness.

Upon initial investigation of the PP film's mechanical behavior, it became clear that the film exhibited strong time dependence. With fur-

ther investigation the modulus was found to be strongly dependent on strain. Because of this interesting nonlinear behavior, several goals were identified. First, we wished to gain a better understanding of the relationship between the microstructure of the highly oriented polypropylene film and its nonlinear viscoelastic behavior. This relationship was investigated by using annealing of the films to alter their structure in a controlled way. The viscoelastic behavior was then examined to see what effect the annealing had had.

Another part of the work was to examine the applicability of the multiple integral representation of nonlinear viscoelasticity to the type of nonlinear behavior seen in these films. The number of terms needed to fit the data and the convergence of the series were checked. Also, the dependence of the multiple integral coefficients on structural changes was examined.

BACKGROUND

Morphology

The structure of highly drawn polypropylene and other semicrystalline polymers has been the subject of a great deal of study in recent years. Several of the morphological features are quite well established, while others remain difficult to understand and are controversial. Some of these features are microfibrils, crystalline orientation, amorphous orientation and tie chains, long period (regular periodicity in the longitudinal direction), presence of voids, and evidence of crystalline bridges. These features may vary depending on the starting material, i.e., its molecular weight and thermal history, and the conditions of draw, i.e., draw rate and temperature. A brief review of the major microstructural features and their dependence on the conditions of draw will follow.

The dominant feature of highly drawn polypropylene is the presence of fibrillar structure. This structure is observed in many ways, including acid etching,[16,31] plasma etching,[17] and by observation of fracture surfaces. Fibrils have diameters on the scale of 1000 Å. They are composed of microfibrils which consist of alternating crystalline and amorphous regions arranged in series along the orientation direction.[34] The c-axes of the crystals, which correspond to the chain helix axis, are oriented in the direction of the microfibril axis. The crystalline blocks in one microfibril may be aligned to a greater or lesser extent with the crystalline blocks in an adjacent microfibril. The extent to which they are aligned is affected by the drawing conditions and annealing. Cold drawn materials[28] (20°C) show a broad line width (in 2θ) in wide angle X-ray diffraction and a poorly defined small angle X-ray pattern. Hot

drawn (120°C) samples, however, show sharper WAXS peaks and a two point (meridional, i.e., spots along the orientation direction) pattern in SAXS, indicating a long period of 260 Å. The presence of a large line broadening indicates either a small crystallite size or large lattice strains and defects.[19] The lack of a clear SAXS pattern in cold drawn material was thought by Owen and Ward[28] to indicate an imperfect, disordered lamellar structure. Because of the low amount of line broadening in WAXS and the regularity of the SAXS pattern, they conclude that in hot drawn materials, the neighboring microfibrils have their crystalline regions aligned. The effect of annealing on the structure will be discussed in a later section.

Taylor and Clark[26] have described a third class of drawing, known as "superdrawing", which results in some unusual features. It is drawn in a two step process. WAXS of superdrawn polypropylene shows very high crystal orientation, while SAXS shows no scattering to a resolution of 40 nm. This result is interpreted in terms of a structure consisting of a continuous crystal matrix with amorphous regions as defects. Garton et al.[16] studied a similarly produced polypropylene fiber after etching with chromic acid[16] and the only morphological features that were observed were some spotting, supporting the continuous crystal matrix proposal. A similar structure was proposed by I.M. Ward and his associates for an ultra-high modulus linear polyethylene[27,29] drawn at 75°C. They based their description of the structure on measurements of longitudinal and transverse crystal thicknesses as measured from broadening of WAXS peaks and on the measurement of SAXS long periods.

Not only are the orientation and arrangement of the crystallites important in the drawn polymer's microstructure, but the amorphous regions also contain features of great importance. During drawing, the crystalline

regions become nearly completely oriented at draw ratios of about 8. Above that draw ratio, modulus, strength and other properties continue to change, indicating that the amorphous material is altering. R.J. Samuels[14,23-25] has described the measurement of both crystalline and amorphous orientation by several techniques including wide angle X-ray diffraction, birefringence, sonic modulus and IR dichroism. (See Appendices A - D.) Other features, in addition to orientation, are needed to describe the amorphous structure. Some of the most important of these are tie molecules, tie molecule length distributions, and the constraint of the amorphous phase.

The tie molecule concept was proposed to explain how the crystallites in a drawn polymer are connected. Peterlin[34] described the process of drawing and proposed a mechanism by which tie molecules developed from the undrawn structure. His description of drawing and of the development of tie molecules assumed that the crystals were folded chain, or adjacent reentry crystals. This implied that, while most chains reentered the same crystal at an adjacent position, a small number of chains, the tie chains, were incorporated in each of two successive crystals in a microfibril. During drawing, Peterlin proposed, each microfibril was formed from a single lamella and the tie molecules between the crystallites in the microfibril lay at the surface of the microfibril.

The nature of the connections between crystallites has been re-examined recently in light of evidence that the folded chain concept of crystallization may need modification. Recently, neutron scattering experiments have shown that there is no change in end-to-end distance or radius of gyration on crystallization from the melt for PE and PP.[35] This has provided support for the suggestion that crystals in the bulk are not strictly chain folded crystals. In the chain folded model the molecular

chain was attached to the growing crystal face and then the rest of its length was "reeled in" and attached to the growing face. The tie chain was the occasional chain that connected two crystalline blocks. Neutron scattering, on the other hand, seems to support the idea that crystallization is an incorporation of nearby chains. These would not necessarily be pieces of the same molecule, but instead would be segments from intertwined molecules near the crystal face. With this model of crystal growth, there are many more chains which may become incorporated in neighboring crystals. These molecules are still called tie chains, but there are many more molecules bridging the gap between crystallites. The concept of tie chain length distribution arises from this idea. With this model an increase in stiffness or strength might be due to an increase in the number of molecules which have been pulled taut during drawing or to a change in the length distribution as the crystals undergo the discontinuous transformation into the fibrillar structure.[32,33] Peterlin[64] (in 1980) has discussed the neutron scattering data and other data concerning crystallization and concludes that half the stems in the crystal lattice must be connected by regular loops with adjacent reentry and one third of all stems must be connected by random loops. He also states that although a structure with regular folds had been used in the basic model of drawing, it was not a condition of that model. He does not, however, describe the effect of this new concept of crystallization on tie molecules and their development during drawing.

Besides the orientation of the amorphous material, and the presence of tie molecules, and a distribution of tie chain lengths, the constraint of the amorphous

material. SAXS intensity[61] decreased with increasing amorphous orientation, indicating a decrease in the density difference between the crystalline and amorphous regions. IR and Raman spectroscopy[59] have been used to study the alignment and length of segments in highly oriented material. Mechanical measurements have also been useful tools in the study of the amorphous phase. Retting[36] measured the relaxation spectrum in various oriented PP samples and showed that the maximum in the relaxation spectra shifts to higher time with increased orientation (up to 7:1 draw ratio). Dynamic mechanical data, particularly the tanδ loss peaks, both along the orientation axis[59,62,66] and as a function of angle to the draw direction,[28] have provided information concerning the constraint of the amorphous regions. Some of these results will be described in the subsequent discussion on the effects of annealing. Table I lists the structural features of interest in drawn semicrystalline polymers along with the techniques that have been used to examine them, and references to some of those who have used the techniques.

TABLE I

IMPORTANT STRUCTURAL FEATURES OF
DRAWN SEMICRYSTALLINE POLYMER MORPHOLOGY

Structural Features	Technique	Reference
Fibrillar structure	SEM	26
	Etching, acid,plasma	16, 17, 31
Crystallinity	Density	23, 4
Orientation functions	WAXS (azimuthal breadth)	1 - 6
	Birefringence	23, 25, 10
	Sonic modulus	23, 25, 10
	IR Dichroism	23, 25, 10
Voids	SAXS	4
	Etching/SEM	16, 17
Long period	SAXS (2θ maximum)	22, 32, 33
Lamellar structure	WAXS (peak broadening)	29
	SAXS	19, 28
Lamellar angle	SAXS	19, 28
Crystal size	WAXS	58
	Etching/GPC	60, 61
Continuity of crystal	WAXS (peak broadening)	58, 27, 29
(intercrystalline bridges)	SAXS	26
	Etching	16
	Dead Bend	26
	Shrinkage	26, 62
	Melting	26, 62
Tie chains,	Mechanical measurements	28, 63, 64, 66
tie chain distribution		65
Constraint of amorphous material	SAXS (intensity)	61
	Area of tanδ β loss peak	59, 62, 66
	Anisotropy of tanδ loss	28
	IR & Raman spectroscopy	59
	Shrinkage	23
	Relaxation spectrum	36

Viscoelasticity

In seeking to use polymers, the time dependence of their properties must be considered. As with any material that is to be used in a mechanical system, its constitutive relation is very important. Even in the simplest case of an isotropic polymer, both its elastic and viscous character must be considered. The theory of linear viscoelasticity (LVE) has been developed to describe the time dependence or "memory" of these materials. However, most polymers show a more complex behavior outside a certain range of stress, strain or time. The behavior in these other regions is known collectively as nonlinear viscoelasticity (NLVE). In this section a brief discussion of the basics of linear viscoelasticity, the criteria for linearity, and the limits of linearity, as well as phenomenological observations of linear and nonlinear behavior will be presented. Also included will be a review of work examining the relationship between structure and nonlinear viscoelasticity.

Linear Viscoelasticity

The description of the time dependence of polymer mechanical behavior usually begins by describing the response of the polymer to a stimulus whose form is a step function. The two most common tests of this type are stress relaxation and creep. In this discussion, the stress relaxation test will be described. This test consists of applying a strain to the sample in a step function, i.e, at $t < 0$ the applied strain is zero, and at $t > 0$ the applied strain is ε_o. The stress, $\sigma(t)$, resulting from the applied strain is then measured over a period of time. If the strain is a tensile strain then the extensional stress relaxation modulus, $E(t)$, is defined as follows:

$$E(t) = \frac{\sigma(t)}{\varepsilon_o}$$

Other functions such as extensional compliance, D(t), shear modulus, G, or compliance, J, are also defined as the response normalized by the applied stimulus. These moduli and compliances are the basis for describing the time dependence of the polymer's behavior.

In developing a description of viscoelasticity, it is helpful to define what behavior is considered linear behavior. The region of linear behavior is described by two criteria:

$$\sigma(C\cdot\varepsilon(t)) = C\cdot[\sigma(\varepsilon(t))]$$

and

$$\sigma[\varepsilon_1(t) + \varepsilon_2(t-t_1)] = \sigma[\varepsilon_1(t)] + \sigma[\varepsilon_2(t-t_1)]$$

It can be shown that the first of these criteria is a special case of the more general second criterion, but it is helpful to consider the two separately. The first criterion means that the modulus function, E(t), is independent of strain. The second criterion is known as the Boltzman superposition theorem and implies that the response of the material to a second strain is unaffected by a previously applied strain, and thus that the response to a combination of strains is simply the sum of the responses to the strains applied separately.

By considering this second criterion, and by dividing any arbitrary strain history into a series of step strains, the response to the strain history can be treated as the sum of the responses to those step strains. Since the response, $\sigma(t)$, to a step strain, ε_o, is just $\sigma(t) = \varepsilon_o\cdot E(t)$, the response to a sequence of such strains is the sum of these responses. Expressed in integral form, this may be written:

$$\sigma(t) = \int_o^t E(t-\xi)\frac{\delta\varepsilon(\xi)}{\delta\xi}\,d\varepsilon$$

where $d[\varepsilon(\xi)]$ has been replaced by $\frac{\delta\varepsilon\ (\xi)}{\delta\varepsilon}\ d\xi$ so that time, ξ, may be the independent variable. Here $E(t-\xi)$ is the extensional modulus function whose argument is the elapsed time between the time of application of a strain and the time, t, at which the stress response is desired. This function $E(t-\xi)$ is sometimes known as the "memory function" because it describes the effect at time t, of a stimulus applied in the past.

This relation, then, underlies linear viscoelasticity. It can be generalized to deal with three dimensional stress and strain states where the elements of the compliance or stiffness tensor are time dependent.

Linear Viscoelasticity in Polypropylene

An overall picture of the linear viscoelastic behavior of isotropic polypropylene is shown in Figure 1.[47] This figure shows the modulus and logarithmic decrement from a torsional pendulum over a temperature range of -260°C to 153°C for three degrees of crystallinity. Note that at room temperature the material is in the middle of a glass transition region. Similar figures and a discussion of the microstructural sources of the various transitions can be found in McCrum et al.[54]

An interesting study of the effect of orientation on the relaxation time spectrum was carried out by Retting (1973).[53] Samples of polypropylene, having draw ratios from 0 to 600%, were tested in the linear range of behavior using three tests: stress relaxation, forced flexural vibration, and constant strain test. Each of these tests covered a specific time range: bending vibration, 10^{-4} to 2×10^{-2} seconds, tensile tests, 2×10^{-2} to 2×10^{-1} seconds, and stress relaxation, 1 to 10^{4} seconds. These tests were done in a temperature range of between -40°C to 60°C. The relaxation spectra, $H(\tau)$, were determined by differentiating the time de-

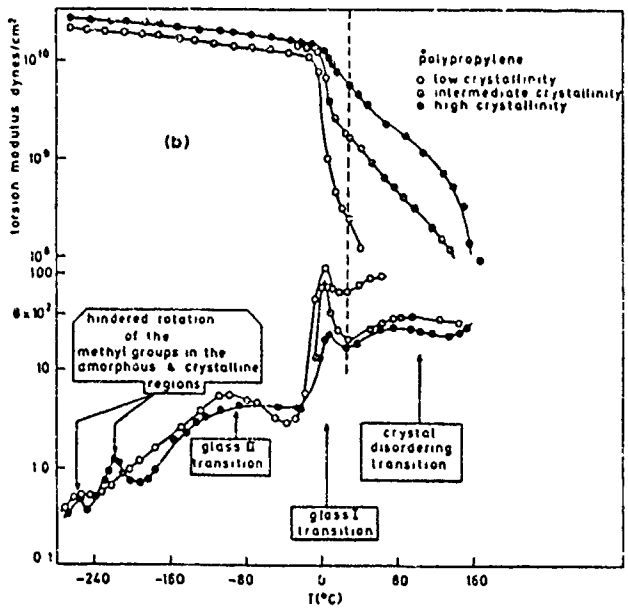

Figure 1: Dynamic mechanical loss traces: Polypropylene of various degrees of crystallinity. A plot of torsion modulus against temperature is included (Muus et al. 1959). (Ref.47)

pendent moduli. Retting found that the maximum in the relaxation time shifted to longer times with increased draw ratio. (See Figure 2.) He suggests that this may happen because upon orientation of the fiber structure, the glass relaxation process parallel to the orientation in the amorphous regions may be hindered and therefore shift to longer times.

Nonlinear Viscoelasticity

Nonlinear viscoelasticity describes the viscoelastic behavior of material which does not fall within the criteria for linearity described previously. The nonlinearity may be seen in two ways. First, the material property, e.g., the extensional modulus, may show strain dependence. This would be seen when, in a series of stress relaxation experiments, the observed stresses cannot be superimposed by normalizing by the applied strains. Nonlinearity may also appear when the response to a multi-step strain is not described well by the Boltzmann superposition theorem. The material is then showing a cross effect wherein an early strain has affected the material's response to a subsequent strain. These features complicate the writing of a constitutive relation, because the material functions are both time and strain dependent. Also, the responses to a series of steps in the strain cannot simply be added together, instead the effect of one strain on the response to another must also be considered.

The transition from linear viscoelasticity to nonlinear viscoelasticity is important to any user of polymers. A clear and extensive review of the nature of the transition was presented by Yannas in his review of 1974.[71] Figure 3 shows the strain limit of linearity for amorphous and semicrystalline polymers for temperatures around T_g. By assigning some level of deviation from linear behavior, the level of strain, stress or time

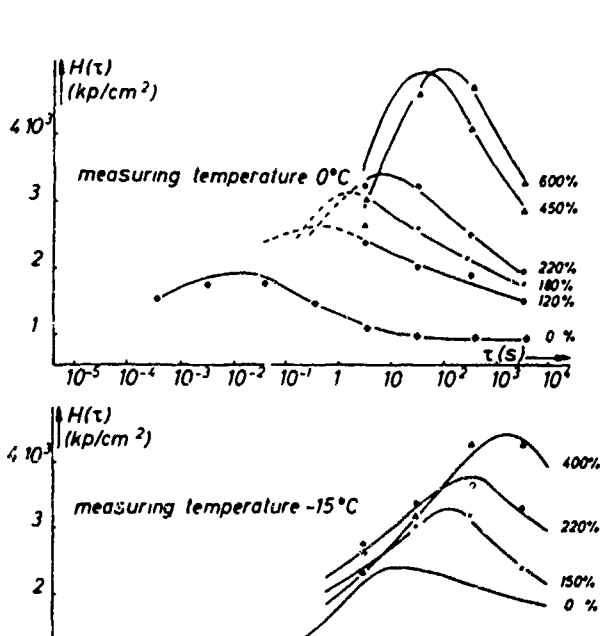

The main relaxation maximum of undrawn and of drawn polypropylene with various draw ratios. The curves were calculated from modulus curves measured at 0 and −15°C.

Figure 2: Effect of orientation on relaxation spectrum of polypropylene.

at which nonlinearity became important was determined, and is shown as percent strain at various temperatures. Polymers below T_g have a strain limit of about 0.01, while above T_g semicrystalline polymers show strain limits of only 0.001 to 0.004.

Nonlinear Viscoelasticity of Polypropylene

A discussion of the observations made by several workers concerning nonlinear viscoelastic properties of polypropylene will follow.

Lockett and Turner (1971)[42] considered the effect of intermittent loading on isotropic polypropylene. They found that the creep response at any specific time increased successively during the first few cycles of a multi-cycle loading-unloading program. This is significant when mechanical "conditioning" is applied to a specimen. It indicates that the state of the conditioned specimen is different from the intital state of the sample.

The nonlinear viscoelastic behavior of oriented polypropylene fibers was studied by Ward and Onat (1963)[50] in one- and two-step uniaxial creep and recovery. Recovery is the reduction in strain upon removal of the load. (Recovery strain is defined as the difference between the strain that would occur if the load remained and the observed strain after the load has been removed. See Figure 4.[37])

They noted several features of behavior: first, the creep strain was not linearly dependent upon the applied load, i.e., the compliance was dependent upon load. Second, the recovery strain was greater than the creep strain. Third, the instantaneous response in creep and recovery were different. And, finally, additional creep due to a load applied at time t_d after the initial load, was always greater than the initial creep and decreased with increasing t_d. These features of nonlinear viscoelastic behavior will be discussed further in a subsequent section, in the description

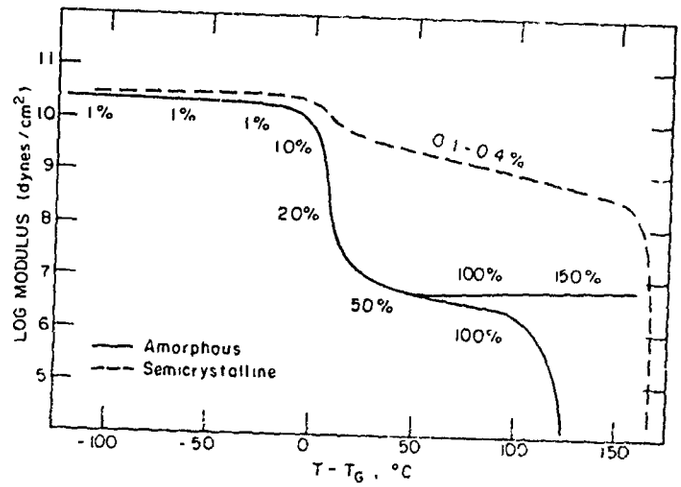

Strain limits of applicability of linear viscoelasticity theory for various amorphous and crystalline polymers.

Figure 3. (Ref.71)

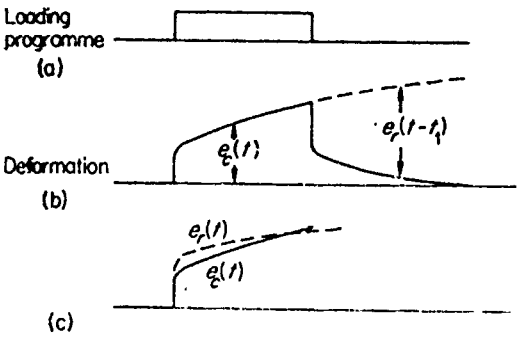

Figure 4 (a) Loading programme; (b) deformation; and (c) direct comparison of creep $e_c(t)$ and recovery $e_r(t)$ for a non-linear viscoelastic solid.

(Ref. 37)

of Buckley's work.

Ward and Wolfe (1966)[52] studied oriented polypropylene fibers in two-step creep tests, applying different combinations of stresses, keeping the time between the two steps constant. They found that the response to a complex loading program could be predicted by simple addition of the responses to the loads applied separately, with only small corrections required. They do not indicate whether or not this holds if the time between steps is changed.

Other work concerning the nonlinearity of polypropylene is discussed in the following section. Work which has been done to understand the molecular level processes and structural basis for nonlinear viscoelasticity will be described.

Relationship Between Structure and Nonlinear Behavior

The microstructural source of nonlinear behavior has been explored by surprisingly few workers in the the past 15 years. In 1965 Hadley and Ward[42] looked at room temperature creep compliance as a function of applied load for samples with low, medium and high orientation and with two molecular weights. (See Figures 5a, b, 6.) They found that the lower orientation fibers showed a parabolic dependence of the compliance, C, on the applied load, σ_o. As the orientation was increased the C *vs.* σ_o plot became linear and, for the highest orientation, sigmoidal. Thus for the most highly oriented fibers C became independent of σ_o at high σ_o. Molecular weight had no effect on the form of C *vs.* σ_o.

Hadley and Ward concluded that overall molecular orientation, as indicated by birefringence, was the major contributor to the form of C vs. σ_o. No explanation of the connection between orientation and the form of the nonlinearity was given. A very interesting exception to the relationship between nonlinearity and orientation was observed in another fiber sample, called the "monofilament", which had been prepared differently. It had a birefringence comparable to that of the most highly drawn fibers, but showed a parabolic dependence of creep compliance on applied load. This was the same nonlinear form shown by the lowest orientation fiber. Thus, the monofilament showed completely different nonlinear behavior from that seen in samples with similar birefringence. This is interesting because it demonstrates that birefringence alone is insufficient to predict the type of nonlinear behavior a sample will exhibit. It is possible that the samples had different crystallinities or different orientation of the amorphous material, such that the birefringence was the same, but the nonlinearity was different. We can conclude that some factors other than the overall molecu-

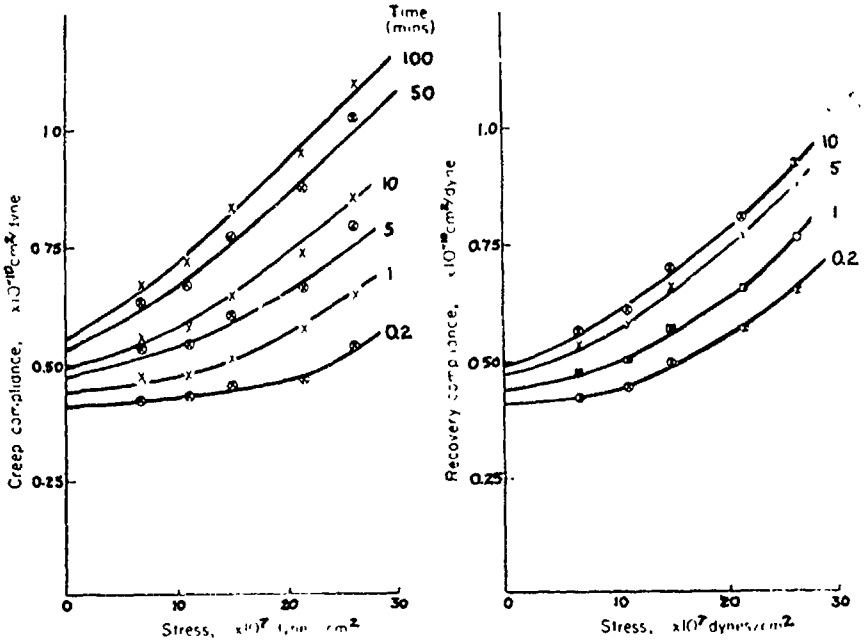

Creep and recovery for high molecular weight, low molecular orientation fibre

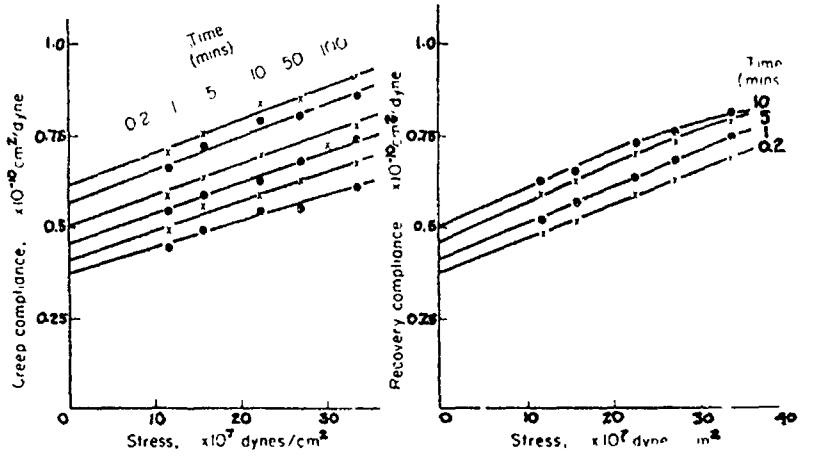

Creep and recovery for high molecular weight, intermediate molecular orientation fibre.

Figure 5(a): Creep and recovery data for low, intermediate and high orientation fibers and for the "monofilament". (Ref. 51)

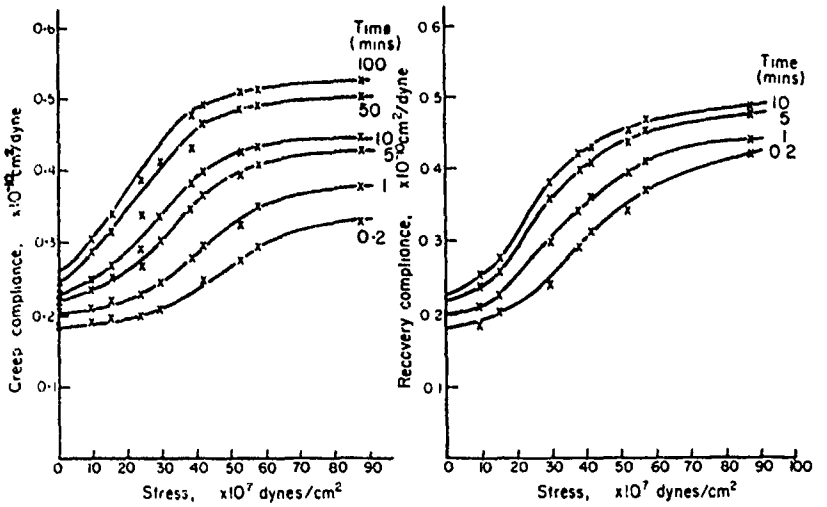

Creep and recovery for high molecular weight, high molecular orientation fibre.

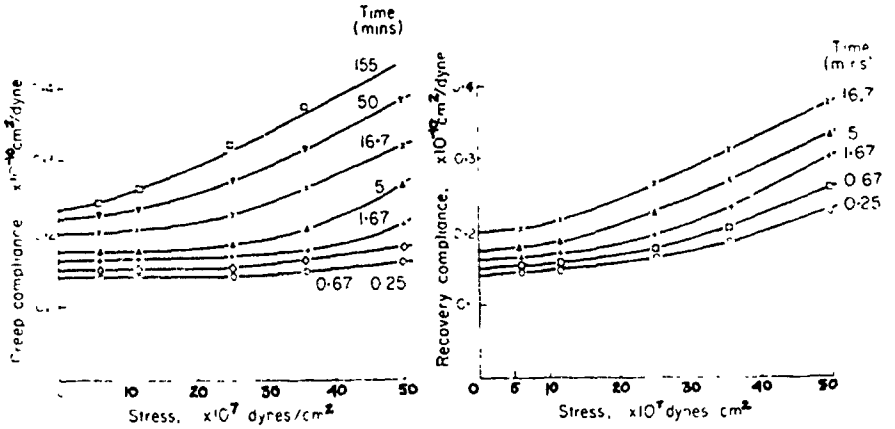

Creep and recovery for original monofilament

Figure 5(b): Comparison between heat set, drawn fibers and the "monofilament", both having birefringence of 30 x 10^{-3}. (Ref. 51)

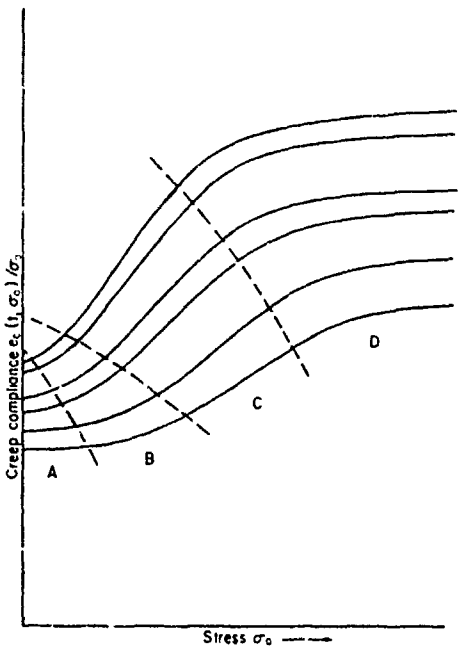

Master diagram for creep and recovery against stress level.

Figure 6: Summary diagram of orientation dependence of creep compliance (Hadley and Ward (1965)[51]).

lar orientation, as measured by birefringence, are important in determining the type of nonlinear behavior a sample will show.

In 1967 Lifshitz and Kolsky[68] discussed a possible mechanism of nonlinearity. They examined isotropic low density polyethylene at room temperature in tensile and torsional creep. They found that in a two-step creep test, as the time under the first load increased, the response to the second load decreased; thus it was less compliant. They attributed this stiffening to an orientation effect which became more pronounced the longer the load was applied.

In 1971, Yannas and Haskell[70] studied the nonlinear behavior of isotropic polycarbonate in stress relaxation over a temperature range from 23°C to 100°C. They applied the Green-Rivlin multiple integral formulation with two terms in the power series. They wished to determine whether or not this representation gave physically meaningful results or was simply a mathematical model. Details of this representation are presented in the section entitled "Modeling". Upon calculating the coefficients for the multiple integral series, they found that the first coefficient monotonically decreased with temperature. The second term did not vary in a regular way with temperature. They concluded that only the first coefficient reflected a physically meaningful phenomenon.

In 1974 Darlington and Saunders[77] looked at the anisotropic creep behavior of LDPE, PMMA and PVC. In LDPE they looked at the 100 second creep modulus (i.e., creep modulus = $\frac{\sigma_o}{\varepsilon(100\ \text{sec})}$) as a function of strain for specimens at an angle, θ, to the draw direction. They found that the strain at which significant nonlinearity first occurred depended strongly on θ, with the onset strain being lowest for angles nearest 90°. This effect was not seen in PMMA. It is difficult to say whether or not this effect

would be seen in other semicrystalline polymers, because LDPE has been found to show unusual anisotropy in modulus. LDPE shows this unusual anisotropy in that the 90° modulus is greater than the 45° modulus. It may be that the features which cause the unusual directional dependence of modulus also give rise to an unusual pattern of nonlinearity.

The most recent attempt to explain the source of macroscopic nonlinearity in terms of microstructure was by Buckley in 1977.[49] He examined isotropic polypropylene at 65°C in combined tensile and torsional creep and looked at changes in linear viscoelastic behavior while the sample was simultaneously undergoing nonlinear viscoelastic deformation. He chose a temperature of 65°C at which polypropylene is dominated (in the linear region) by one relaxation mechanism, the α-relaxation. He discussed several interpretations of nonlinear behavior. First he dispatched the theory that internal damage accumulates while the sample is under load and recovers gradually upon removal of the load. This was not a feasible explanation because the response to a second step in stress, applied at a time t_d after the first step was applied, was reduced as t_d was increased. Thus the sample had become stiffer with time under load, whereas if damage had been accumulating it would have become more compliant.

The complexity of nonlinear behavior was pointed out by Buckley when he noted that both stiffening and softening seem to occur under creep. An appearance of "softening" behavior was seen in creep-recovery experiments. If a creep stress was applied for a time, t_c, and was followed by recovery, the recovery strain was for a while greater than the creep strain at an equivalent time. Thus for a time under no load the sample was more compliant in recovery than in creep. Also, as t_c was increased, the recovery compliance increased. This is in contrast to the two-step creep in which the additional creep compliance decreased with increasing time under the first

load. Thus the idea proposed by Lifshitz and Kolsky that the sample orients and so stiffens, cannot be correct, since it should be stiff in recovery also.

Buckley concluded that up to strains of 0.01 the nonlinearity could be described by making the shear creep compliance stress-history sensitive while the creep compressibility behaved just as it would in simple Boltzman superposition. He explained this in microstructural terms by saying that viscoelastic regions were dispersed in an elastic matrix and that only a small part of the structure was responsible for the α-relaxation. The properties of the viscoelastic regions were controlled by the magnitude of the local stress. He tentatively suggested some possible molecular level interpretations.

First, the restraining elastic matrix may consist of crystals and noncrystalline "tie molecules" linking neighboring crystals. The viscoelastic component then would arise from the noncrystalline molecular segments at or near the lamellar crystal surface, as has been suggested to explain the α-relaxation. Another possible structural explanation may be that the elastic component is as above, while the viscoelastic regions deform as a non-Newtonian viscous liquid. These ideas were put forward as suggestions only. Arridge and Barham[13] in 1978 made a comment which suggested a similar explanation for nonlinearity. They said that nonlinear behavior is inevitable in semicrystalline polymers because of the irregularity of the stress distribution throughout the polymer.

In conclusion, we can see that the connection between microstructure and nonlinear viscoelasticity is not well understood. This work seeks to explore that connection.

The Effect of Annealing on Structure

In this work annealing was used to alter structure and properties. Thus it is important to review the literature concerning the effects of annealing on the structure of highly-drawn semicrystalline polymers.

In 1973 Samuels[23] found that the total amount of shrinkage of oriented polypropylene fibers and films was controlled by the noncrystalline chain orientation. This is important because shrinkage was allowed in some of our films during annealing. In our work, however, shrinkage was limited to 1 - 2%, while Samuels examined free shrinkage.

In another study published in 1973, Owen and Ward[28] compared the structure and the anisotropy of the dynamic properties of three polypropylene samples. Cold drawn (at room temperature), hot drawn (at 120°C) and hydrostatically extruded (at 100°C) samples were prepared. The cold drawn samples were subsequently annealed by mounting them in a jig, but not under tension, in an oil bath at either 120°C, 145°C, or 158°C. The samples annealed at 120° and 145° showed a small amount of shrinkage, while those annealed at 158°C shrank about 50%. Wide angle X-ray diffraction (WAXS) and small angle X-ray scattering (SAXS) were used to examine the structure. Creep (at 10 seconds), vibrating reed, and TFA (Transfer function analyser) were used to examine the anisotropy of the moduli over a temperature range from -110 to +90°C.

From these data, Owen and Ward concluded that while cold and hot-drawn material showed very high crystalline orientation, the hot-drawn material showed a well-developed lamellar texture, while the cold-drawn material did not. From WAXS and SAXS studies, the cold-drawn material seemed to have small, strained and disordered crystals. The effect of annealing on the cold-drawn structure was to allow a relaxation of the intercrystalline

material, which reduced the number of interlamellar tie molecules such that constraints on the deformation of the amorphous regions were reduced. A second effect of annealing was to permit recrystallization, which created a more clearly defined lamellar structure.

In 1978, Nardella, Spruiell and White[19] carried out a study of the drawing behavior of various polypropylene spun fibers. They also examined the effect of annealing on cold-drawn fibers. Their drawing conditions were cold drawing at 25°C, hot drawing at 140°C and annealing at 140°C for 15 minutes. No indication is given as to the constraint, if any, given during the annealing procedure. They concluded that cold drawing gave a material having a reduced crystallite size and large amounts of lattice strains and defects. They found that annealing caused a removal of internal residual strains, increased the perfection of the unit cell and the size of the crystallites, and caused a new long period to develop. These results are similar to those found by Owen and Ward.

In 1978 an interesting phenomenon termed "self-hardening" was reported by Arridge and Barham.[12,13,67] The phenomenon was observed when a highly drawn polyethylene was held at constant length, heated to between 129 and 132°C (within the melting region) until all contractile tension had dissipated, and was subsequently cooled to room temperature under constraint. They found that if the modulus of the sample was measured immediately it had decreased to 10% of the modulus of the original fiber, but upon remaining at room temperature for several hours, either constrained or not, it recovered up to 75% of the original modulus. Similar effects were observed in polypropylene, although the magnitudes of the changes were smaller.

The mechanism they proposed to explain this self-hardening was that upon heating under constraint, most of the crystals melt, leaving only

a small amount of crystallinity remaining. Upon cooling to room temperature, recrystallization occurs from these remaining crystals, giving a highly oriented crystalline region which causes a restoration of the modulus. The resulting material shows no contraction upon heating and shows a "dead bend", i.e., extensive fibrillation upon bending the fiber.

Some similar properties were seen in polypropylene fibers created by Taylor and Clark[26] in 1978. They termed their fibers "superdrawn" fibers because they were made by a two-step drawing process. First the fiber was rapidly drawn to its natural draw ratio. Then at the same temperature (optimal temperature was found to be 130°C) the drawn portion was further drawn very slowly, at 4%/min. The resulting fibers showed both the lack of shrinkage at 155°C (in the usual melting peak) and the dead bend effect seen in the self-hardened polyethylene. They also saw a very sharp melting peak on the DSC and no SAXS up to a resolution of 40 nm. They concluded that the unusual drawing procedure had produced a continuous crystal matrix in which the amorphous material was limited to disconnected regions (see Figure 7). This structure is similar to that proposed for the self-hardening polyethylene.

Other work which showed similar phenomena was carried out by Gibson, Davies and Ward[27] and by Clements, Jakeways and Ward.[29,58] Clements et al.[58] in 1978 examined a high density polyethylene drawn at 75°C at about 500%/min. They used WAXS peak broadening to examine the average crystal dimensions from the (200), (020) and (002) reflections. Upon drawing above a deformation ratio of 10, they found little change in the (200) and (020) reflections, i.e., those dimensions perpendicular to the draw direction. However, from the (002) reflection (parallel to the draw direction) a crystal thickness of 460 Å was found. The same sample showed a SAXS long

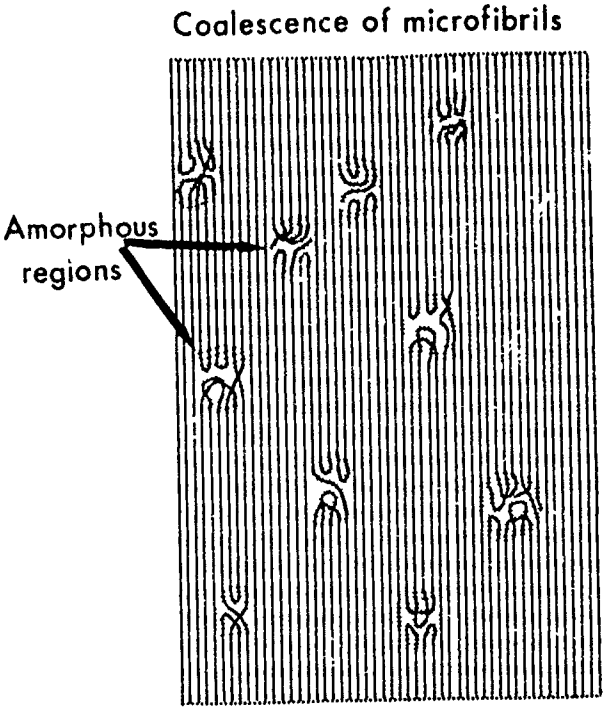

Proposed morphology of superdrawn filament illu rating concept of continuous crystal matrix.

Figure 7. (Ref.26)

period of 200 Å. The authors concluded[27] that the structure consisted of fibrillar stacks of crystallites linked by intercrystalline bridges, or as a continuous crystal containing disordered regions which are periodic in the C direction (the orientation direction). (See Figure 8.)

In these three groups of work, the self-hardening phenomenon, superdrawing, and the intercrystalline brdiges of Clements et al., similar structures were proposed even though different processing was used in drawing. This work is relevant to the discussion of the effect of annealing on structure because it is a form of annealing under constraint, and in the case of superdrawing, annealing under increasing strain. In each of these models the continuity of crystals along the orientation direction is seen to have a stiffening effect due to a parallel type stress transfer along crystalline regions.

The effect of annealing on the high modulus polyethylene of Clements et al.[58] was examined by Clements, Jakeways, Ward, and Longman[29] in 1979. These samples were annealed at constant length. Some were annealed for 3-1/2 hours in an air oven (temperature 125 - 130°C) and cooled slowly. Other samples were annealed for 2 hours in a silicone oil bath (temperature 80 -135°C) and quenched in ice water.

The authors concluded that upon annealing, the initial 200 Å lamellar structure grew at the expense of the crystalline bridges with an increase in the long period and the crystallinity. Thus, they concluded, the effect of annealing was to produce a simple parallel lamellar texture in which the crystalline and non-crystalline material behaved as if they were connected in series.

In 1980 an examination of a highly drawn polypropylene and the effect of annealing was described by Wills, Capaccio and Ward.[62] Their

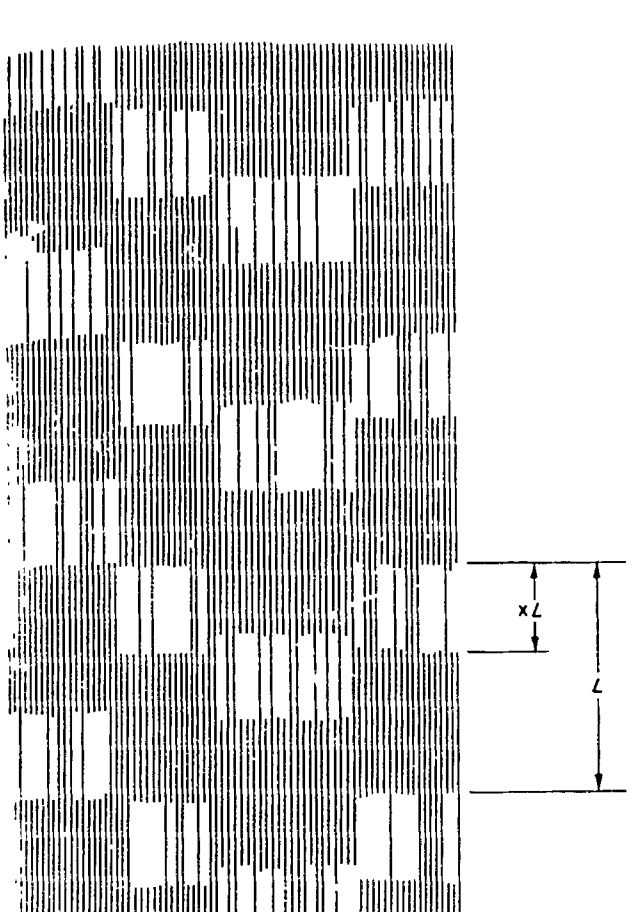

A schematic representation of the structure of the crystalline phase of highly oriented linear polyethylene

Figure 8. Schematic representation of the structure of the crystalline phase of highly oriented linear polyethylene. (Ref. 27)

samples were drawn at 110°C at a crosshead speed of 10 cm/min., reaching draw ratios of up to 18. High molecular weight samples were annealed for 60 minutes at 135°C under a tension of 5.5 MPa (~800 psi). Low molecular weight samples were annealed for 15 minutes at 100°C under a tension of 10.4 MPa (~1500 psi). A similar annealing procedure, 15 minutes at 135°C under 10 MPa (~1450 psi), on samples of high molecular weight, gave a shrinkage of 8.5%; under the same conditions the low molecular weight sample shrank only 0.7%.

The effect of annealing on the structure was to cause a reemergence of the β loss peak which the authors concluded was due to the relaxation of the intercrystalline material. The relaxation allowed the occurence of interlamellar shear. (See Figure 9.) In addition, at low temperatures (T<30°C), the dynamic modulus increased on annealing, indicating that a considerable degree of structural rearrangement had occurred. Annealing also caused an improvement in crystal perfection and crystal size, as seen by sharpening of WAXS peaks and an increase in the melting temperature as seen by DSC.

In summary, various studies of the annealing of highly oriented polypropylene and of linear polyethylene have been reviewed. Various conditions of annealing were examined, including annealing under constant length, or constant tension, and annealing at various temperatures. The earliest of these annealing studies were made on cold-drawn (T~25°C) materials and later studies were made on moderate temperature-drawn materials (PP: T~110 - 130°C; PE: T~75°C). Generally these studies have found an increase in crystalline perfection, little change in crystalline orientation (except at high temperatures), an increase in the regularity of lamellar structure, often a change in long period, and some report an increase

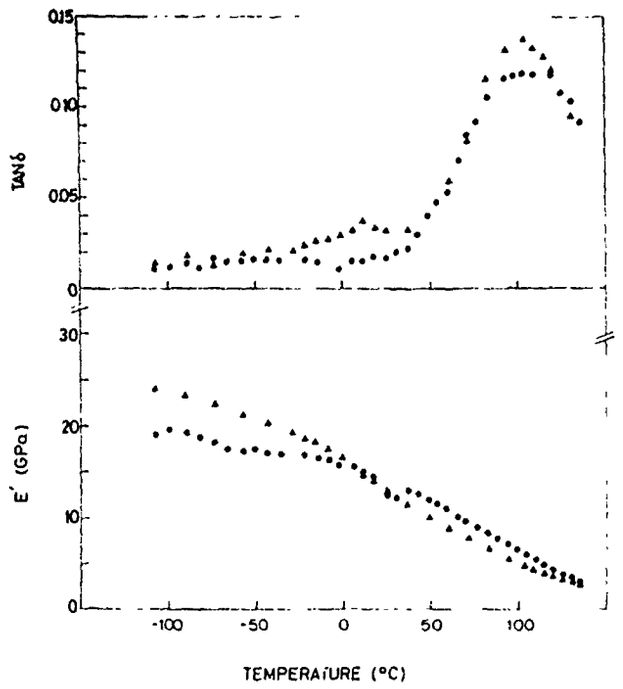

Figure 9 : Temperature dependence of tan δ and storage modulus E' for ultra-drawn polypropylene (M.W. = 400,000) (●) as drawn, (▲) after annealing under tension. (From Ref. 62)

in interlamellar shear. From this last observation the conclusion is drawn that taut tie molecules relax on annealing. Whether or not the effects of annealing on cold-drawn structures would occur in the annealing of a hot-drawn material such as that examined in this study is uncertain.

MATERIAL

A description of the polypropylene films that were studied will be given. Both general information and specific measured properties will be offered.

The polypropylene films used in this work were taken out of laminates and films made by Phillips Scientific Corporation for the Army Materials and Mechanics Research Center (AMMRC). They are designated XP laminates and were developed for use in constructing battlefield radomes (radar domes). The description of the process which was used to manufacture these panels is shown in Figure 10. This figure and information on the process were obtained from an AMMRC report (Ref. 56).

The films were stretched continuously between two motor-driven rolls, passing through a radiant-heat oven between the rolls. The surface temperature of the heaters was controlled in the range 320 - 480°C. The film temperature as it left the oven was 170°C, as measured by an infrared pyrometer.[59,61] The drawing speed was approximately 50 meters/minute.[61] Draw ratios up to 12:1 and 14:1 were achieved.

After drawing, the films were cross-plied at 90 degrees to produce pads. Eight-inch-wide strips of film were wound on a mandrel at opposite 45 degree angles. The pad was then cut off the mandrel and cut into smaller sections. Several techniques were used to press these pads to remove entrapped air between the layers and to provide structural integrity. It was found that rigid, air-free laminates could be made with little loss in polymer orientation under pressing conditions of 176°C and 2000 psi. The pressure prevented film shrinkage and relaxation of the oriented polymer. Laminates were held at temperature for 70 minutes, causing the center of the laminate to be at platen temperature for 5 minutes. Pressure was maintained

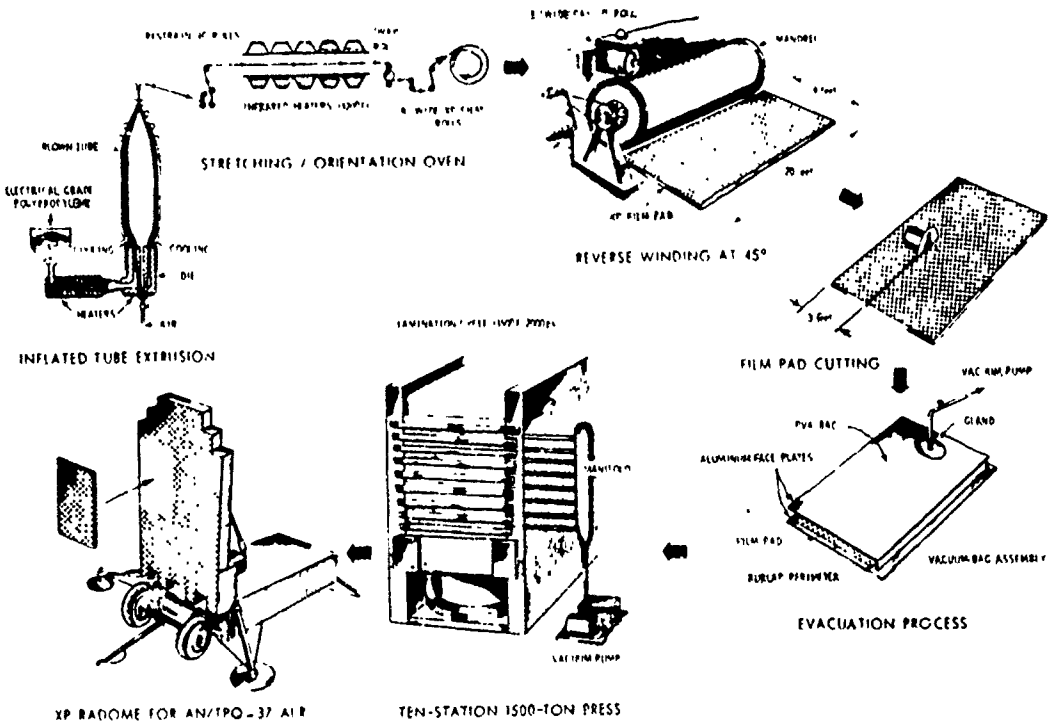

Figure 10: Flow diagram illustrating the production of PP cross-ply panels. (from Ref. 56)

during a 60-minute cooling cycle until room temperature was reached. Figure 11 shows a finished laminate.

Samples for tests in these studies were prepared by cutting off the edges of a laminate and peeling off the top layers. Then a section containing from eight to ten layers was peeled off, care being taken to prevent serious delamination among those layers. This "sheet" was then cut into specimens. Specimen preparation will be discussed in the next section.

C.R. Desper has, in publications and presentations from 1973 to 1979,[11,59,60,61] presented structural data for some of the films produced by AMMRC. This data will be described briefly. Replicas of the surface of the films show a fibrillar structure. Crystalline orientation was around 0.992 to 0.997, with crystallinities of 0.66 to 0.69. Amorphous orientations of from 0.38 to 0.69 were found.[11] Dynamic mechanical behavior showed that as the orientation increased the tanδ β loss peak became smaller (see Figure 12). Curves D and E are the most highly oriented films. This supression of the β loss peak was also seen in oriented polypropylene by Wills et al.[62] in 1980 (see Figure 9). From IR and Raman spectroscopy, Desper concluded that the non-crystalline regions are not random mixtures of random conformers, but are collections of short helical runs, separated by no more than a hand reversal.[59]

Other studies of these highly drawn polypropylene films included the measurement of crystal size by wide angle X-ray peak broadening. Desper found that crystal size was 120 Å in all directions. From SAXS, the long period was found to be 170 Å, and the pattern was a clear meridional pattern, indicating a well-developed lamellar structure (as seen by Owen and Ward and Nardella et al. in hot drawn PP as described earlier). See Figure 13. Etching in boiling 70% nitric acid was used to investigate the presence of taut tie molecules, or extended chain crystals. The effect of the etch was pre-

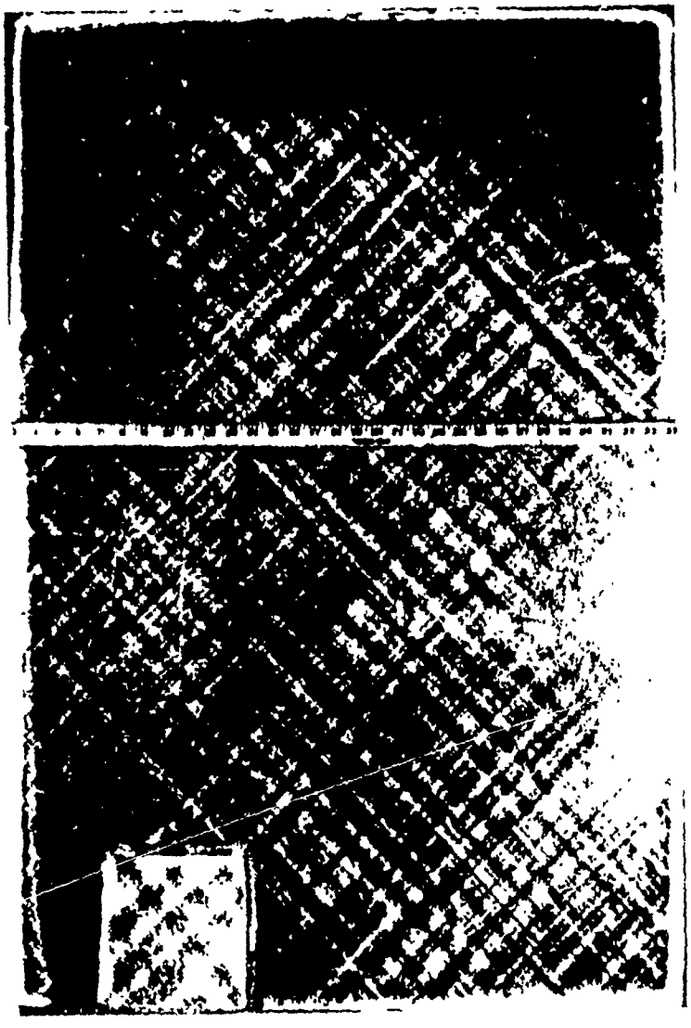

Figure 11: Photo of polypropylene cross-ply laminate. (Ref. 56)

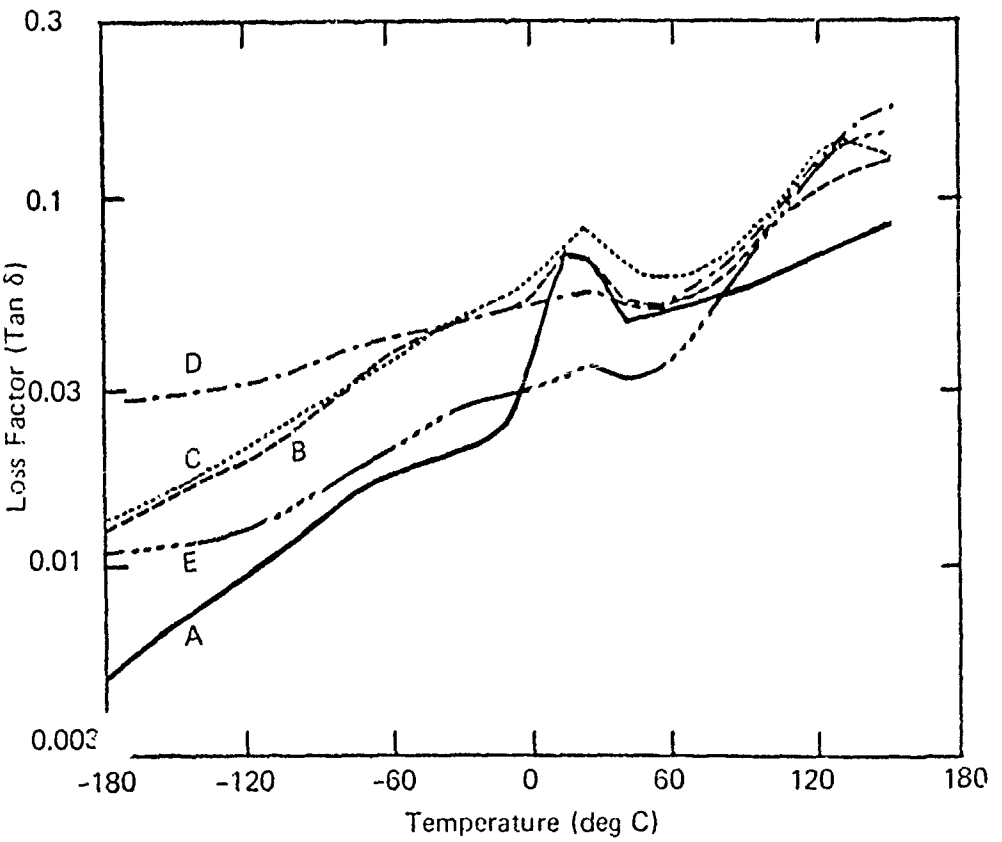

LOSS FACTOR TAN δ VERSUS TEMPERATURE AT 110 Hz FOR FIVE POLYPROPYLENE FILMS OF DIFFERENT DEGREES OF ORIENTATION

Figure 12: Effect of orientation on tan δ β loss peak. Curves D and E have highest orientation. (Ref. 61)

Figure 13. Small angle X-ray scattering pattern of hot drawn polypropylene. Draw direction is vertical. Meridional maximum indicates 170 Å long period.

sumed by Desper to be cleavage of the molecules at folds, leaving fragments whose lengths would indicate the length between folds. The length distribution of the fragments was examined by gel permeation chromatography. See Figure 14. In unstretched film, a bimodal distribution was seen with maximums at lengths of 85 Å and 200 Å and with 17% of the fragments having lengths greater than 200 Å. For stretched films a broader distribution was found with a maximum at 100 Å and with 33% of the fragments having lengths greater than 200 Å.[60,61] The increase in the number of fragments having lengths greater than 200 Å was thought to be due to an increase in the number of tie molecules or to development of a continuous crystal matrix. Finally, on examining shrinkage behavior, Desper reported[61] that samples shrank appreciably in one hour at 155°C. In this feature these polypropylenes differ from superdrawn fibers (described earlier). These data give a general idea of the structure of the films formed by large scale drawing.

Measurements of the structural properties of the film examined in this work were carried out to get a general characterization of the material. To that end, thermal, X-ray and IR absorption were checked. Figure 15 shows the measurement by Differential Scanning Calorimetry (DSC), using a Perkin Elmer DSC-2, of the melting temperature (243°K, 151°C). Figure 16 shows results from a Digilab Fourier Transform Infrared Spectrometer.

Figure 17 shows a transmission X-ray photograph made using a technique described by Alexander.[4] Figure 18 is an illustration from Samuels[10] showing the planar assignments to the spots (or arcs) obtained from transmission photos of cold drawn and annealed or spun polypropylene fibers. Note that the photo from the film studied here resembles that of the cold drawn fibers.

In summary, this section has reviewed how the polypropylene films studied in this thesis were produced. The structural characterization of the

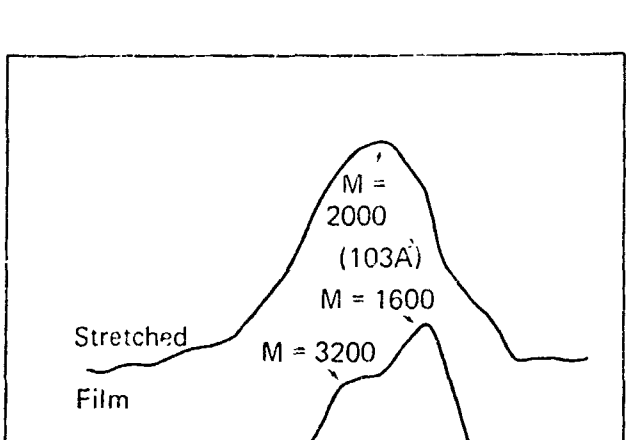

Gel Permeation Chromatograms - HNO_3 Etched Polypropylene

GPC Data

HNO_3 Oxidized PP Film

Sample	Molecular Length Maxima	Fragments Above 200Å
Unstretched	85Å, 200Å	17%
Stretched	100Å	33%

Figure 14. Nitric acid etch of stretched and unstretched PP film (Ref. 61)

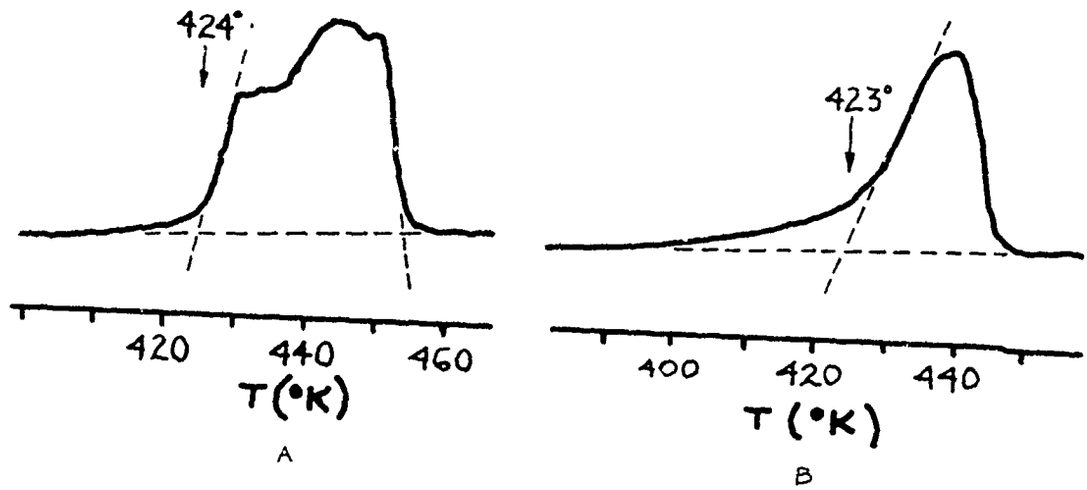

Figure 15: Differential Scanning Calorimetry of PP film: (a) Melting of oriented film showing shrinkage effects; (b) Same film after cooling and reheating. (All heating rates were 20°/min.)

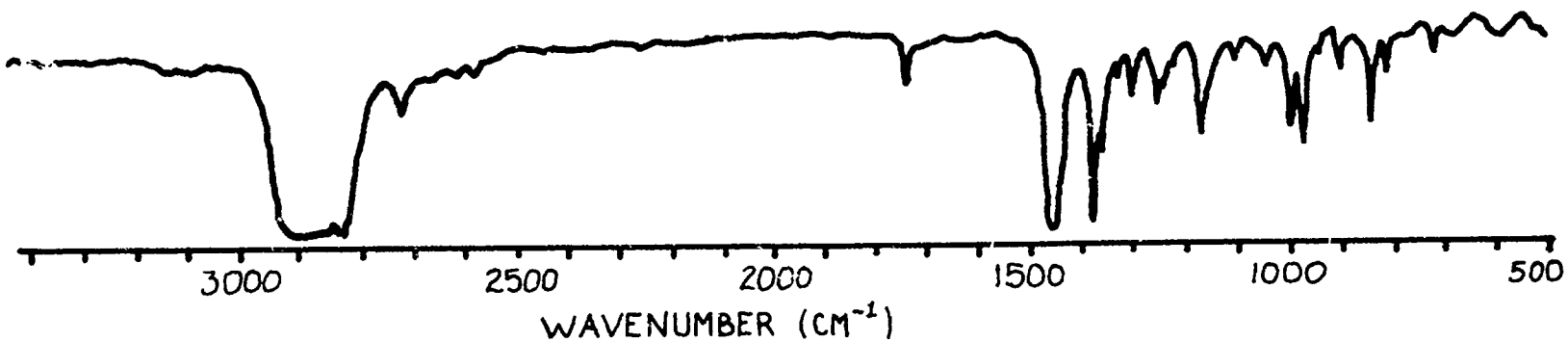

Figure 16: Transmission spectra from Fourier Transform Infrared Spectrometer of PP film.

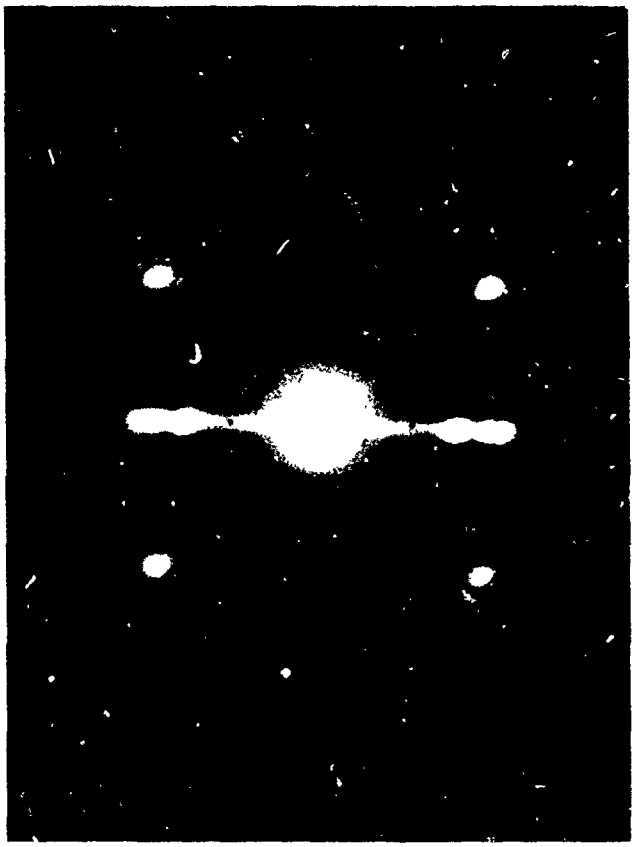

Figure 17 : Transmission X-ray photograph of oriented PP film, orientation direction is vertical. (thickness:1mm-35 minute exposure).

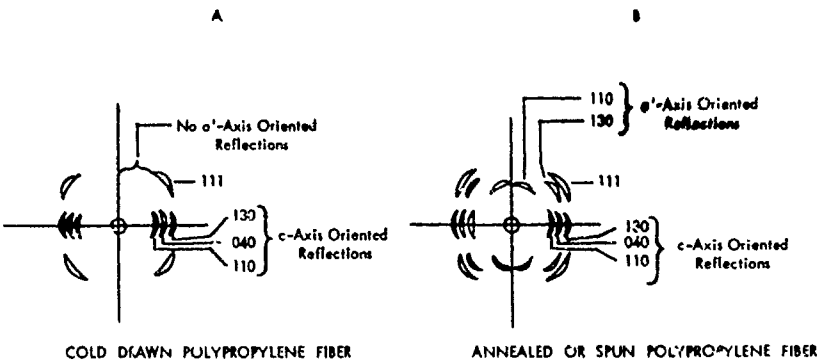

X-ray diffraction diagrams of isotactic polypropylene fibers.

Figure 18: Transmission X-ray photographs of PP identifying diffraction planes(10).

films has also been described. Finally, some general characterization of the film used in this thesis has been presented, including thermal properties, IR absorption spectrum, and crystal structure.

EXPERIMENTAL

In this section, sample preparation, testing geometry, mechanical tests, techniques to measure strain, and the range of parameters which were examined will be described. In addition, the equipment and techniques used to measure orientation and the annealing procedure will be described.

Specimens were straight-sided strips of film. They were made by separating an 8 - 10 layer section from a laminate pad (described earlier). The section was then cut into specimens. This was done by clamping the section and a cutting guide (a metal bar with a width equal to the desired sample width) to a table. Using a new industrial razor blade, the section was cut completely through on each side of the guide. The cutting guide reduced the variation in the specimen's width. Using new razor blades reduced damage on the specimen edges. This was especially important for the specimens whose lengths were perpendicular to the orientation direction. Because the strength in this direction was so low, any defect at the edge caused the specimen to fail prematurely. Once the multi-layer section had been cut into specimen strips, the layers were separated. Since, in the laminate, adjacent layers are oriented 90° to one another, the cut pieces yielded specimens in which the orientation was in different directions.

The angle the orientation direction made with the direction in which the specimen was tested (the specimen length) was used to identify the film specimens. The specimens which were examined were 0°, 45° and 90° specimens, i.e., the first was tested in tension along the orientation direction, the second at 45° to the orientation direction and the last perpendicular to the orientation direction.

In deciding on specific sizes of the specimens, several things were considered. First, the length was limited by the size of the laminate

pads. They were 12" x 12" and the orientation of the layers was diagonal across the pad. This meant that the longest possible 0° specimen was about 16.5". The other constraint on sample size was that the individual strips of oriented film making up the laminate were 8" wide. This meant that the 45° specimens were limited to about 10" and the 90° specimens to about 8". The width for the specimens was set by the strengths in the various directions. For the 45° and 90° specimens, the strengths were low so widths of approximately 1" were typical. The 0° specimens were very strong and did not require large widths. In fact, because of the anisotropy of the film, the aspect ratio (length/width) of the specimen had to be considered as noted by Arridge et al.[58] They found that for a tensile specimen of highly oriented polyethylene, a length/width ratio of approximately 50 was required before the modulus, determined using grip displacement to measure strain, became independent of sample aspect ratio. Therefore, the length was kept as long as possible and the width was kept to about 0.2" in order to keep it large enough to cut and measure accurately.

Another factor in testing these specimens was finding an appropriate gripping arrangement. Ordinarily, a dog-bone shaped specimen would be used to provide a large gripping area, making it possible to apply the required stress on the gage region. This was not possible for this material because of its tendency to split along the orientation direction. For this reason the straight sided geometry was used. For testing the 45° and 90° specimens, gripping was not difficult. Flat plate, rubber coated grips, which were tightened by a screw, were found to be adequate. The only problem that arose using this arrangement was that when the plates were tightened, torque had to be exerted, which could cause the specimen to tear. With care, this could be avoided. In addition, a very careful alignment was

necessary so the specimen would be evenly loaded in the test.

Because the main interest was not in failure behavior but in stiffness behavior, the simple flat plate, rubber coated grips were used to test 0° specimens. The specimen was placed between the plates without any other attachment. The 0° specimens could not be brought to failure in this way, as slippage intervened at high loads, but the lower stress behavior could be quite satisfactorily observed using this arrangement.

Both constant strain rate (stress-strain) tensile tests and stress relaxation measurements were made. Also, some two-step stress relaxation measurements were made. Strain measurements in stress relaxation experiments were made by measuring the location of gage marks with a cathetometer before and after application of load. In constant strain rate tests the strain was determined from grip displacement. This was possible because the grips were flat plate, not wedge type, and because the specimens were straight-sided, not dog-bone shaped. Marks on the films were aligned with the edges of the grip faces so that any slippage in the grips would be noticeable. The thickness of the films was measured using a weighing technique. The films were approximately 1.5 mil (0.038 mm) thick.

Two-step stress relaxation tests were also performed to check the time-invariance criterion of linear viscoelasticity. The time invariance criterion states that the the response to an input does not change with the time at which the input is applied. To test this, two sets of two-step tests were done. In each test, an initial strain, ε_o, was applied at time $t = 0$, and at a later time, $t = t_D$, a second strain of the same size was applied, bringing the total strain to $2\varepsilon_o$. Values of ε_o were 0.015 and 0.025. The additional stress due to the second step, $\sigma_2(t - t_D)$, was found by subtracting the stress due to the first strain, $\sigma_1(t)$, from the total stress at time t, $\sigma(t)$. Strain measurements in these tests were made using

using the cathetometer.

In stress relaxation tests, the strain had to be applied as quickly as possible. For this reason, the highest cross-head speed (20"/min) was used for the 0° and 45° specimens. Because the displacements were quite small, the time to load was small. To prevent the 90° specimens from breaking, the cross-head speed was 5"/min. To set the strain, ε_o, the "Gage Length" and "Return" dials on the Instron machine were used. These stopped the motion of the cross-head at a displacement which was preset. However, because of its speed, the cross-head normally overshot the set limit. This meant that the displacement could not be set precisely. The range over which the tests were performed is described below.

	Constant Strain Rate	Stress Relaxation
	Range of strain rate (min^{-1})	Range of Strain
0°	0.0002-0.02	0.001-0.06
45°	0.0003-0.02	0.003
90°	0.0003-0.02	0.0015

Orientation measurements were made using density, X-ray azimuthal width, birefringence and sonic modulus. The equipment and details of the techniques of these measurements are described in Appendices A through D. The density was measured using a Techne Incorporated Density Column with a gradient made from isopropanol and ethylene glycol. Details of the density measurement can be found in Appendix C. The crystalline orientation was measured in two ways, as described in Appendix A. First, a Siemens pole-figure goniometer was used. Also, transmission X-ray photographs were made using the X-ray camera and film holder of a Laue X-ray camera. These were used for a qualitative comparison of the crystalline orientation of the annealed and unannealed films.

Birefringence measurements were made using a Berek compensator in a Reichert light microscope (No. 323 474). Details of the measurements can be found in Appendix B. Sonic modulus measurements were made on an H.M. Morgan Co. (Cambridge, MA) Dynamic Modulus Tester, Model No. PPM5, at AMMRC, Watertown, MA. Details of the measurement may be found in Appendix D.

To better understand the relationship between the microstructure of the highly oriented film and its nonlinear viscoelastic behavior, a series of annealing procedures was carried out. The annealing was done in such a way that the degree of crystallinity and the crystalline orientation were unchanged. This meant that the effect of annealing was limited to changes in the amorphous structure.

To anneal the specimens, each film section was placed on a frame, gripped at two ends, and the distance between the grips was adjusted to place the film under tension or to leave it slack to allow shrinkage. The frame and film were then placed in an oven for one and one-half hours. After that time the frame was removed, allowed to cool, and the film specimen was removed from the frame. At least a week passed before the film specimens were mechanically tested at room temperature.

In summary, the details of the mechanical tests, the equipment used in the orientation measurements, and the annealing procedure have been described.

RESULTS

Mechanical Properties

Several types of mechanical tests were carried out to examine the modulus of the polypropylene film. First, constant strain rate (stress-strain) tests and stress relaxation tests were performed on 0°, 45° and 90° specimens to examine the mechanical anisotropy of the film. Some remarks will be made concerning the relationship between the results of stress-strain and stress relaxation tests. Next, stress relaxation tests on 0° specimens over a range of strain from 0.001 to 0.06 were carried out. Two-step stress relaxation tests were also performed. Finally, the polypropylene films were annealed to cause a controlled change in structure, and consequently in mechanical properties. After annealing, the specimens were tested in stress relaxation so that comparison could be made between the unannealed and annealed specimens. The results of these mechancial measurements is the subject of this section.

Mechanical Anisotropy

The mechanical anisotropy was examined by testing the films along the orientation direction (0°), at 45° to the orientation direction (45°), and perpendicular to the orientation direction (90°), all in the plane of the film. First the constant strain rate tests in the 0°, 45° and 90° directions are shown in Figure 19. Curves from tests having about the same strain rate (approximately 0.003 min^{-1}) are compared. Note that the 0° specimen was not brought to failure in this test. At the maximum stress slipping in the grips began. In another test, using a different grip arrangement, the failure stress for 0° was 5.9×10^8 Pa (8.5×10^4 psi).

Figure 20 shows a summary of the results from the constant strain

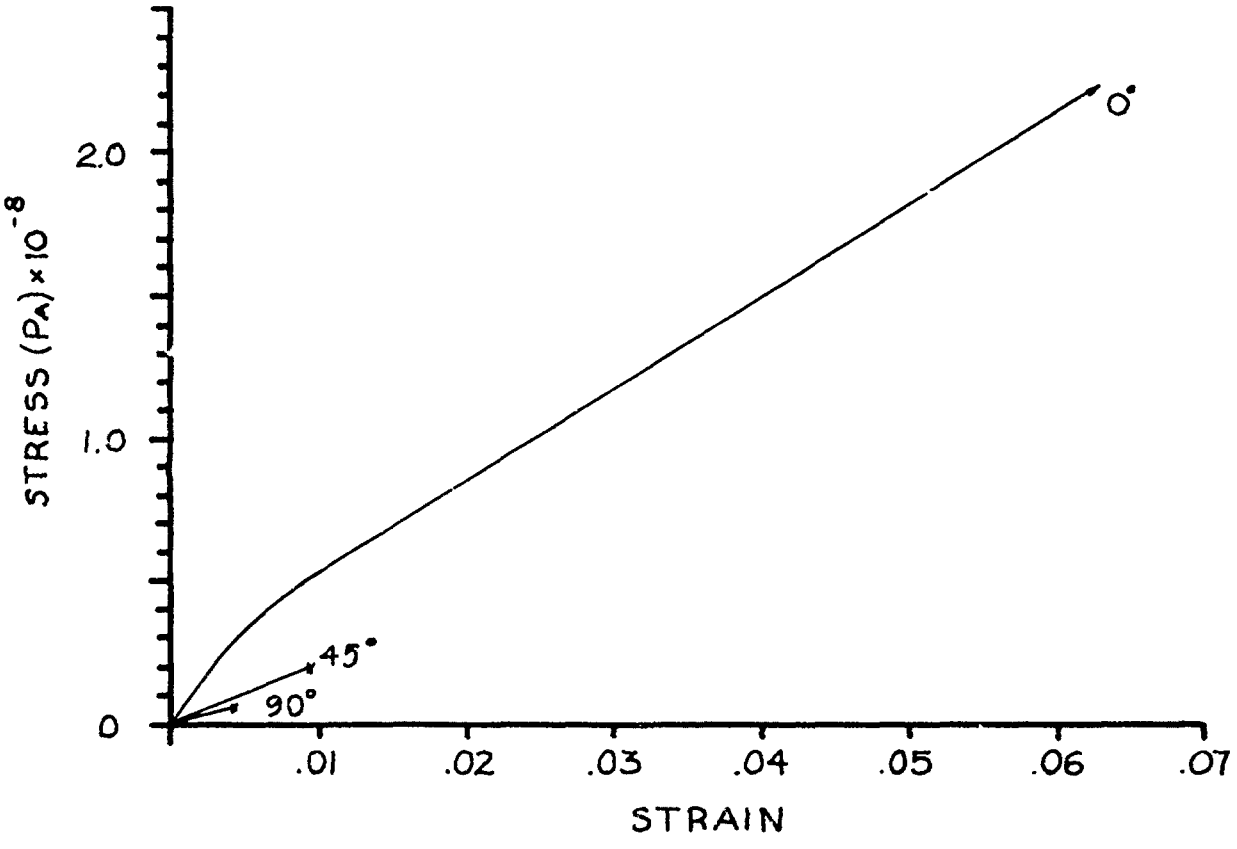

Figure 19: Directional dependence of stress-strain behavior in PP films (strain rate of 0.003 min^{-1}) Note that 0° did not go to failure.

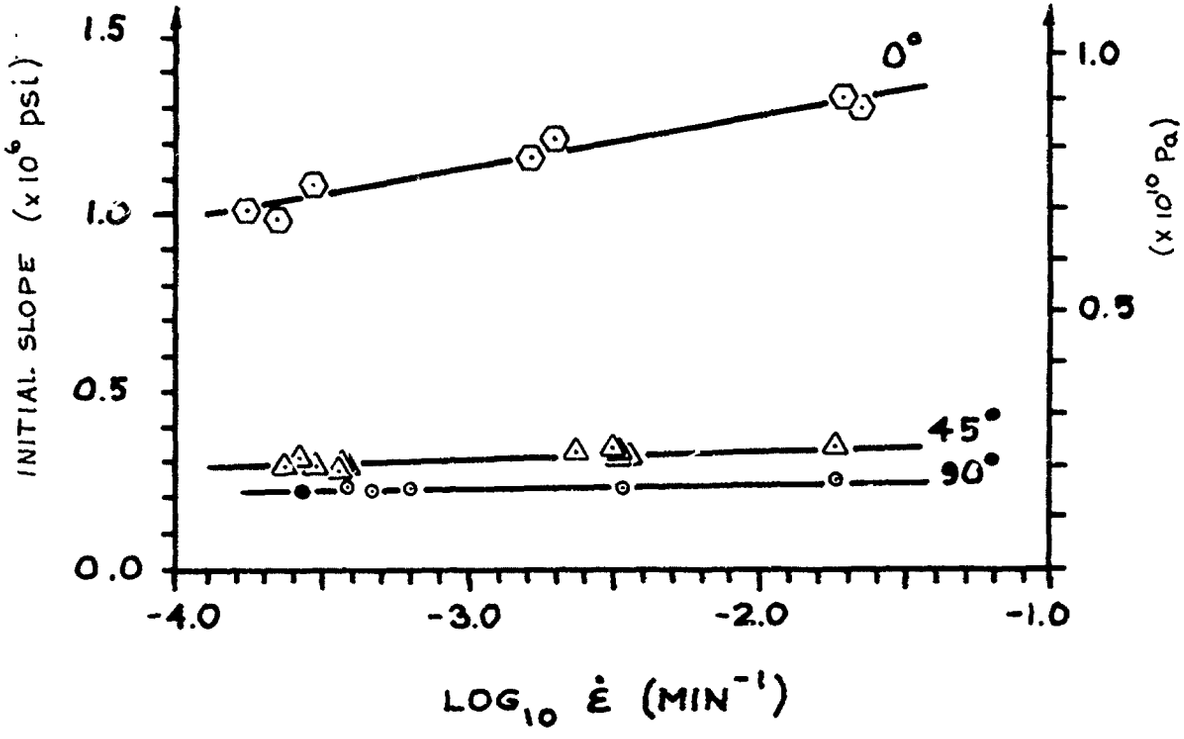

Figure 20: Strain-rate dependence of initial slope of stress-strain curves.

rate tests at different strain rates. The initial slope from the stress-strain curve is plotted here. The difference in magnitude of the modulus for the 0°, 45° and 90° specimens is apparent as is the difference in the sensitivity of the initial modulus to the strain rate. The sensitivity varies as follows: the increase in modulus per decade of rate is 12.4% for 0°, 7.5% for 45° and 5.7% for the 90° specimens.

Another example of the variation of properties with angle from the orientation direction is presented in Figure 21. This figure compares the stress relaxation modulus as a function of time for the 0°, 45° and 90° specimens, all having about the same imposed strain. These data show the same dependence of the modulus on direction as the stress-strain tests just discussed.

Another interesting feature is that the shape of the stress relaxation modulus curves changes with the angle to the orientation direction. In the 0° case, there is distinct curvature. The 45° specimens show some curvature but much less than the 0° specimens. The 90° log modulus vs. log time data are linear as far as could be determined. Measurement of the 90° stress relaxation was complicated by temperature fluctuations which caused stress variations due to thermal expansion. These were noticable because of the low strains necessitated by the low strength of the film and because of the smaller variation in the stress with time.

Comparison of stress-strain and stress relaxation

Comparison between the stress-strain (constant strain rate) and the stress relaxation results is made in Figures 22 and 23. Figure 22 shows a plot of log modulus vs. log time with a representative stress relaxation curve shown ($\varepsilon_o = 0.0128$). Along with this, the slopes of the tangents to the stress-strain curves are shown as bars. The time range over which these bars

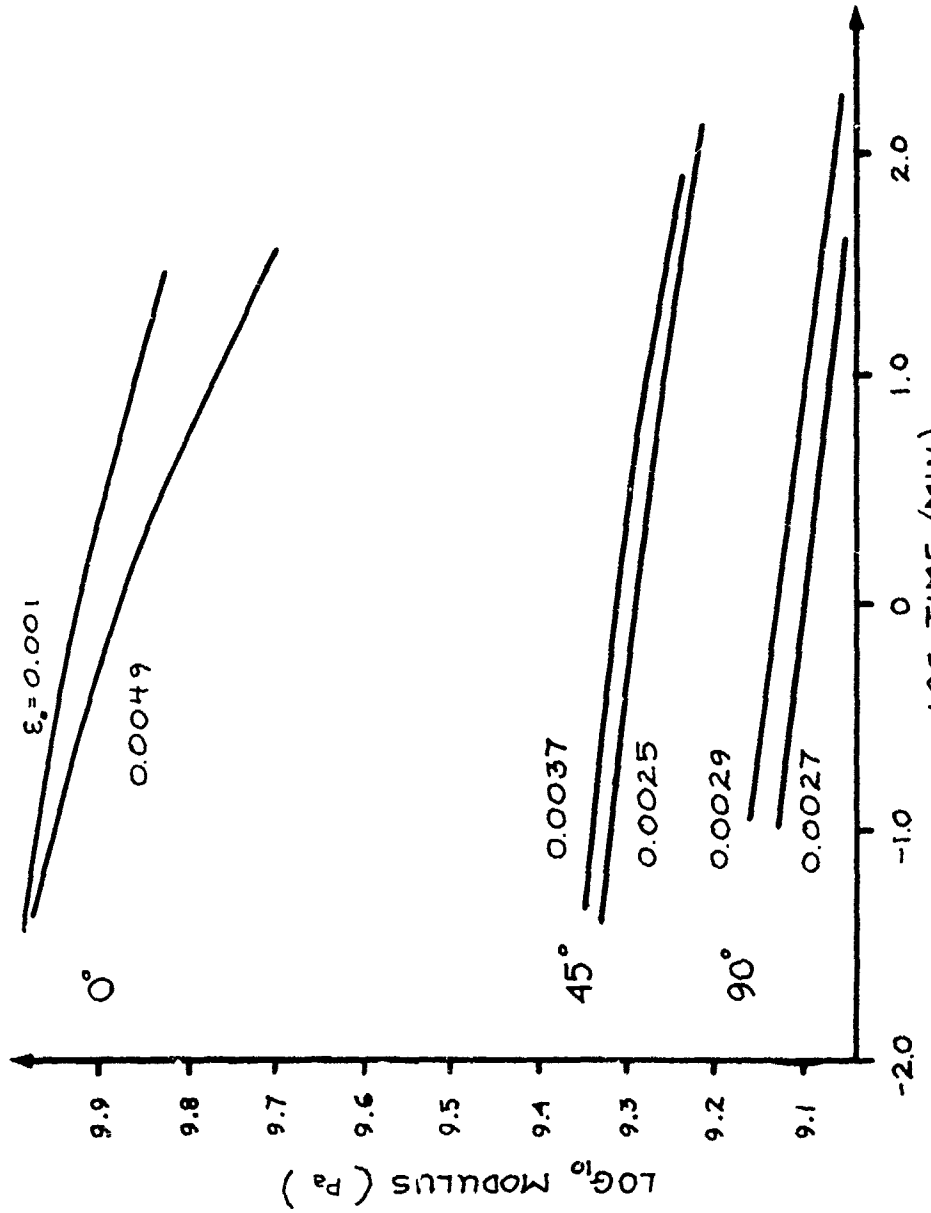

Figure 21: Comparison of stress relaxation modulus for 0°, 45° and 90° specimens.

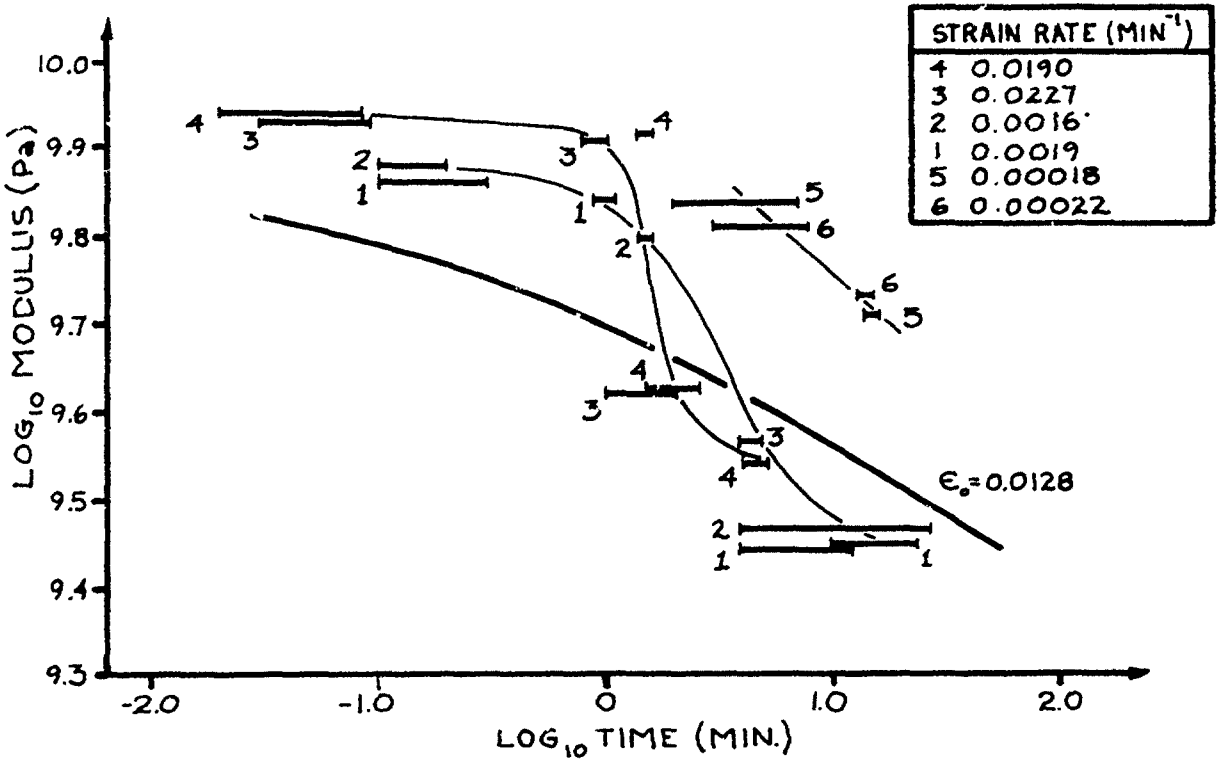

Figure 22: Comparison of constant strain rate test with stress relaxation data (——). Short bars are moduli measured from slopes of stress-strain curves for 0° specimens.

extend is determined by the strain over which the tangent touched the curve. The strains are related to the time by the strain rate. Figure 23 shows the stress-strain curve for a strain rate of 0.002 min^{-1} as a solid line. Plotted with this is data from stress relaxation experiments showing the stress at three different times plotted against the applied strain, ε_o, of each test. Note that the minimum strain of the stress relaxation tests falls at or a little above the yield strain in the stress-strain test.

Stress Relaxation for 0°

Because of the low strain to failure of the 45° and 90° films, and the limited ability of the Instron to provide small displacements accurately, variation in the stress relaxation data with strain could not be studied. Also, a minimal strain was required to ensure that the strain would be applied evenly over the whole specimen.

The 0° specimens, however, had a large range of strain that could be studied. Figure 24 shows the stress relaxation modulus in the 0° direction at four different applied strains. In Figure 25 the results of the stress relaxation tests on the 0° specimens are summarized. The stress relaxation moduli of one minute after the application of strain, E(1 min), are plotted against ε_o. The figure clearly shows that the stress-strain linearity criterion for linear viscoelasticity is not found.

Even at the lowest strains that could be applied with the equipment available, no linear region was found.

Two-Step Stress Relaxation

The time invariance criterion of linear viscoelasticity was checked following the example of Lifshitz and Kolsky.[68] The test is described in the Experimental section. Results of the tests are shown in

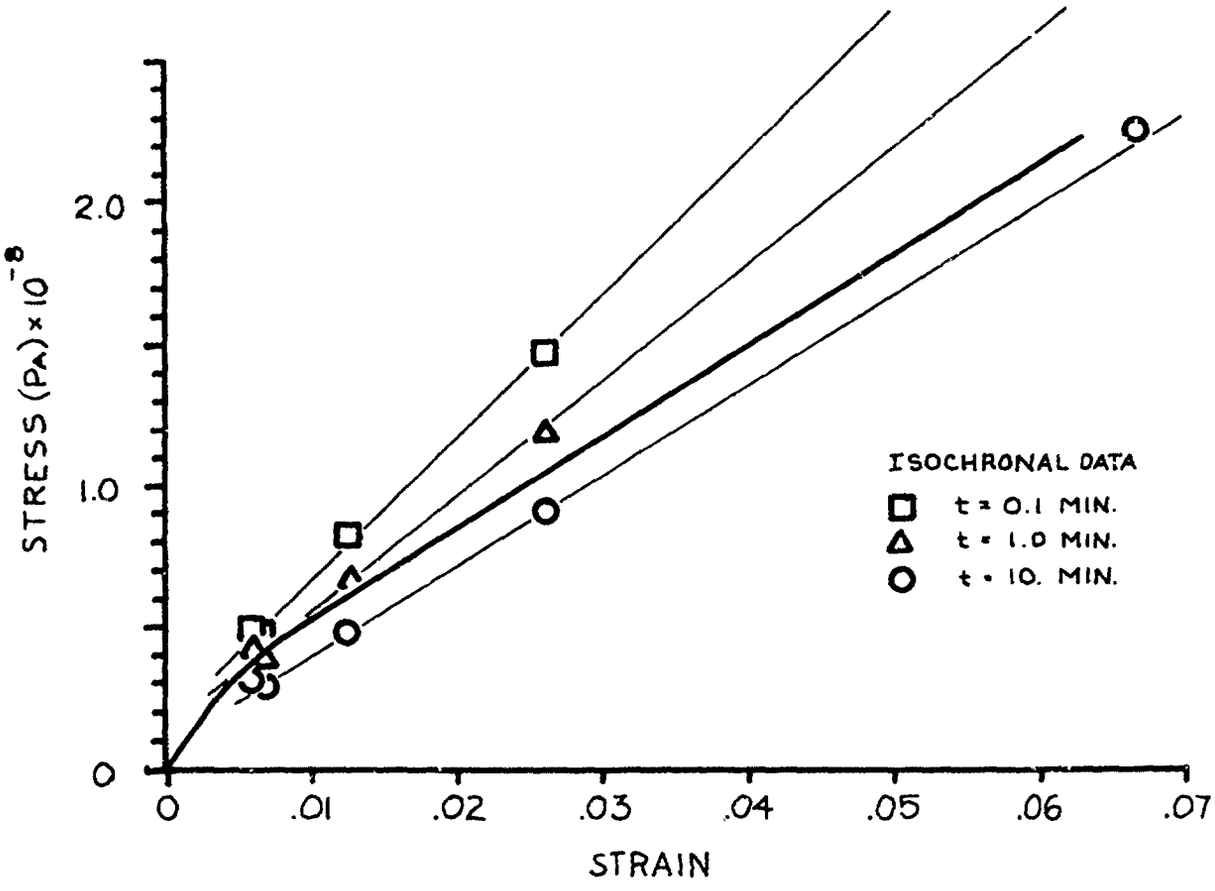

Figure 23: Isochronal stress-strain curves constructed from stress relaxation data compared to stress-strain data for 0° specimens tested with a strain rate of 0.002 min^{-1}.

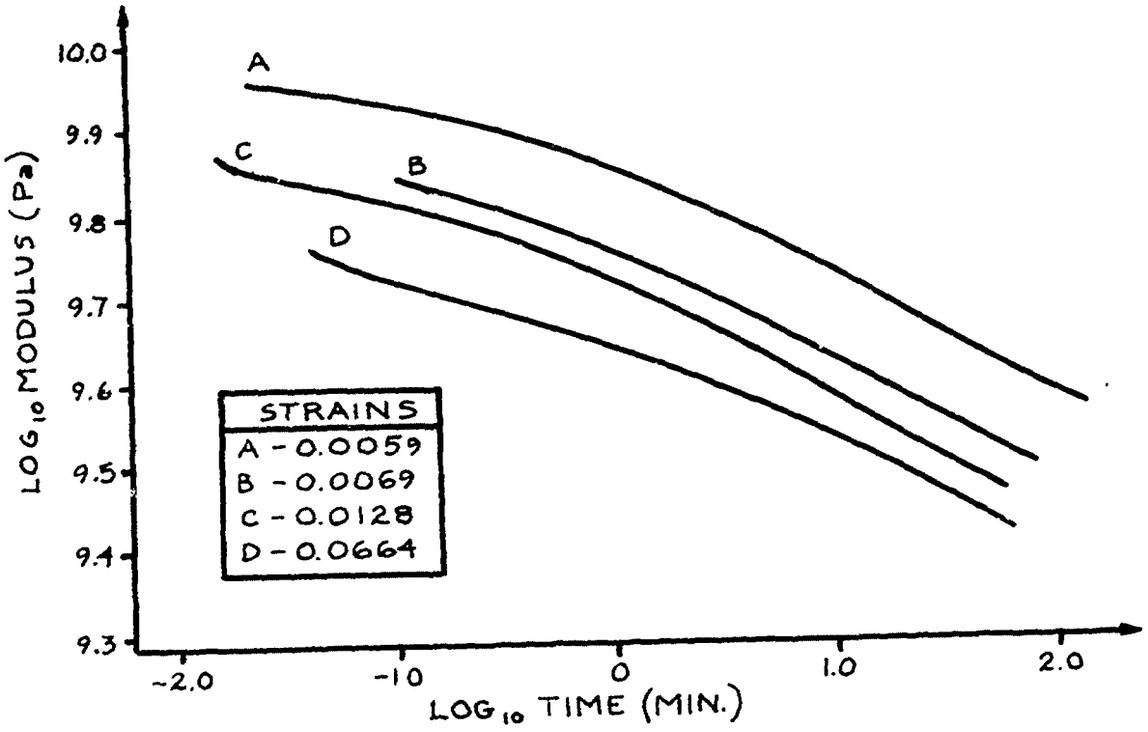

Figure 24: Time dependence of stress relaxation modulus at various strains for 0° specimens.

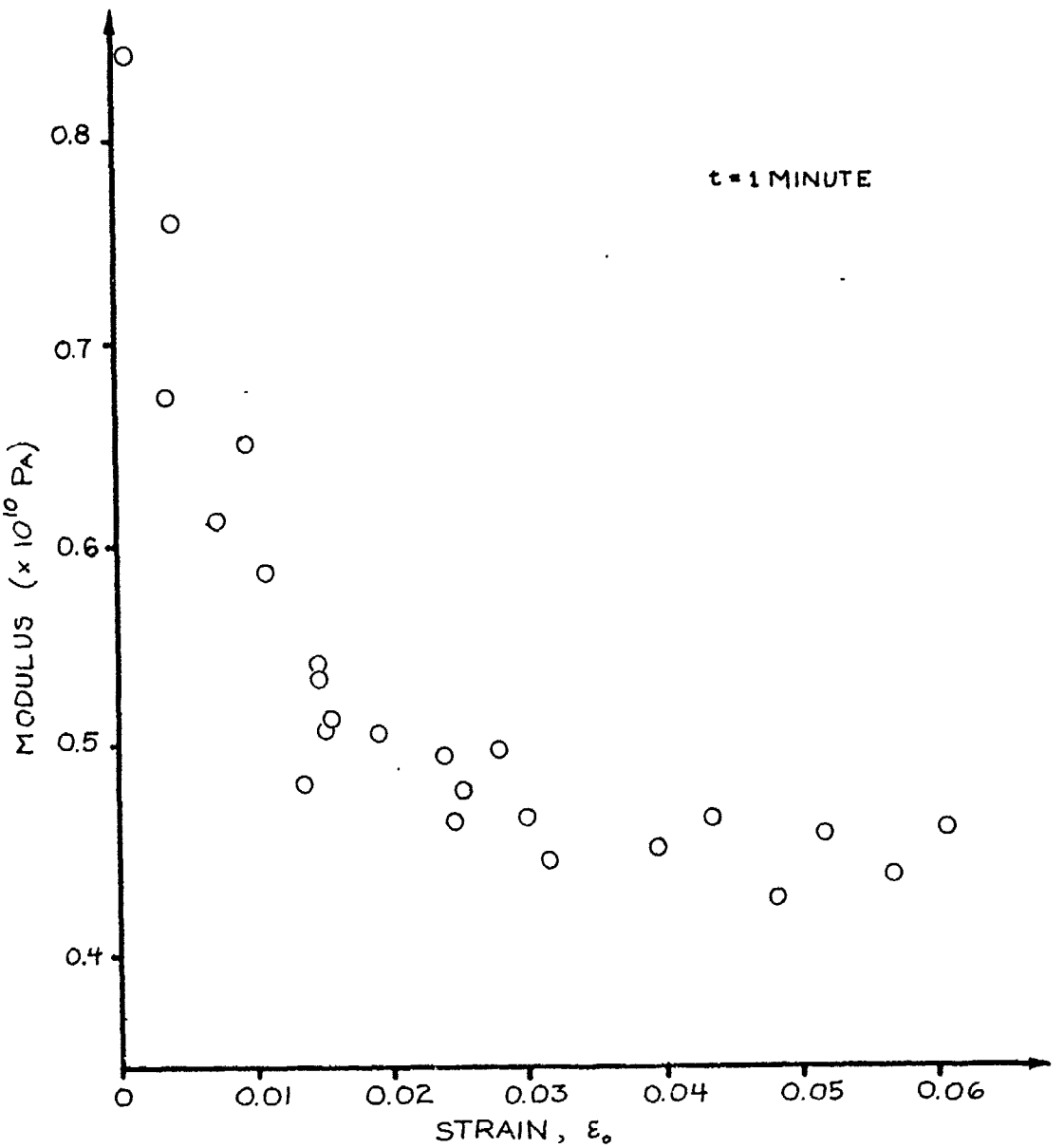

Figure 25: 0° data E (1 min.) vs. ε_o, unannealed.

Figure 26 for $\varepsilon_o = 0.0125$ and in Figure 27 for $\varepsilon_o = 0.025$. In each $\sigma_1(t)/\varepsilon_1$ (solid line) and $\sigma_2(t-t_D)/\varepsilon_2$ (dashed line) are shown. Delay times of 4, 10 and 100 minutes were used between the two steps in both of these tests.

Upon examination of these figures, two features are apparent. First, the shape of the modulus-log time curve is different for the first and second steps in strain. The relaxation is more rapid in the response to the second step in strain. However, the magnitude of the moduli in the first and second steps is not markedly different and shows no regular trend with delay time. It should be noted that, because exactly the same strain could not be applied in each step, the calculation of the modulus due to the second step in strain was complicated and error was introduced. Therefore, the small differences in the magnitude of the modulus between the first and second step responses and between the responses for the various t_D cannot be taken as significant. It seems, therefore, that the time invariance criterion of linear viscoelasticity is obeyed, because the magnitude of the modulus did not change with the delay time. However, the change in the shape between the first and second step response is a violation of the time invariance criterion, albeit a small one.

Effect of Annealing

The effect of annealing on the mechanical properties of the polypropylene films, depended on the type of annealing that was performed. The first film specimens were annealed at 113, 120, 135 and 155°C while the film was extended to 1% strain. After annealing, the specimens were cooled and stored for approximately one week. They were then tested in stress relaxation. The stress relaxation moduli of these films at one minute as a function of the applied strain are shown with data from the unannealed film in

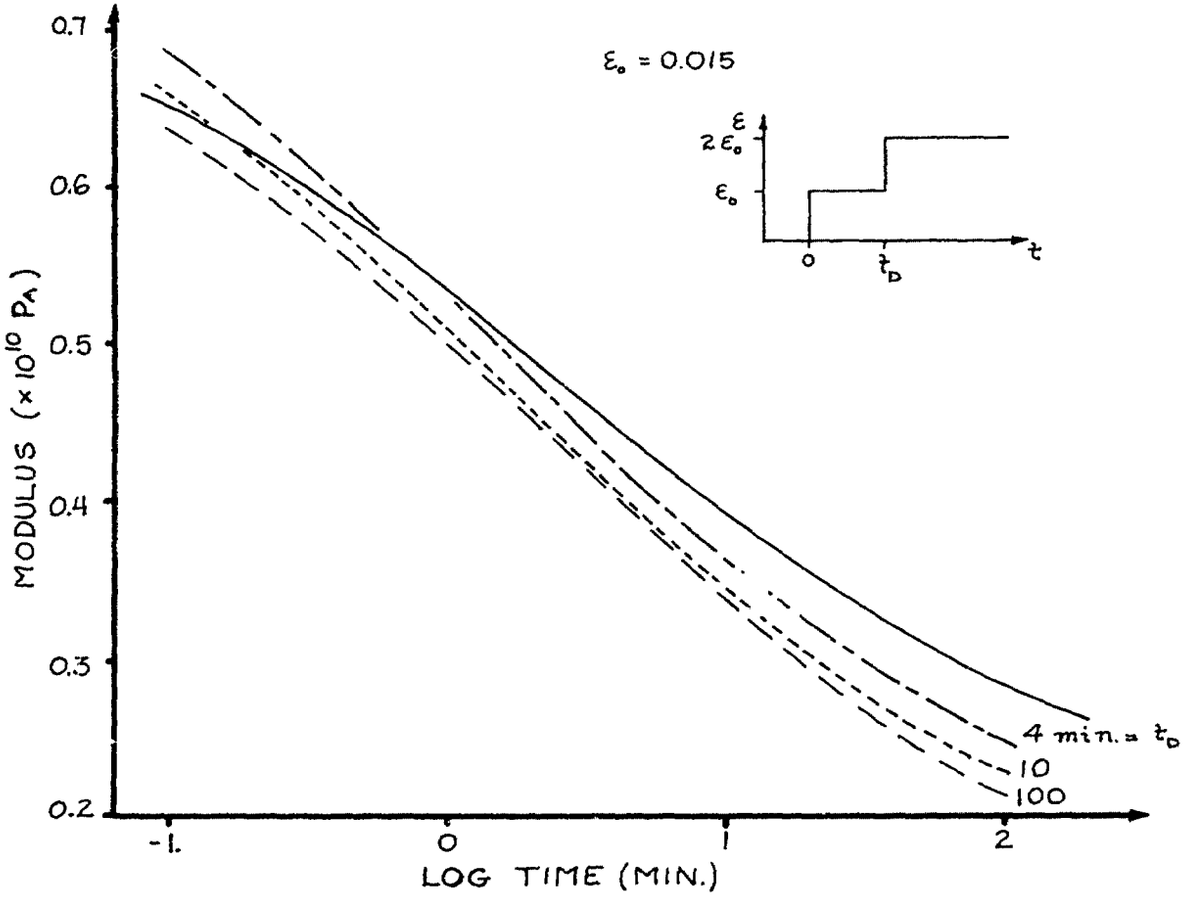

Figure 26: Check of time invariance: Two-step test where an initial step strain, ε_o, is applied at t = 0 and a second step strain is added at $t = t_D$. Comparison of t_D = 4, 10, 100 min. ε_o = 0.015.

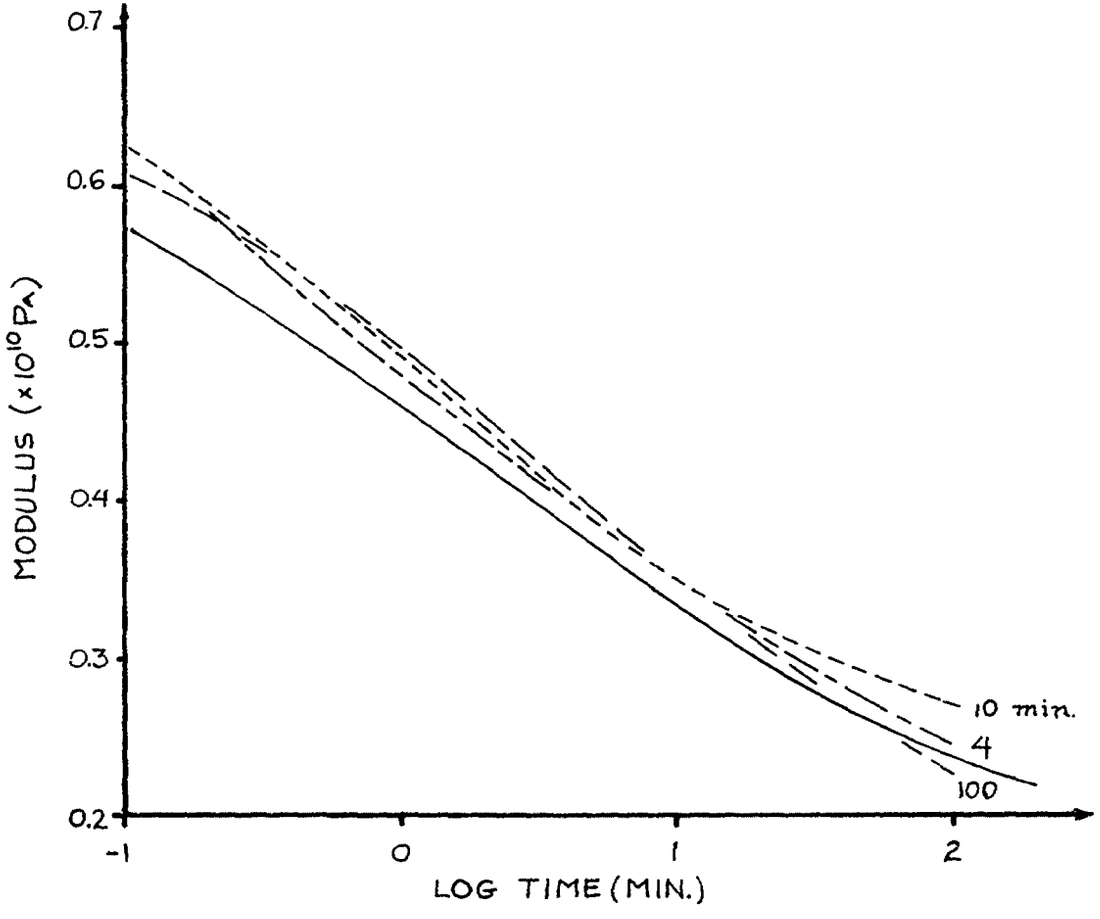

Figure 27: Check of time invariance: Two-step test where an initial step strain, ε_o, is applied at t = 0 and a second step strain is added at t = t_D. Comparison of t_D = 4, 10, 100 min. ε_o = 0.025.

Figure 28. Some small changes in modulus can be seen in those specimens annealed at the lowest and highest temperatures. For those specimens annealed at 113° and 120°C a small increase in modulus was seen. For specimens annealed at 155°C the modulus decreased slightly.

Because the change in modulus was small, a more severe annealing procedure was used. In this procedure, the film specimens were annealed at 1[illegible]nd 133°C with the frame's grips set to allow 1% shrinkage during the 1-1/2 hour annealing period. These specimens were tested after one week of storage. The stress relaxation moduli at one minute for these specimens are shown in Figure 29. It is apparent that the annealed specimens which were permitted to shrink showed a strong decrease in modulus over the strain range examined. However, the form of the modulus' dependence on strain was not changed for the annealed compared to the unannealed samples.

From the measurements described above, it is clear that the effect of annealing on the highly oriented film depends on the annealing temperature and on the amount of constraint on the specimen during annealing. Annealing with 1% shrinkage showed a decrease in modulus, whereas a specimen annealed at the same temperature but under extension showed little or no change in modulus. The freedom to shrink allowed an internal structural rearrangement which led to a decrease in modulus. The nature of that rearrangement is of interest, and will be taken up in the Discussion section after the results of structural measurements are described.

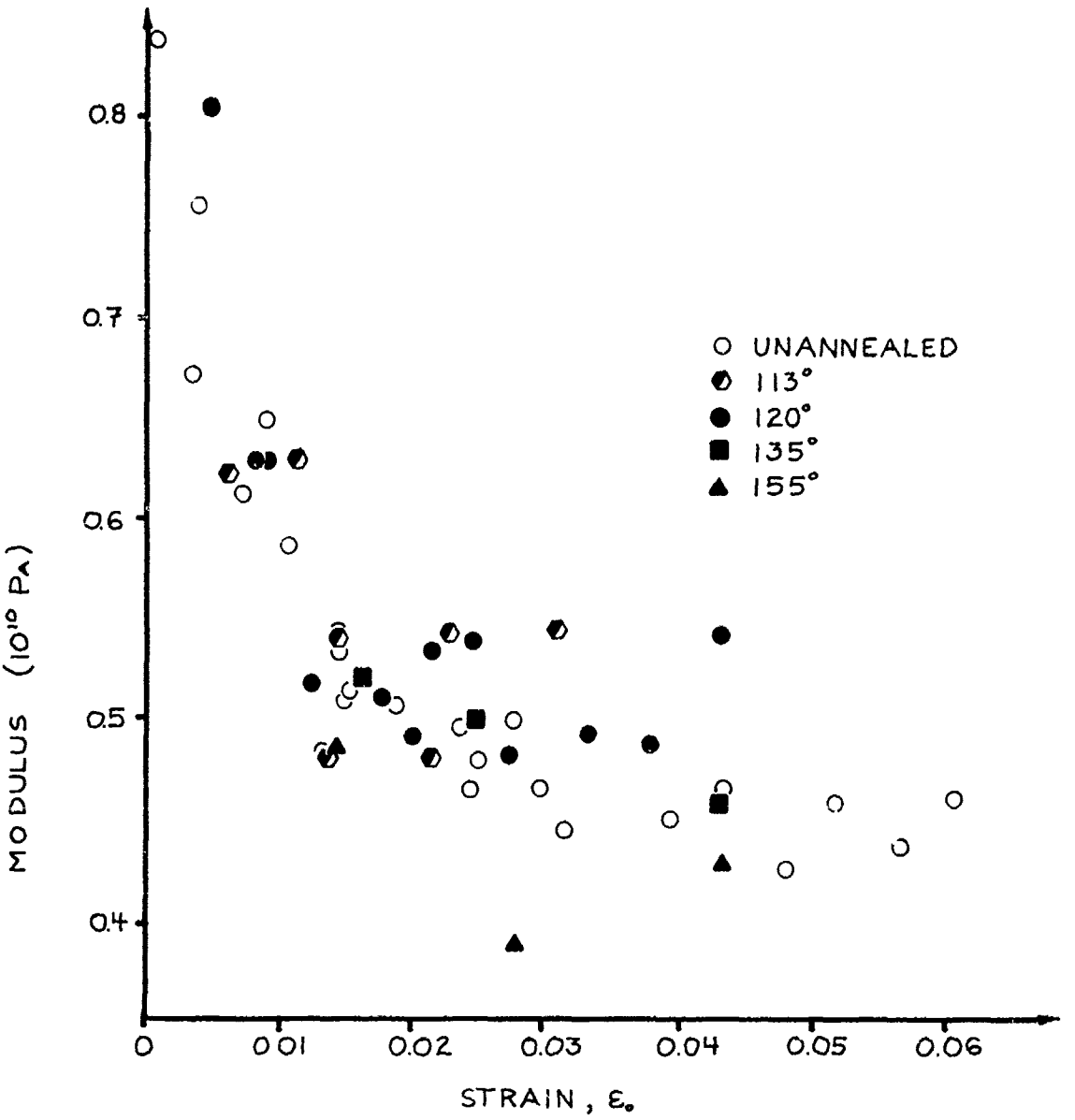

Figure 28: Comparison of the one minute stress relaxation modulus vs. strain for unannealed samples and samples annealed under constant extension of 1% at the indicated temperatures for 1.5 hours. Specimens were cooled to room temperature after annealing and tested in stress relaxation approximately one week later at room temperature. Separate specimens are represented by each symbol.

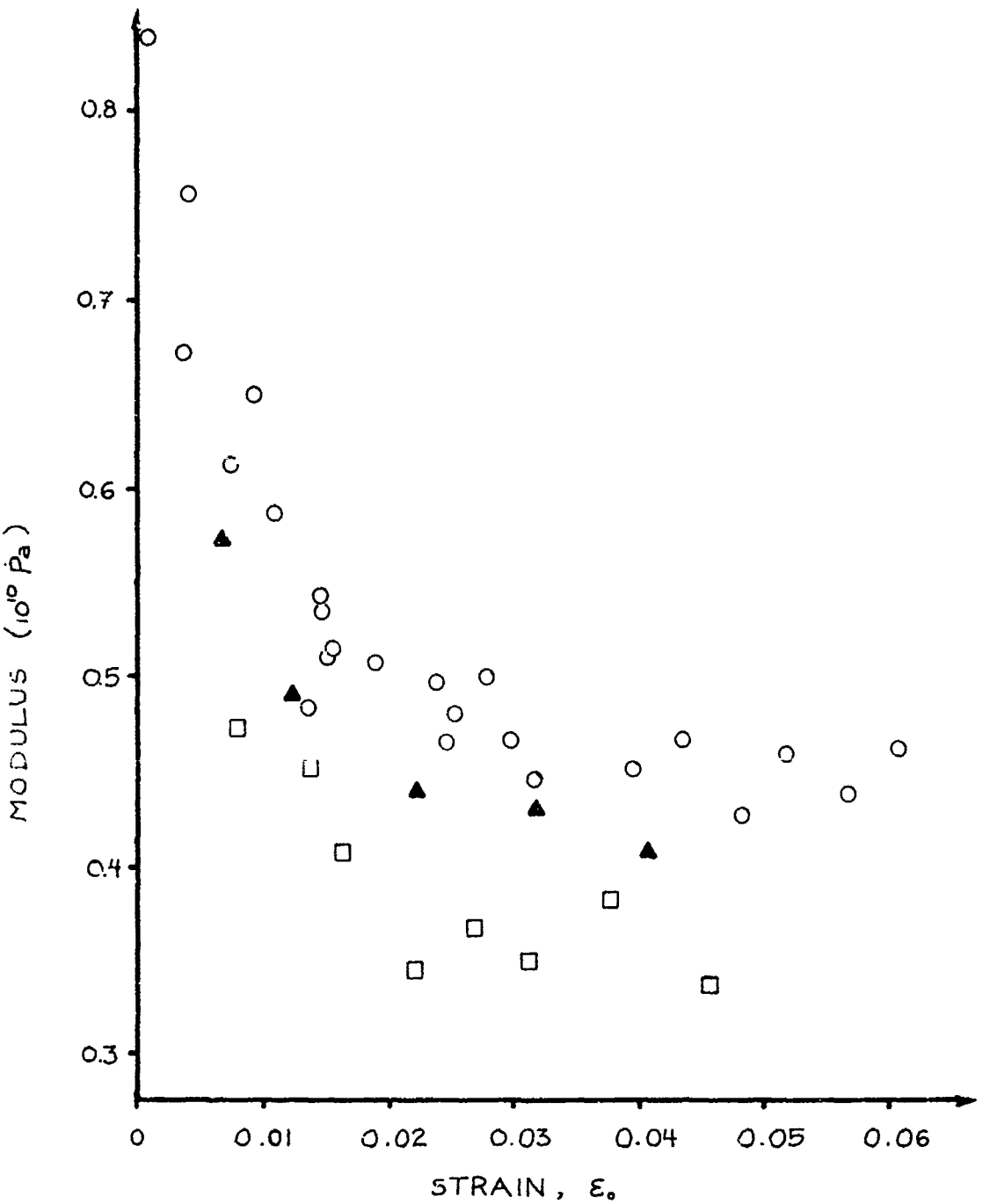

Figure 29: Stress relaxation modulus at one minute vs. strain for unannealed specimens (O) and specimens annealed at 120°C (▲) and 133°C (□). Specimens were annealed for 1.5 hours with 1% shrinkage allowed. Specimens were cooled to room temperature and tested in stress relaxation approximately one week later at room temperature.

Structural Measurements

In this section the results of structural measurements including density, wide angle X-ray diffraction, birefringence, and sonic modulus will be given. Details of the measurements are given in Appendices A through D.

Density

Density was determined using a density gradient column to be 0.914 g/cm^3. All the samples that were annealed and are discussed in this thesis showed the same density as that of the unannealed material. We concluded from this that the degree of crystallinity was unchanged by annealing. The maximum variation in density between the samples was ± 0.1%, corresponding, to, at most, a change in crystallinity of 1.6%.

Wide Angle X-ray Scattering

The crystalline orientation of the unannealed film was measured and the crystalline orientation function f_c was found to be 0.97. To check whether or not the crystalline orientation had been disturbed by annealing, transmission photographs[4] were taken as described in Appendix A. No broadening of the diffraction spots was seen, indicating that the orientation of the crystals was not altered by the annealing procedure.

Birefringence Measurements

Birefringence measurements were made on unannealed and annealed films, to look for changes in amorphous orientation. A detailed description and discussion of the technique is given in Appendix B. An average value of birefringence for the unannealed films was found to be 0.0324 with a standard deviation of 3.6% of the average. The birefringence values measured for annealed specimens fell within the values of the unannealed specimens. Thus if any changes in birefringence did occur upon annealing, it was not

possible to detect them because of the large variation between the individual films' birefringences.

Sonic Modulus

Sonic modulus measurements were made on unannealed specimens and on specimens which had been annealed at 121° and 133°C and had experienced 1% shrinkage. The unannealed specimens had a sonic modulus of 1.76×10^6 psi. Annealed samples showed an increase of up to 8% in sonic modulus as compared to the unannealed films. Because the increase was greater than the 95% confidence limits, it represented a real increase in amorphous orientation.

Comparison of Sonic Modulus and Birefringence

A comparison between the sensitivity of birefringence and sonic modulus to changes in amorphous orientation explains why a change in orientation can be seen by sonic modulus and not by birefringence. Figure 30 shows this comparison. Each curve was calculated from the equations relating orientation to sonic modulus and to birefringence, for values of $f_c = 0.97$ and $x_c = 0.72$. The sonic modulus is more sensitive to amorphous orientation than birefringence. For our case, the observed 8% increase in sonic modulus corresponds to a change in f_{am} from 0.55 to 0.60. By calculation, the change in birefringence from that change in f_{am} would be 2%. Thus the change in birefringence would be less than the 3.5% scatter in the birefringence data; therefore, the change in f_{am} was not detectable by birefringence. Because of its superior sensitivity and ease of use, sonic modulus is the preferred method for measuring small changes in amorphous orientation in highly oriented polypropylene.

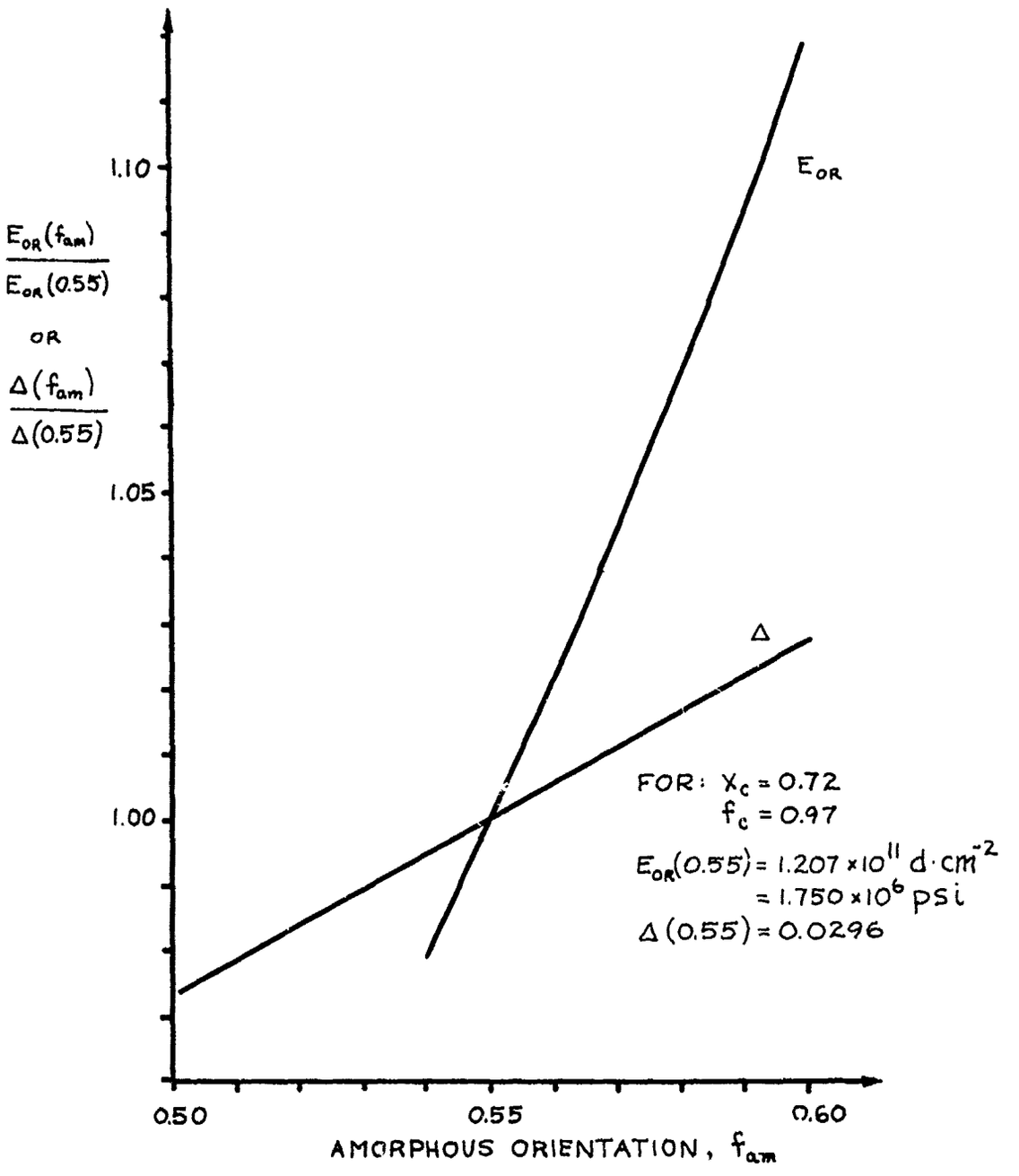

Figure 30. Comparison between sensitivity of sonic modulus and birefringence to amorphous orientation.

DISCUSSION

Structure of Unannealed Film

To reach its present structure, the polypropylene film as taken from the laminate had gone through several processes. It had been blown and then drawn at 170°C at 50 meters/min. to a draw ratio of 12:1. It had then been laminated and pressed at 176°C at 2000 psi for 70 minutes and cooled for 60 minutes. This process resulted in a clear film. The pressing probably healed voids created during drawing.

The films produced in this way had a fibrillar structure, as seen by TEM replicas, virtually complete crystal orientation, a high crystallinity of 72%, and a crystal size of about 100 Å wide and 120 Å long. SAXS indicated a lamellar structure. The amorphous material had an orientation of 0.55 and was constrained, as indicated by a suppression of the tanδ β loss peak and the high orientation indicated by IR and Raman dichroism.

Other information concerning the film's structure was gathered from the anisotropy of its mechanical properties. This film showed a straightforward pattern of anisotropy in several mechanical properties. Strength and modulus both were greatest along the draw direction. This is attributable to the deformation of the molecular chains aligned in the draw direction, with the stresses transmitted by the molecules between the crystallites. The lower strength and stiffness in the 45° and 90° directions indicate the predominance of van der Waals type forces and a lesser amount of covalently bonded chains in those directions.

Another feature of mechanical anisotropy in these films is the anisotropy in time dependence. In this work the modulus was examined by constant strain rate (σ-ε) tests and by stress relaxation. In the former, the initial slope of the σ-ε curves showed strongest time dependence in the

draw direction (0°) and the time dependence decreased as the angle to the draw direction increased to 45 and 90°. (Refer to Figure 20.) A similar trend was seen in the stress relaxation modulus. The decrease of modulus with time was strongest in the draw direction. (Refer to Figure 21.) This time dependence indicated the presence of some type of structure allowing motion. This motion arose at room temperature in polypropylene, from the motion and flow of amorphous material. Because of the high orientation and especially because of the suppression of the tanδ β loss peak, it might seem that the time dependence of the modulus would be eliminated. However, this was not the case. Clearly, despite the high constraint of the amorphous regions, movement was still possible. It was also clear that the direction perpendicular to the draw direction (90°) was not devoid of amorphous material. The 90° specimens retained some time dependence, though the effect was decreased as compared to the draw direction.

From the consideration of the structural information on the film, a comparison to the proposed models of highly drawn semicrystalline structures was of interest. The major structures proposed have been the tie-molecule fibrillar model of Peterlin, the crystalline bridge model of Ward, and the continuous crystal network proposed by Taylor and Clark. The last of these seemed to be eliminated for several reasons. First, the method of production of these films was quite different from Taylor and Clark's. While they drew their fibers very slowly (4% / min.) at 130°C, giving them a form of annealing under stress, the films studied here were formed by high-speed drawing (50 meters minute) at high temperatures (170°C). Also some important properties especially indicative of the continuous crystal (CC) structure were not seen. The CC structure gave no SAXS pattern to a resolution of 40 nm, and thermal stability at 155°C. Our film, however,

showed a clear meridional SAXS pattern and shrank 13% in 15 minutes with 145 psi load at 150°C. Thus we concluded that the CC structure was not present in our film.

Another model that has been proposed for highly drawn semi-crystalline polymers was presented by Clements et al.[29,58] and Gibson et al.[27] They examined the drawing of linear polyethylene (LPE) and the resulting microstructures. From WAXS broadening they found a crystal size which was greater than the repeat period seen by SAXS. From this they concluded that the structure consisted of fibrillar stacks of crystallites linked by intercrystalline bridges, shown in Figure 8. However, in 1980 Wills, Capaccio and Ward[62] published a similar study of the drawing behavior of polypropylene. They found that they could produce material having moduli which were comparable percentages of the theoretical moduli to those which had been achieved in the drawing of LPE. They found, however, that the lack of sharp melting behavior forced the conclusion that the structural homogeneity seen in LPE was not present in their drawn PP. They concluded that their structural measurements were consistent with the general features of the model of drawn structures put forward by Peterlin.[34] The films in this study also showed broad melting behavior indicating that the crystalline bridge concept was not appropriate to describe their microstructure. We too concluded that in general Peterlin's model was best.

Effect of Annealing

When hot-drawn, highly oriented polypropylene films were annealed at T = 121 and 133°C, allowing 1% shrinkage, a decrease in the stress relaxation modulus over a range of strain and a small increase in sonic modulus were observed. The freedom to shrink proved to be important. Films annealed at the same temperatures with no shrinkage did not show any large change in modulus. In none of these samples was there any change in crystallinity or crystalline orientation.

The changes in properties and structural measurements outlined above indicated that an internal structural rearrangement had occurred upon annealing. To understand the effect of the annealing procedure, we first looked at what has been found in the literature. Most annealing studies had been done on cold-drawn material. In such material annealing resulted in an increase in the regularity of lamellar structure and a relaxation of taut tie molecules, as evidenced by an increase in interlamellar shear.[28] In none of these studies had either the crystallinity or the orientation functions been monitored. When cold-drawn material had been annealed, the temperature of annealing was greater than the draw temperature. This was quite different from our work, where annealing was done at temperatures 40°C lower than the draw temperature. The question arose, whether or not the effects of annealing hot-drawn material were the same as those observed in cold-drawn material.

One effect seen in annealing cold-drawn material was the development of a more perfect lamellar structure. In hot-drawn materials, a lamellar structure already existed. It might seem, therefore, that this effect had already occurred during drawing. However, further reorganization into more perfect lamellae might still be possible. Another effect seen in anneal-

ing cold-drawn material, simultaneous with lamellar rearrangements, was the relaxation of taut tie moleucles. It was unclear whether or not these two phenomena were linked, that is, whether in order to relax taut tie molecules the large motions involved in reorganizing lamellae were necessary. If they were linked, it would be harder for taut tie molecules to relax in hot-drawn material because the amount of lamellar rearrangement would be less.

The effect of annealing on PP films which had been drawn at a temperature between cold-drawn (25°C) and our hot-drawn (170°C) films was observed by Wills et al.[62] They annealed PP films which had been drawn at 110°C, at 135°C under tension of 5.5 MPa for an hour. They do not state how much shrinkage occurred, but from other data on the same films, shrinkages of between 8 and 15% were found. On such films annealing resulted in restoration of the β loss peak, indicating an increase in the mobility of the amorphous material.

Thus several possible effects might be occurring upon annealing. First, the decrease in modulus which occurred when our PP film was annealed with 1% shrinkage, suggested that the amorphous material was retracting, thus relieving the taut tie molecules. This would explain the shrinkage and the drop in modulus, but structural measurements did not indicate the decrease in amorphous orientation that would be expected if simple retraction were occurring. In fact, the sonic modulus measurements indicated an increase in amorphous orientation.

Another possible explanation of the increase in sonic modulus with a decrease in the stress relaxation modulus is that relaxation of the amorphous material did occur but was accompanied by a small increase in crystallinity. This might increase the sonic modulus enough to mask the

relaxation of the amorphous material. We knew from density measurements that the density of the annealed films was within the scatter of the density of the unannealed film. The scatter in the density was $\pm$ 0.0008 g/cm^3, that is, approximately $\pm$ 0.1%. This corresponded to a scatter in crystallinity of 1.6%.

To check the effect of such a change in density, the calculation of f_{am} from sonic modulus for the annealed films was repeated. In the new calculations a value of crystallinity was used that was 1.6% higher than that used in the earlier calculations. The values of f_{am} calculated in this way were found to be 3% lower than earlier calculations of f_{am}. However, this still meant there was a 4% change in f_{am} from that measured for the unannealed film. So, even if we took a change in crystallinity into account, we still found a small increase in amorphous orientation. Thus a retraction of the amorphous material did not seem to be a viable explanation of our data.

Reconciliation of the drop in stress relaxation modulus, the shrinkage and the increase of sonic modulus upon annealing was possible by considering a larger scale reorganization, rather than a simple retraction of amorphous material. In cold-drawn material, annealing caused a lamellar structure to develop, in which crystallites in adjacent microfibrils became aligned. In hot-drawn material such as ours, a lamellar structure already existed, but it had an amorphous phase which constrained the lamellae. Annealing of this structure may have permitted changes similar to those seen in cold-drawn material, though the changes would not have been as large.

With this in mind it is suggested that annealing, with shrinkage, allowed a movement of microfibrils past one another, causing a further reorganization of the crystallites into a more ordered lamellar structure. This would explain the mechanism of shrinkage. The decrease in stress relax-

ation modulus may be rationalized as follows. Before annealing, some adjacent microfibrils were positioned so the crystallites were not aligned, but were staggered. See Figure 31. In unannealed film, the misalignment of the crystallites would allow stress to be, in part, transferred along crystal-crystal connections. On annealing, the amount of misalignment would be reduced and the crystallites in adjacent microfibrils would be better aligned. Because of this the stress transfer from crystal to crystal is reduced and the stress must be transferred through the amorphous regions, resulting in a decrease in modulus. It is possible that during such a rearrangement, chains in the already highly-ordered amorphous regions are forced into greater alignment, causing the increase in sonic modulus. Possibly in this case as well, some small increase in crystallinity may contribute to the increase in sonic modulus.

In conclusion, the effect of annealing on our PP film when 1% shrinkage was allowed was to cause a decrease in the stress relaxation modulus and a small increase in sonic modulus, indicating an increase in amorphous orientation. Because of the latter observation, a simple relaxation of the amorphous material leading to a decrease in modulus and shrinkage was not a consistent explanation. A mechanism was tentatively presented which explained these observations. The mechanism, in short, is as follows. Upon annealing, shrinkage takes place by movement of microfibrils past one another. As a consequence, crystallites in neighboring microfibrils align, reducing crystal-crystal connections which had increased the stiffness. Consequently, crystal-amorphous connections become more important in stress transfer and thus the modulus is reduced.

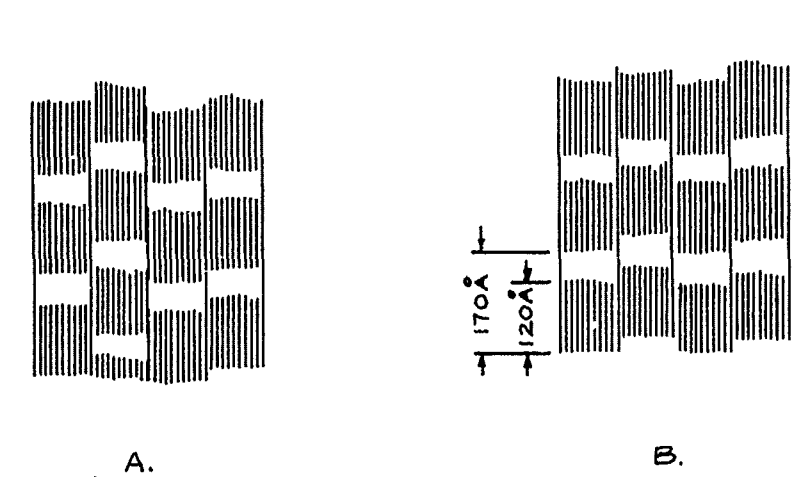

Figure 31: Proposed development of lamellar structure upon annealing.

Discussion of Nonlinear Viscoelastic Behavior

In this section a review will be given of the aspects of nonlinear behavior exhibited by the PP film along the draw direction. Also, the effect of annealing on the mechanical behavior will be described. The discussion will conclude with a comparison of this work to the work described in the literature concerning the relationship between microstructure and nonlinear viscoelasticity.

We have examined the stiffness of a highly-oriented PP film along its draw direction and found that it showed nonlinear viscoelastic behavior. First, nonlinearity was seen in violation of the so-called "stress-strain linearity"[71] criterion. For stress relaxation, the prediction of linear viscoelasticity was that the modulus ($E(t) = \sigma(t)/\varepsilon_o$) did not depend on the applied strain, ε_o. From Figures 24 and 25, it was clear that for the 0° specimens this was not the case. It was not possible to determine whether or not this was the case for the 45° and 90° specimens, since their low strain to failure prevented an examination of the strain dependence of stress relaxation. Another feature of this data was that no region of linearity was found down to strains of 0.001. Because our equipment could not apply smaller strains that this, and because measurement of smaller strains than 0.001 was not possible by the cathetometer, the strain limit of linearity was not found.

A second criterion of nonlinearity was the time invariance criterion. As described in the Results section, for times from 4 to 100 minutes, the time invariance criterion was seen to hold.

A third way the linearity of the film's behavior was tested was by comparing stress-strain tests to stress relaxation. Linear viscoelasticity predicted that the instantaneous slope of a constant strain rate test

at some time t_i, would correspond to the stress relaxation modulus at $t = t_i$. This prediction seemed to provide a way to relate the data from stress-strain tests to the stress relaxation data. To check this, tangents were constructed to the load-displacement data for 0° specimens from constant strain rate tests. These tangents were constructed at several strains. The corresponding times and moduli were determined. These modulus-time "points" are shown in a log modulus vs. log time plot along with data from a stress relaxation test in Figure 22. These "points" were shown as bars because the curvature of the load-displacement curve was small and the tangents touched the curves over a range of strain/time. The prediction of linear viscoelasticity, that the slopes would correspond to the stress relaxation modulus, was not observed.

The nonlinearity that was observed was interesting. The drop in slope in the stress-strain plot shifted with strain rate, and did not correspond to a specific time only. A relaxation time concept in which specific molecular motions had specific relaxation times controlling the behavior was not the only factor here. It seemed that the transition from high to low modulus (slope) occured at a shorter time for the high strain rate than for the lower strain rates. It didn't seem, however, to be solely controlled by strain either. This was further evidence of the complexity of this material's behavior in which strain or time alone were insufficient to describe behavior.

Another attempt to relate the stress relaxation and stress-strain behavior is shown in Figure 23. Here isochronal stress-strain curves were constructed from stress relaxation data at times of 0.1, 1.0 and 10 minutes. This was compared to a constant strain rate test having a strain rate of $0.002\ min^{-1}$. Note that to reach a strain of 0.02 in the stress-strain test,

ten minutes were required. It was interesting that the slope of the isochronal stress-strain curve for ten minutes was about the same as that for the constant strain rate test. These comparisons of stress relaxation data and constant strain rate data showed that the material behavior was similar in both tests, but that the behavior predicted by linear viscoelasticity was not observed.

With the desire to examine the microstructural control of nonlinearity, films were annealed as has been described. The effect of the annealing on stress-strain linearity was checked by performing stress relaxation tests at various applied strains. A marked drop in modulus was found over all strains examined, but there was no change in the form of the E vs. ε_o curve. Thus the modulus was more sensitive to the changes in structure that occurred on annealing than was the form of nonlinearity. It is possible that in order to change the form of nonlinearity larger changes in structure may have been needed. Later these points will be discussed further. For the rest of this section, proposals which have been put forward to describe the structural basis of nonlinearity are discussed and compared to the data presented in this thesis. Also, a discussion of related points will be made.

The effect of orientation on the creep of polypropylene was examined by Hadley and Ward.[51] They found that fibers having different amounts of orientation had different forms of the stress dependence of the creep compliance. The isochronal compliance-stress data for their most highly-oriented fibers had a similar form to the present isochronal modulus-strain data. Unfortunately, Hadley and Ward did not present any other structural data besides birefringence and molecular weight. The value of birefringence they measured for their spun, heat set and drawn fibers of highest orientation was 30×10^{-3}, as it was for their "monofilament". This was sim-

ilar to the birefringence of our film: $\Delta \cong 32 \times 10^{-3}$. As described in the background section, they found that the shape of the compliance vs. applied load curve was different for the heat-set and drawn fibers compared to the "monofilament", even though the birefringences were the same. (See Figure 5b.) (The behavior of the polypropylene films studied in this thesis resembled the behavior of the spun, heat-set and drawn fibers rather than the behavior of the "monofilament".) Thus, even with little or no difference in birefringence, a variation in the form of the nonlinearity was seen. This was similar to the observation in the present work that with little or no change in birefringence, crystallinity or crystalline orientation, the modulus dropped with no change in the form of the nonlinearity. Hadley and Ward's differences in nonlinearity could have been due to variations either in crystallinity or in crystalline or amorphous orientation, which would alter the nonlinear behavior but give similar values of birefringence. Interpretation of our data is more restricted since the crystallinity and crystalline orientation did not change. Because the overall orientation did not change very much and the crystallinity did not change, we must conclude that other features of the microstructure were altered which did not change those parameters to a large extent, but did allow a significant drop in modulus.

The data presented here concerning time invariance was compared to that found by Lifshitz and Kolsky[68] for isotropic LDPE. They found that the response to a second step in load decreased when the time between application of the first and second loads was increased. This was not found in the present case of oriented polypropylene. When similar experiments were carried out in stress relaxation, the stress response to the second step in strain was found to have little or no dependence on the time between application of the first and second strains. The difference can be explained

by noting the difference in materials. The present material is a highly-oriented polypropylene, while Lifshitz and Kolsky examined isotropic low-density polyethylene. In our work with polypropylene, the two-step tests were done at strains in the range where modulus was independent of strain. Because the LDPE was isotropic it probably had no leveling-off of the compliance at higher stresses and thus showed the effect of time to a greater extent. Also, Lifshitz and Kolsky covered a range of delay times from 1 to 1235 minutes, whereas our delay times only ranged from 4 to 100 minutes. Therefore we may have seen less effect because we observed a smaller time range.

The theory suggested by Buckley[49] and echoed by Arridge and Barham[13], that nonlinearity in semicrystalline polymers arose from an irregular structure and the consequent irregular local stresses, was intuitively reasonable. Some features of Buckley's work had to be noted before comparison to the present work could be made. Buckley's data in support of the irregular structure concept was collected on isotropic polypropylene at 65°C. From dynamic mechanical data, polypropylene at 65°C is in the α loss region. This was quite different from the present work. In our work all tests were performed at room temperature, where the β loss process is located. Thus the specific findings of Buckley may not be precisely applicable to this work. However, his conclusion that the irregularity of local stresses on individual viscoelastic regions causes a nonlinear response, may be important not only for isotropic polypropylene but also for oriented polypropylene.

In the present work, this theory was examined by annealing oriented polypropylene with the goal of altering the structure and examining the resulting changes in nonlinearity. It was thought that the effect of anneal-

ing might be to reduce the irregularities of stress throughout the structure, and thus to reduce the nonlinearity. However, if such changes did occur, their magnitude was too small to affect the nonlinearity noticeably. It may be that the changes in structure that are possible while the crystallinity and crystalline orientation are kept the same are so minimal that they cannot give rise to changes in the form of the nonlinearity. It is possible that changes in crystalline orientation are required before changes can be seen in the form of the nonlinearity.

In summary, a surprisingly small amount of work has been done to understand the microstructural features controlling nonlinearity. This work approached the issue by using structural characterization as a partner to mechanical property measurements. We found that substantial changes in the stress relaxation modulus were possible with no change in the strain dependence of the modulus. Also, we found that the stress relaxation modulus was a more sensitive measure of changing structure than orientation function and crystallinity. We concluded that other microstructural changes, such as the rearrangement of crystallites into lamellae, which cannot be detected by changes in orientation function or crystallinity, were responsible for the decrease in modulus. Also, it was apparent that those changes did not affect the form of the nonlinearity, i.e., the dependence of modulus on strain.

In conclusion, it is apparent that microstructure is critical in the type of nonlinear viscoelasticity that a material shows. Thus, both better ways to characterize semicrystalline structures and an application of established techniques are vitally needed to gain a fuller understanding of nonlinear behavior. A problem in the study of microstructural control is that the microstructure of isotropic and oriented semicrystalline polymers

is still an issue of great debate. Because of the lack of agreement over what the microstructure is, the effect of annealing on the microstructure, the structural causes of stiffness and strength, and, in this case, the effect of structure on nonlinear or linear viscoelasticity, are difficult to assess. Thus, studies which seek to understand the detailed nature of semicrystalline microstructure are exceedingly worthwhile if we are ever to understand the mechanical behavior of these useful polymers.

MODELING VISCOELASTICITY

Linear Viscoelasticity

Attempts to model linear viscoelastic behavior have, to a large extent, consisted of efforts to explain or predict the form of the material functions, such as the extensional modulus, E(t). The general form of the modulus' dependence on time is shown in Figure 32. Arrangements of springs and dashpots were some of the earliest models of the time dependence of modulus. These mechanical analogs provided a way to incorporate both the elastic and viscous elements of the material's behavior. A spring and dashpot arrangement called a standard linear solid is shown in Figure 33.

The relaxation time, τ, of an element was defined as the viscosity of the dashpot divided by the stiffness of the spring. When compared with an experimentally measured modulus, E(t), the standard linear solid's E(t) was found to change too abruptly from the initial glassy modulus to a final rubbery modulus. To deal with this, the concept of the relaxation spectrum, or spectrum of relaxation times, was developed. This corresponds to a spring and dashpot model having many arms, each having a different relaxation time. This would result in a more gradual change from the high modulus to the low modulus. In the actual material, the separate relaxation times are thought to correspond to the motion of different portions or lengths of the polymer chains.

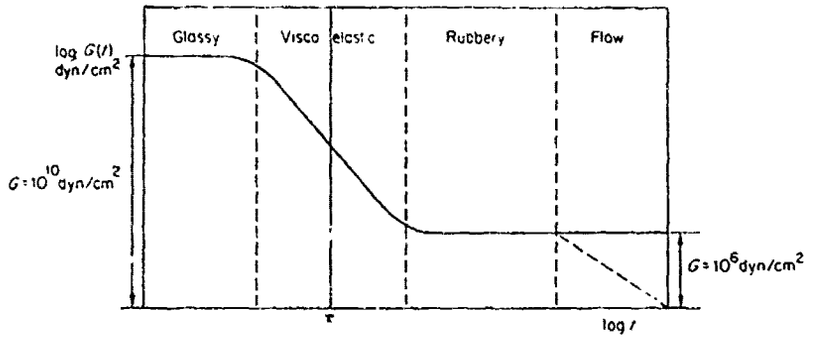

The stress-relaxation modulus $G(t)$ as a function of time t
τ is the characteristic time (the relaxation time).

Figure 32: A schematic stress relaxtion curve. (Ref. 37, p. 83)

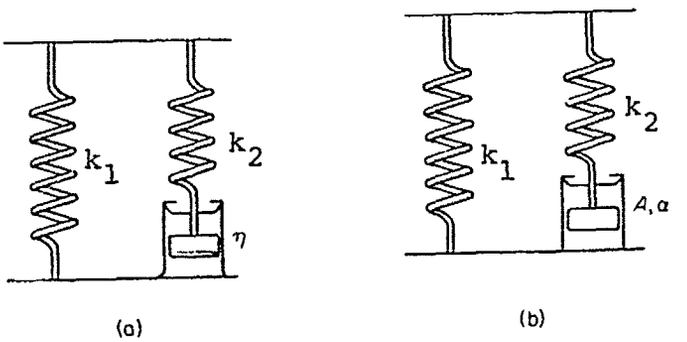

(a) The standard linear solid; (b) Eyring's modification of the standard linear solid with the activated dashpot

Figure 33: Standard linear solids. (Ref. 37, p. 206)

Modeling Nonlinear Viscoelasticity

The question arises, "Why model?" There are at least three reasons. The first and most elegant use of modeling is to compare data to some theoretical physical process. Next, a model can provide a "common language" by which data may be compared between workers. Finally, a model can provide a summary of the data over a range of parameters, so it may be conveniently used and applied to new circumstances. This latter use is not always possible, especially if the conditions of use are different from those under which the data were collected. Eyring's model of viscoelastic behavior as a thermally activated flow process is an example of the first type of model. The mathematical models, including the multiple integral representation, are developed with the latter two goals in mind. The many attempts to model nonlinearity have been thoroughly reviewed by Hadley and Ward[42] in 1975 and by Yannas[71] in 1974. In the discussion below, a description of both the Eyring model and a brief review of mathematical models, with a major discussion of the multiple integral technique, will be given. Other mathematical models will be mentioned when they have been used to model the nonlinear viscoelasticity of polypropylene.

Thermally Activated Flow

Eyring's[44] model is one of the few attempts to associate molecular level processes with nonlinear properties. He began by assuming that flow in a polymer was related to the thermally activated motion of segments of polymer chains into loose or empty places in the structure. The assumption was made that the externally applied stress altered the potential energy barrier to motion. The rate of motion of the segment was given by the difference between the rate of flow forward and backward over the barrier. This gave a net rate of flow for the segment in the forward direction which

was assumed equal to the strain rate of the polymer. This yields a strain rate for a thermally activated dashpot:

$$\dot{\varepsilon} = A \cdot \mathrm{SINH}(\alpha \cdot \sigma)$$

where $A = 2k' \frac{V_h}{V_m}$ and

$$\alpha = \frac{V_h}{2kT}$$

k' = frequency of jumps

V_h = volume of the flow hole

V_m = volume of segment

k = Boltzman constant

Using this non-Newtonian dashpot in a standard linear solid spring-dashpot arrangement (see Figure 33), the following was the relation between stress and strain:

$$\dot{\varepsilon} = \frac{\sigma}{k_2} - \frac{k_1}{k_2}\dot{\varepsilon} + A \cdot \mathrm{SINH}(\alpha\sigma - \alpha k_1 \varepsilon)$$

In a stress relaxation test where $\varepsilon(t) = \varepsilon_o$ and $\dot{\varepsilon} = 0$, we find that

$$0 = \frac{\dot{\sigma}}{k_2} + A \cdot \mathrm{SINH}(\alpha\sigma - \alpha k_1 \varepsilon_o)$$

The use of this model will be described in the Discussion section.

Mathematical Models of Nonlinear Viscoelasticity

Attempts to describe nonlinear behavior in a succinct mathematical form have been of three types.[42] The first was based on separable stress or strain and time functions. Empirical descriptions of creep for materials with small creep strains using separable stress and time functions were proposed by Findley and Khosla (1955, 1956) and Pao and Marin (1952,1953).[42]

Notable representations of stress relaxation and stress-strain curves as separable functions of strain and time were given by Smith (1962) for plasticized PVC ($\varepsilon<20\%$), by Bernstein et al. (1963), (i.e., BKZ), for elastomers at small times and for fluids of long times, and by Lianis (De Hoff et al., 1966) for the stress-relaxation behavior of elastomers. The first approach to polypropylene's nonlinearity used separable stress and time variables. Turner's[42] empirical approach consisted of using a relatively simple set of tests to predict the creep strain over a region of stress and time. The limitation of these tests was that though they were able to predict creep they were not able to predict recovery (the strain in the specimen when the stress is removed).[42]

Polypropylene was also examined by Buckley and McCrum (1974) and Buckley (1977) in a combined tension-torsion loading. By measuring combined tensile and torsional creep and assuming that the compressive compliance, B(t) was independent of the stress invariants I_1 and I_2, they found that the shear compliance depended on both I_1 and I_2, the deviatoric and hydrostatic components of stress respectively. Hadley and Ward[42] pointed out that these conclusions were analogous to the one-dimensional treatments of the BKZ theories, each of which resulted in single integral representations, all seeking separation of stress and time variables.

The single integral theories of nonlinear viscoelasticity were reviewed by Smart and Williams (1972).[42] The BKZ theory and those of Leaderman and Schapery were compared. They concluded that the BKZ theory, which was basically a finite strain theory, had nothing to offer for polypropylene. Also, Leaderman and Schapery's representations had the problem that though creep data was modeled satisfactorily, recovery data was not.

The second type of mathematical model consisted of intuitive modi-

fications of linear viscoelastic theory. This approach was demonstrated by Leaderman and Eyring (Leaderman 1943) for textile fibers. Schapery (1969) incorporated the features of nonlinearity and temperature dependence in a comprehensive form applied to several materials from nitrocellulose to polyisobutylene.

Multiple Integral Representation

The third mathematical model is the multiple integral representation proposed by Green and Rivlin (1957)[42]. It is of special interest here because Hadley and Ward[42] concluded that for semicrystalline polymers, especially polypropylene, it has proved to be most satisfactory. Green and Rivlin suggested that the stress response to a continuous strain could be written for the one dimensional case:

$$\sigma(t) = \int_{-\infty}^{t} E_1(t-\tau)\,\frac{d\varepsilon(\tau)}{d\tau}\,d\tau + \int_{-\infty}^{t}\int_{-\infty}^{t} E_2(t-\tau_1,\, t-\tau_2)\,\frac{d\varepsilon(\tau_1)}{d\tau_1}\,\frac{d\varepsilon(\tau_2)}{d\tau_2}\,d\tau_1 d\tau_2 + \cdots + \int_{-\infty}^{t}\cdots\int_{-\infty}^{t} E_n(t-\tau_1,\, \cdots,\, t-\tau_n)\frac{d\varepsilon(\tau_1)}{d\tau_1}\cdots\frac{d\varepsilon(\tau_n)}{d\tau_n}\,d\tau_1\cdots d\tau_n$$

This reduces to the Boltzmann superposition principle if n = 1 and if $E_1(t) = E(t)$, the stress relaxation modulus.

The meaning of this representation was elucidated by a description given by Findley et al.[45] Consider the time dependent stress resulting from a constant strain, ε_o, expressed as a polynomial.

$$\sigma_o(t) = \varepsilon_o\psi_1(t) + \varepsilon_o^2\psi_2(t) + \varepsilon_o^3\psi_3(t) \cdots$$

To demonstrate the development of the multiple integral represen-

tation, only terms up to the third term of the polynomial will be included. The response to a strain ε_1 applied at a time t_1 would be:

$$\sigma_1(t) = \varepsilon_1\psi_1(t-t_1) + \varepsilon_1^2\psi_2(t-t_1) + \varepsilon_1^3\psi_3(t-t_1)$$

If the strains ε_o and ε_1 were applied successively at $t = 0$ and at $t = t_1$, respectively, the response would consist of not only a sum of $\sigma_o(t)$ and $\sigma_1(t)$, but also would have to include the effect of ε_o on the response to ε_1. This can be seen in the following way.

If the strains are applied successively, we could write the total response at $t > t_1$ as follows:

$$\sigma(t) = (\varepsilon_o + \varepsilon_1)\psi_1(t) + (\varepsilon_o + \varepsilon_1)^2\psi_2(t, t-t_1)$$
$$+ (\varepsilon_o + \varepsilon_1)^3\psi_3(t, t-t_1, t-t_1)$$

Multiplying out the terms:

$$\sigma(t) = \varepsilon_o\psi_1(t) + \varepsilon_1\psi_1(t-t_1) + \varepsilon_o^2\psi_2(t, t)$$
$$+ 2\varepsilon_o\varepsilon_1\psi_2(t, t-t_1) + \varepsilon_1^2\psi_2(t-t_1, t-t_1)$$
$$+ \varepsilon_o^3\psi_3(t,t,t) + 3\varepsilon_o^2\varepsilon_1\psi_3(t, t, t-t_1)$$
$$+ 3\varepsilon_o\varepsilon_1^2\psi_3(t, t-t_1, t-t_1) + \varepsilon_1^3\psi(t-t_1, t-t_1, t-t_1)$$

Rearranging the terms we get:

$$\sigma(t) = \varepsilon_o\psi_1(t) + \varepsilon_o^2\psi_2(t, t) + \varepsilon_o^3\psi_3(t, t, t)$$
$$+ \varepsilon_1\psi_1(t - t_1) + \varepsilon_1^2\psi_2(t-t_1, t-t_1) + \varepsilon_1^3\psi_3(t-t_1, t-t_1, t-t_1)$$
$$+ 2\varepsilon_o\varepsilon_1\psi_2(t, t-t_1) + 3\varepsilon_o^2\varepsilon_1\psi_3(t, t, t-t_1)$$
$$+ 3\varepsilon_o\varepsilon_1^2\psi_3(t, t-t_1, t-t_1)$$

The first two lines are simply the sum of the responses to the strains applied separately. The remaining terms express the joint contributions of the strains to the stress response. The assumption is made that the cross effects are symmetric with respect to the time argument, i.e.,

$$\psi_2(t,\ t-t_1) = \psi_2(t-t_1,\ t)$$

The addition of further steps would, of course, increase the number of cross terms which could be written. If n steps were applied, the response would be:

$$\sigma(t) = \sum_{i=o}^{N} \varepsilon_i \psi_1(t-t_i)$$

$$+ \sum_{i=o}^{N} \sum_{j=o}^{N} \varepsilon_i \varepsilon_j \psi_2(t-t_i,\ t-t_j)$$

$$+ \sum_{i=o}^{N} \sum_{j=o}^{N} \sum_{k=o}^{N} \varepsilon_i \varepsilon_j \varepsilon_k \psi_3(t-t_i,\ t-t_j,\ t-t_k)$$

An interesting feature of this formulation is that if ψ_2 and ψ_3 are zero for all arguments this reduces to the Boltzmann superposition theorem. Another point to note is that even if $\psi_2(t,\ t)$ and $\psi_3(t,\ t,\ t)$ are zero (this corresponds to $\sigma(c\cdot\varepsilon(t)) = c\cdot\sigma(\varepsilon(t))$), nonlinearity may arise from terms such as $\psi_2(t,\ t - t_1)$. Continuous and varying strain inputs may be considered as a series of infinitesimal step strains. In that case, the Green-Rivlin integral formulation shown earlier is obtained.

This treatment can be extended to treat three dimensional stress and strain states. However, since all the work in this thesis will concern only uniaxial tests, the multiaxial case will only be touched on lightly, and only where it contributes to an understanding of the correct

treatment of the uniaxial case. In creep tests, where a stimulus of a simple uniaxial stress can be applied, the uniaxial strain response is related in a simple manner to the applied stress through one component of the compliance tensor, the extensional compliance. In stress relaxation, on the other hand, the situation is more complicated. In a stress relaxation test, a uniaxial strain is imposed on the sample. However, the applied strain is not the only strain the sample experiences; Poisson's contraction gives rise to some lateral strains as well. Because the material's time dependent Poisson's ratio is not known, the values of those strains are unknown and vary with time. We can write the resulting strain tensor as follows:

$$\varepsilon_{ij} = \begin{bmatrix} \varepsilon_o & 0 & 0 \\ 0 & x(t) & 0 \\ 0 & 0 & x(t) \end{bmatrix}$$

The resulting axial stress is not only a response to a constant imposed strain, but it will also be influenced by the varying lateral strains. Because of this we cannot determine the time dependent material function which corresponds to the first element of the stiffness tensor, E_{11}, through this test.

The multiaxial form of the Green-Rivlin formulation does give us, however, a description of the stress resulting from this strain tensor. It gives:

$$\sigma_{11}(t) = (\psi_1 + \psi_2)(t)\cdot\varepsilon_o + \int_o^t 2\psi_1(t-t_1)\dot{x}(t_1)dt_1 + (\psi_3+\psi_4+\psi_5+\psi_6)(t,\ t)\cdot\varepsilon_o^2 + \cdots$$

and $$\sigma_{22} = \sigma_{33} = 0 = \psi_1(t)\cdot\varepsilon_o + \int_o^t (2\psi_1+\psi_2)(t-t_1)\cdot\dot{x}(t_1)dt_1$$

Here ψ_1, ψ_2, ψ_3, ... are the material functions which are analogous to elements of a stiffness tensor. Since we know that σ_{22} and σ_{33} are zero, theoretically we could solve the second relation for x(t) in terms of the materials functions ψ_i. The value of x(t) could ther be used in the first equation and the material functions could be determined by comparison to experimentally determined values of $\sigma_{1i}(t)$. If this were done, a relation of the form

$$\sigma_{11}(t) = \int_0^t \psi_a \dot{\varepsilon} dt_1 + \int_0^t \int_0^t \psi_b \dot{\varepsilon}^2 dt_1 dt_2 + \int_0^t \int_0^t \int_0^t \psi_c \dot{\varepsilon}^3 dt_1 dt_2 dt_3$$

would be obtained. For a constant strain, ε_o, this gives:

$$\sigma_{11}(t) = \psi_a \varepsilon_o + \psi_b \varepsilon_o^2 + \psi_c \varepsilon_o^3$$

It should be pointed out, however, that ψ_a,ψ_b and ψ_c cannot be easily related to ψ_1, ψ_2, ... This is unfortunate since ψ_1, ψ_2, ... are more basic to material characterization. One should bear in mind that ψ_a, ψ_b, and ψ_c contain not only the material functions ψ_1, ψ_2, ..., but also the effect of the time dependent lateral strain in the axial stress. They will be referred to as the Kernel functions.

Oriented Polypropylene

The need for models that include the synergistic effects of time and stress became apparent in Ward and Onat's (1963)[50] study of simple and two-step uniaxial creep and recovery in oriented polypropylene, described earlier. Their observations were certainly beyond the predictions of linear viscoelasticity, and were beyond those models (e.g., Leaderman's modified superposition theorem) predicting identical linear elastic (instantaneous) responses in creep and recovery.

This led Ward and Onat to consider the multiple integral representation proposed by Green and Rivlin in 1957. For simple one-dimensional creep the representation for creep strain is given by:

$$\varepsilon(t) = J_1(t)\sigma_o + J_2(t, t)\sigma_o^2 + J_3(t, t, t)\sigma_o^3$$

When compliance $\varepsilon(t)/\sigma_o$ was plotted against the applied stress it was observed that the curves had a parabolic shape. This suggested to Ward and Onat that $\varepsilon(t)/\sigma_o = A + B\cdot\sigma_o^2$ where $\varepsilon(t)$ could be creep, recovery or additional creep. Here the second term $J_2(t)$ is zero.

Ward and Wolfe (1966)[52] studied the same oriented polypropylene fibers, performing a series of two-step creep tests applying differing stresses and keeping the time between the steps constant. They found that the creep strains in these tests were predicted well from the data from the previous creep, recovery, and two-step creep tests. An interesting feature was noted: that the predictions of the multiple integral representation and the predictions obtained by adding the responses to stresses applied separately were not too different. This means that the value of the cross terms, i.e., $\psi_i(t_1, t_2, \ldots t_i)$ were not large compared with the single step terms, i.e., $\psi_i(t, t, \ldots)$. Their data were also fitted well by the modified superposition law proposed by Findley and Lai (1967)[42] and by Pipkin and Rogers (1968) in which the difference between the creep under the first and second stresses is used to modify the linear predictions. However, this modified superposition law, using multi-step creep tests which included only increasing loads, was insufficient to describe the whole behavior in that it could not predict the recovery behavior.

In the literature, some problems and objections concerning the use of the multiple integral representation have been raised. The first objection is that the kernel functions, ψ_i, have no intrinsic physical meaning,

but at most are associated with a certain level of strain.[70] This was borne out to some degree by Yannas and Haskell's[70] study of the temperature dependence of the ψ_i's for polycarbonate creep. They found that only the first kernel, ψ_1, varied monotonically with temperature, and that ψ_2 did not vary in a consistent manner with temperature.

A second difficulty inherent in the use of the multiple integral representation is that, for a strong nonlinearity, many terms may be required. In that case a very large number of tests would be needed fully to determine the value of the kernel functions, $\psi_i(t_1, t_2, \ldots t_i)$.[71]

A third and quite serious problem arises when the material functions are calculated from experimental data. Hall (1967)[69] described and discussed some of the problems associated with the use of the multiple integral representation. As described earlier, the stress is given as a power series in strain with the kernel functions, $\psi_i(t)$, as the power series coefficients. One way to find the value of the several ψ_i would be to use a least squares regression analysis. Hall described some of the problems which would arise if this procedure were followed directly. First, he pointed out that it is not known at what order the series should be truncated. If the series is divergent, the solution for the low order coefficients, $\psi_i(t)$, will be strongly affected by the point of truncation. Also, he noted that the large matrices which are involved in the solution of the equations are apt to be ill-conditioned, such that small errors in the data can have a large effect on the magnitude of the solutions. These problems can be overcome, however, by replacing the power series by an equivalent Chebychev series:

$$f(x) = a_o T_o(x) + a_1 T_1(x) + a_2 T_2(x) + \ldots$$

$$T_o(x) = 1$$

$$T_1(x) = x$$

$$T_n(x) = 2x\, T_{(n-1)}(x) - T_{(n-2)}(x)$$

Here $f(x)$ corresponds to the stress relaxation modulus, $\sigma(t)/\varepsilon_o$, and x corresponds to strain, ε_o.

Hall points out that the use of the Chebychev series has the advantage that it is the most strongly convergent of any series expansion of the function, $f(x)$. (He cites Modern Computing Methods, National Physical Laboratory H.M.S.O., London, 1957.) This means that the values obtained for the coefficients of the lower order terms would not be very sensitive to the point of truncation of the series.

Even when the Chebychev polynomial was used, Hall found that the absolute value of ψ_i was greater than ψ_{i-1}. However, even though the series was divergent, at low strains the series would converge because $\psi_i \varepsilon^{i-1} < \psi_{i-1} \varepsilon^{i-2}$. He found this to be true up to strains of about 3 - 4%. He found that when he considered the effect of experimental error, he could only determine up to 3 terms reliably with the experimental data on polypropylene. With these three terms, convergence up to strains of only 1.5% could be obtained.

Yannas and Haskell[70] conclude that the "predictions of the Green-Rivlin theory cannot be compared meaningfully with experimental data when more than two to three kernels characterize the behavior. This conclusion is based on currently acceptable levels of experimental uncertainty (1-5%) and . . . leads us to consider the possibility that the Green-Rivlin theory might usefully describe the behavior of amorphous, but not that of

semicrystalline, polymers."

The final limitation of the multiple integral representation was pointed out by Lockett and Turner (1971).[42] They noted that since the representations are simply polynomial fits, they are only valid over the region in which they were obtained, and so for example cannot predict compressive behavior from data on tensile behavior.

Some of these objections and difficulties have been addressed by Soussou and Moavenzadeh (1972).[72] Both the problem of divergence of the power series and the problem of the large number of tests required to determine the kernel functions were circumvented by these authors. They used an approach used in the study of nonlinear electrical systems. To carry out such tests, equipment such as an MTS testing machine is used to input a random load program having a constant power spectral density over a practically attainable broad range of frequencies, called a "white Gaussian process".

In conclusion, a description of models of linear and nonlinear viscoelasticity has been put forward. Emphasis has been on the multiple integral representation of Green and Rivlin. A description of the representation, some examples of its use, some limitations and problems with its use, and some ways of overcoming those limitations have been presented.

Results and Discussion of Modeling

Eyring Activated Flow Model

The details of the use of the Eyring activated flow model for nonlinear viscoelasticity are described and discussed in Appendix E. No values of the dashpot parameters could be obtained which would describe the modulus-time behavior for the whole strain range. Thus the hope that a connection between nonlinear viscoelasticity and molecular processes could be found was not fulfilled by this model.

Multiple Integral Representation

The following is a discussion of the use of the multiple integral representation for stress relaxation data on the oriented polypropylene film examined in this work. The multiple integral form for stress relaxation is:

$$\sigma(t) = \psi_1(t)\varepsilon_o + \psi_2(t,t)\varepsilon_o^2 + \psi_3(t,t,t)\varepsilon_o^3 + \cdots$$

The stress relaxation modulus is then

$$E(t) = \psi_1(t) + \psi_2(t,t)\varepsilon_o + \psi_3(t,t,t)\varepsilon_o^2 \cdots$$

At any time, t_o, after a step in strain is applied, the modulus at t_o is a power series polynomial in strain. To find the value of the kernel functions, $\psi_i(t_o)$, a procedure described by I.H. Hall[69] and mentioned earlier, was followed using Chebychev polynomials.

By use of a computer program[78] which was able to perform a least square regression analysis on any given polynomial of functions, the values of the Chebychev coefficients, a_i, were computed. These coefficients were then transformed back into the power series coefficients which correspond to the kernel functions, $\psi_i(t_o)$. Note that the kernel

functions were calculated from modulus data at one minute and at no other times. To show how the $\psi_i(t)$ values depend on time, further calculations would be necessary using modulus data at a variety of times. From these coefficients, ψ_i, the $E(t_o)$ vs. ε_o plots were made. The effect of the point of truncation was examined by plotting the curves for polynomials having two to six terms. This is shown in Figure 34. Figure 35 shows the variation of the values of the kernel functions ψ_i, with the number of terms used in the calculation.

A comparison between the least square regression analysis for a power series and the solution when the Chebychev polynomial is used in the analysis is compared in Figure 36. The data set is a preliminary data set, but the comparison between the solutions is marked. As Hall described, the point of truncation, ie., the number of terms of the series, affects the form of the solution very strongly for the solution calculated from the power series. The Chebychev polynomial shows less of an effect of the point of truncation on the form of the curve.

The effect of manipulating the data set was examined and is shown in Figure 37. Curve I was calculated using the original, unaltered data set. This data set consisted of the one minute stress relaxation moduli from twenty-four tests at strains ranging from 0.001 to 0.006. (See Figure 37, symbols 0 and Ø.) Curve II was calculated from a modified data set in which the data points at strains of 0.015 and 0.025, where there was a preponderance of data, were replaced by their averages, symbolized by ▲. The range of strain of data set II was reduced, resulting in data set III, so that the latter had the same strain range as the data for the unannealed film. Eliminated points are symbolized by Ø. Finally data set II was weighted to emphasize the higher strain data which had less error. This re-

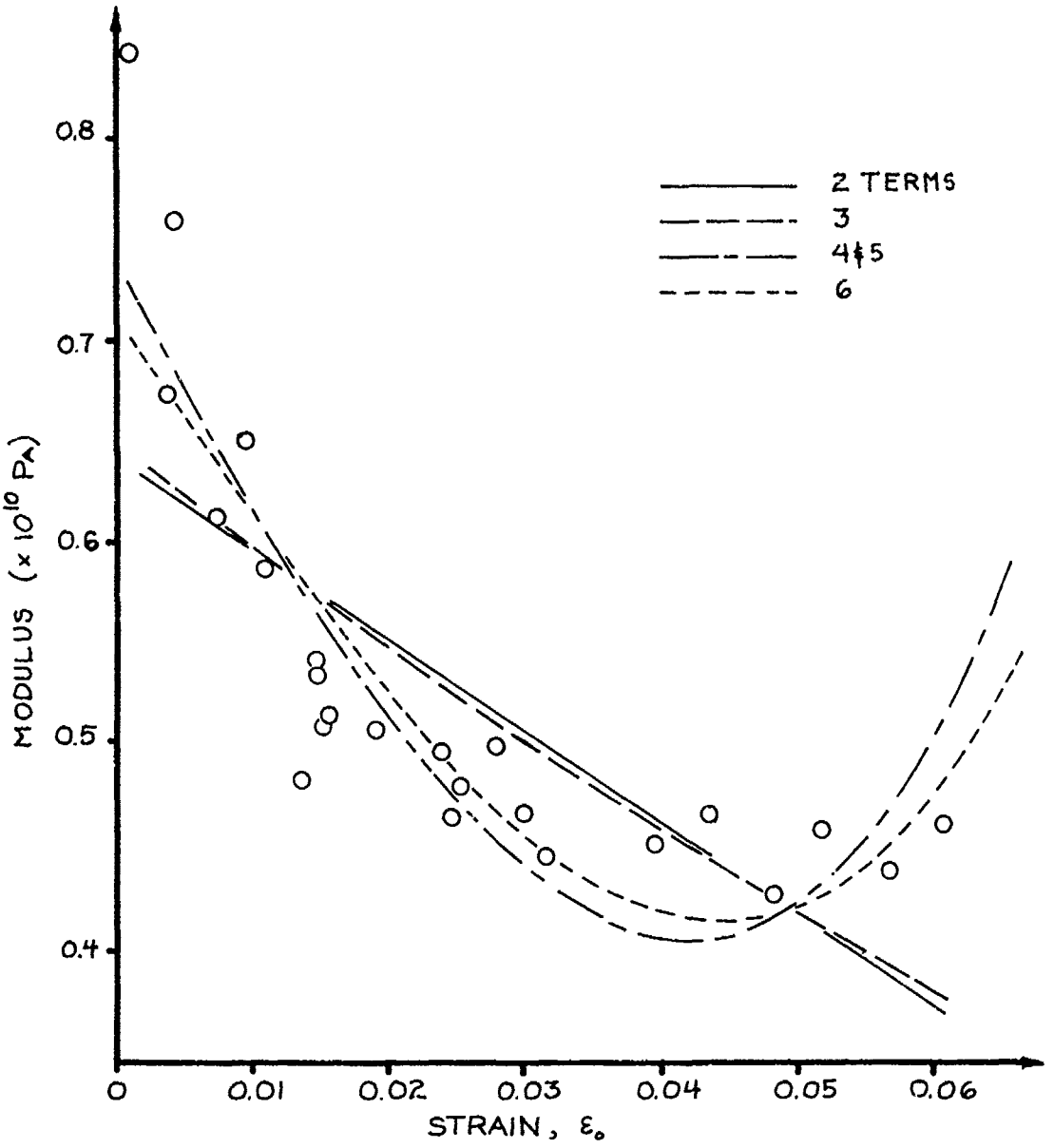

Figure 34: Least square regression fit of Chebychev polynomial of from 2 to 6 terms to data for the one minute stress relaxation modulus vs. strain.

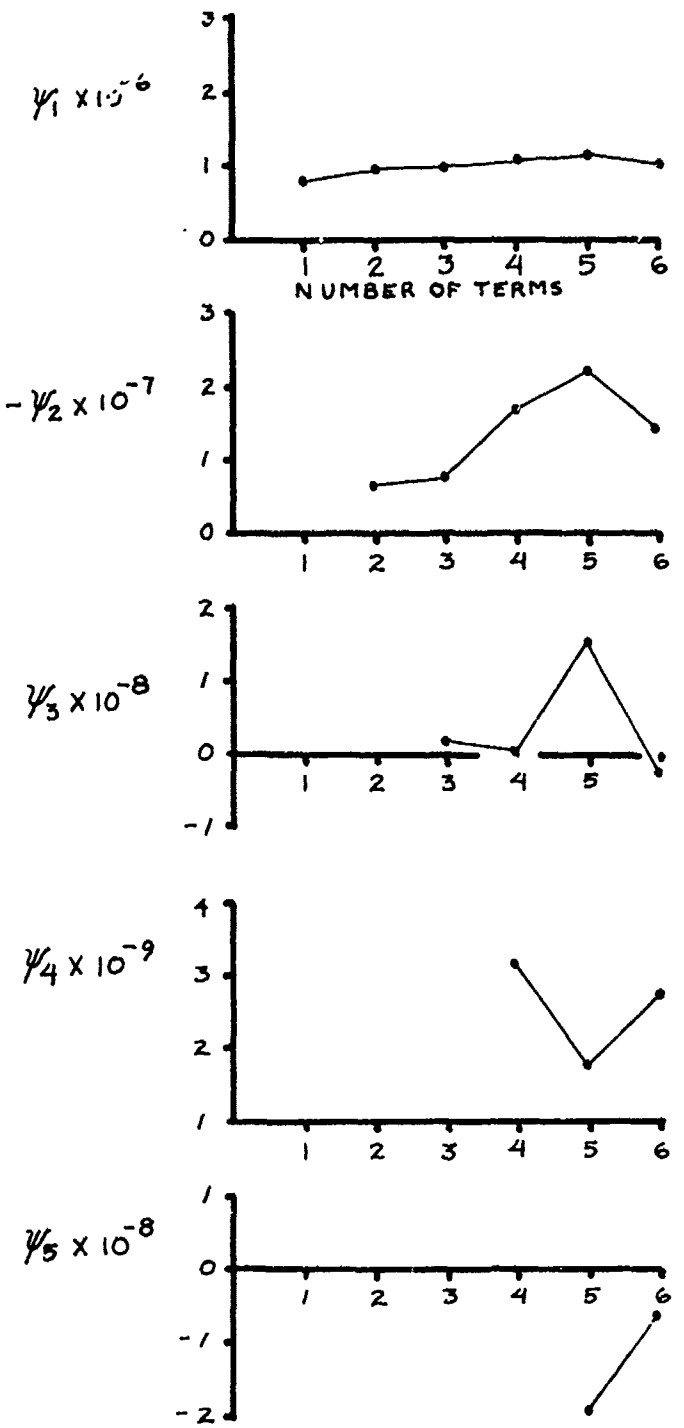

Figure 35: Dependence of Kernel Functions on number of terms in Chebychev series.

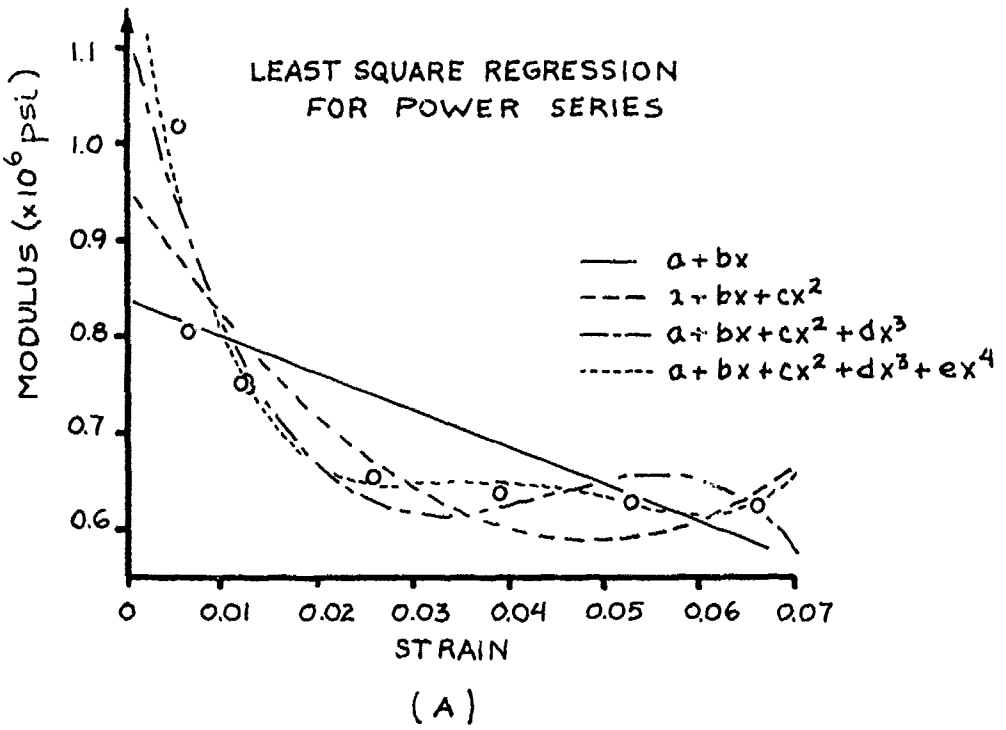

(A)

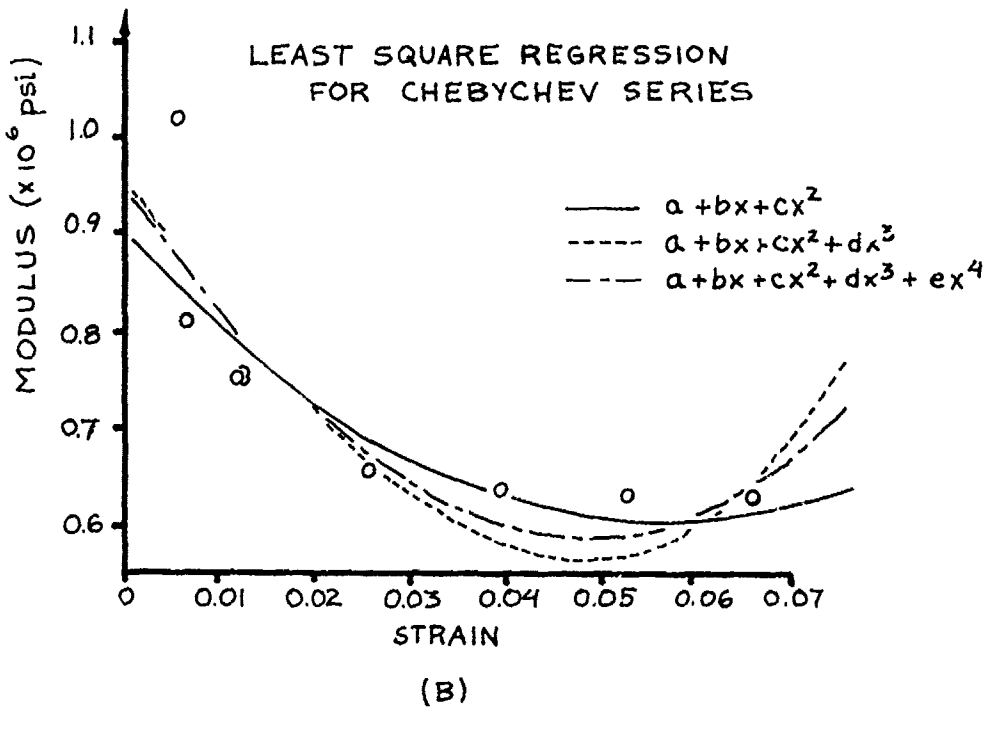

(B)

Figure 36: Comparison between use of power series and Chebychev series.

sulted in data set IV. Weighting was done by entering the data points having strains between 0.02 and 0.04 twice, and data points having strains greater than 0.04 three times.

These changes in the data set do not greatly alter the form of the curve. This comparison may be similar to Hall's test of the effect of experimental error on the error in the coefficients. He perturbed the data, and if the change in the value of the coefficient calculated from the perturbed and original data, was greater than the value of the coefficient, it was not accepted. When the values of our coefficients are compared between the data sets described in Figure 37, the next-to-last coefficient varies by two times the value of the coefficient if the number of coefficients is greater than 3. (See Table II.) This is similar to Hall's finding that more than three coefficients had great sensitivity to error. However, the curve of the three-term solution does not reproduce the form of the experimental data well, compared to the four- and five-term solutions as shown in Figure 34.

From these comparisons, it appears that unless four or more terms are included, the fit of the polynomial to the data is very poor. Even with four or more terms, the fit to the data is only good to a strain of about 0.03 to 0.04. This is also somewhat similar to Hall's results. If we compare the coefficients we can determine up to what strain the series is convergent. Table III shows the values of coefficients calculated from the original, unaltered modulus-strain data set. The strain above which the series is not convergent is given by: $\varepsilon = \psi_{i-1} / \psi_i$, as determined by the test for convergence,

$$\psi_i \varepsilon^{i-1} < \psi_{i-1} \varepsilon^{i-2} .$$

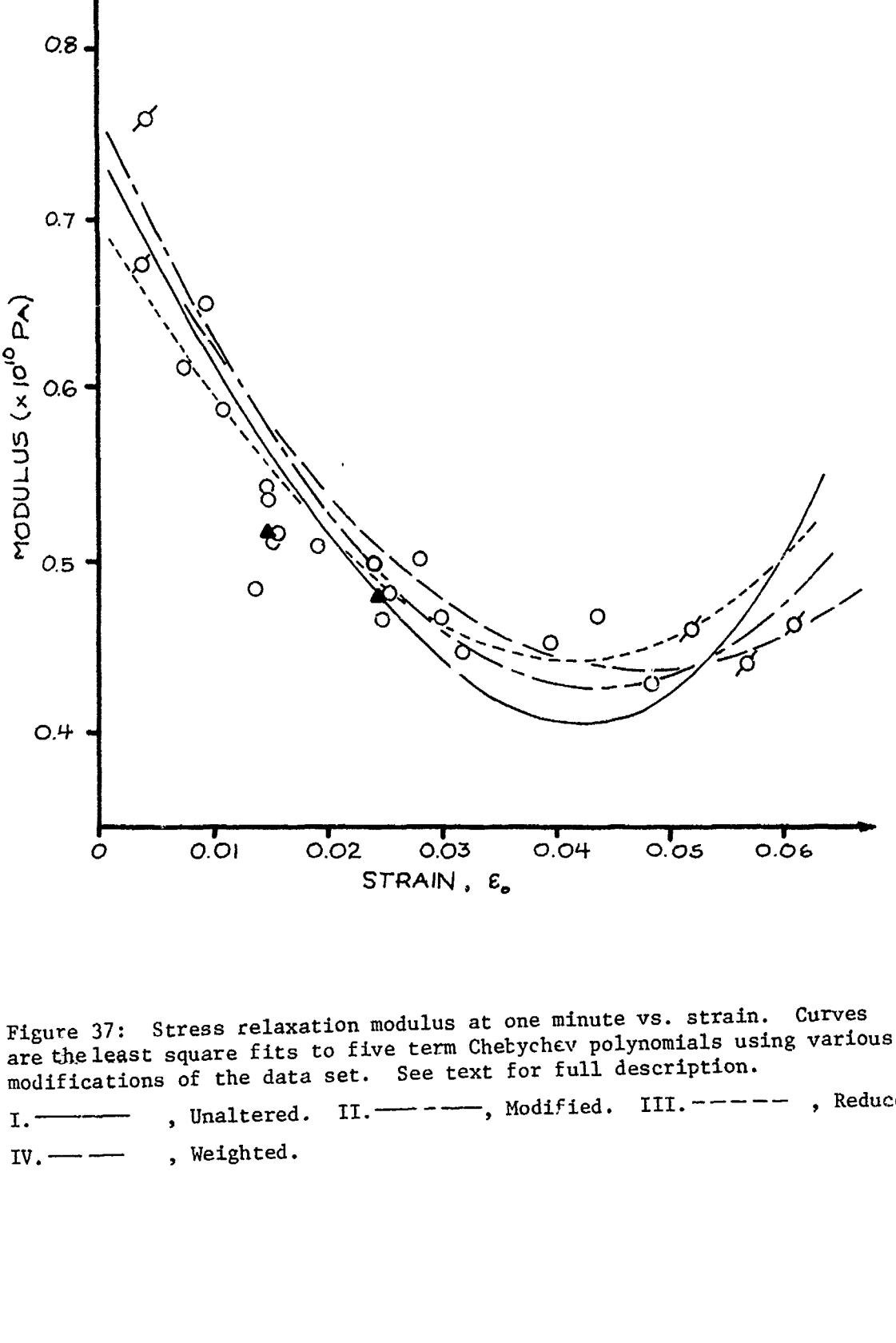

Figure 37: Stress relaxation modulus at one minute vs. strain. Curves are the least square fits to five term Chebychev polynomials using various modifications of the data set. See text for full description.

I. ———— , Unaltered. II. — - — - —, Modified. III. - - - - - , Reduced.

IV. — — , Weighted.

TABLE II

VARIATION BETWEEN COEFFICIENTS CALCULATED FROM SEVERAL DATA SETS: FROM THREE-, FOUR-, AND FIVE-TERM SOLUTIONS*

Data Set (see text for description)	Values of Coefficients				
	ψ_0	ψ_1	ψ_2	ψ_3	ψ_4
DA	9.44×10^5 (6)	-7.65×10^6 (20)	1.81×10^7 (54)		
DAR	9.35×10^5 (7)	-9.40×10^6 (2)	5.28×10^7 (35)		
DAX	9.80×10^5 (2)	-9.042×10^6 (6)	5.32×10^7 (36)		
DAM	1.00×10^6	-9.61×10^6	3.91×10^7		
DAW	9.51×10^5 (5)	-6.99×10^6	1.49×10^7 (62)		
DA	1.07×10^6 (2%)	-1.74×10^7 (5%)	4.88×10^6 (24)	3.14×10^9 (17)	
DAR	1.12×10^6 (3)	-2.45×10^7 (48)	1.66×10^8 (2500)	3.60×10^0 (34)	
DAX	1.01×10^6 (7)	-1.00×10^7 (39)	2.05×10^7 (219)	5.43×10^8 (80)	
DAM	1.09×10^6	-1.65×10^7	6.42×10^6	2.69×10^9	
DAW	$.985 \times 10^6$ (10)	-0.91×10^7 (45)	1.99×10^7 (210)	5.00×10^8 (81)	
DA	1.11×10^6 (0%)	-2.22×10^7 (3)	1.62×10^8 (24)	1.77×10^9 (281)	-1.94×10^8 (27)
DAR	1.01×10^6 (9)	-1.65×10^7 (23)	1.47×10^8 (31)	8.04×10^8 (73)	-1.53×10^8 (43)
DAX	1.13×10^6 (2)	-2.44×10^7 (13)	3.48×10^8 (64)	-1.45×10^9 (212)	-5.02×10^8 (88)
DAM	1.11×10^6	-2.15×10^7	2.12×10^8	4.65×10^8	-2.67×10^8
DAW	1.07×10^6 (4)	-1.78×10^7 (17)	1.74×10^8 (18)	1.43×10^8 (69)	-2.02×10^8 (24)

* Note: Numbers in parentheses are the % difference between the coefficient and the modified data value (DAM).

TABLE III

TEST OF CONVERGENCE OF COEFFICIENTS
CALCULATED FROM ORIGINAL, UNALTERED DATA SET

ψ_o	ψ_1	$\frac{\psi_o}{\psi_1}$	ψ_2	$\frac{\psi_1}{\psi_2}$	ψ_3	$\frac{\psi_2}{\psi_3}$	ψ_4	$\frac{\psi_3}{\psi_4}$	ψ_5	$\frac{\psi_4}{\psi_5}$
7.7×10^5										
9.3×10^5	-6.5×10^6	0.14								
9.4×10^5	-7.6×10^6	0.12	1.8×10^7	0.42						
1.07×10^6	-1.7×10^7	0.063	4.9×10^6	3.5	3.1×10^9	0.002				
1.11×10^6	-2.2×10^7	0.050	1.6×10^8	0.14	1.8×10^9	0.089	-1.9×10^8	9.5		
1.03×10^6	-1.4×10^7	0.074	-3.0×10^7	0.47	2.8×10^9	0.011	3.3×10^7	85.	-5.8×10^9	0.006

This data set is shown in Figure 34. The four-term solution is the lowest order curve which fits the data well. The covergence test gives a limit of 0.06 from the first two terms, and a limit of 0.002 for the last two terms. By eye, these coefficients give a good fit up to a strain of 0.03.

Finally, Figure 38 shows a comparison of the five-term solutions to both the unannealed data and the data for samples annealed for 1.5 hours at 121°C and 133°C with 1% shrinkage allowed. The most characteristic difference between the annealed and unannealed samples, i.e., the decrease in modulus, is preserved. The variation in the shape of the curves can be attributed to scatter in the data rather than to significant differences in behavior. These results are reminiscent of Yannas and Haskell's finding that only the first coefficient showed a monotonic decrease with temperature. The higher order coefficients did not show a regular change with temperature.

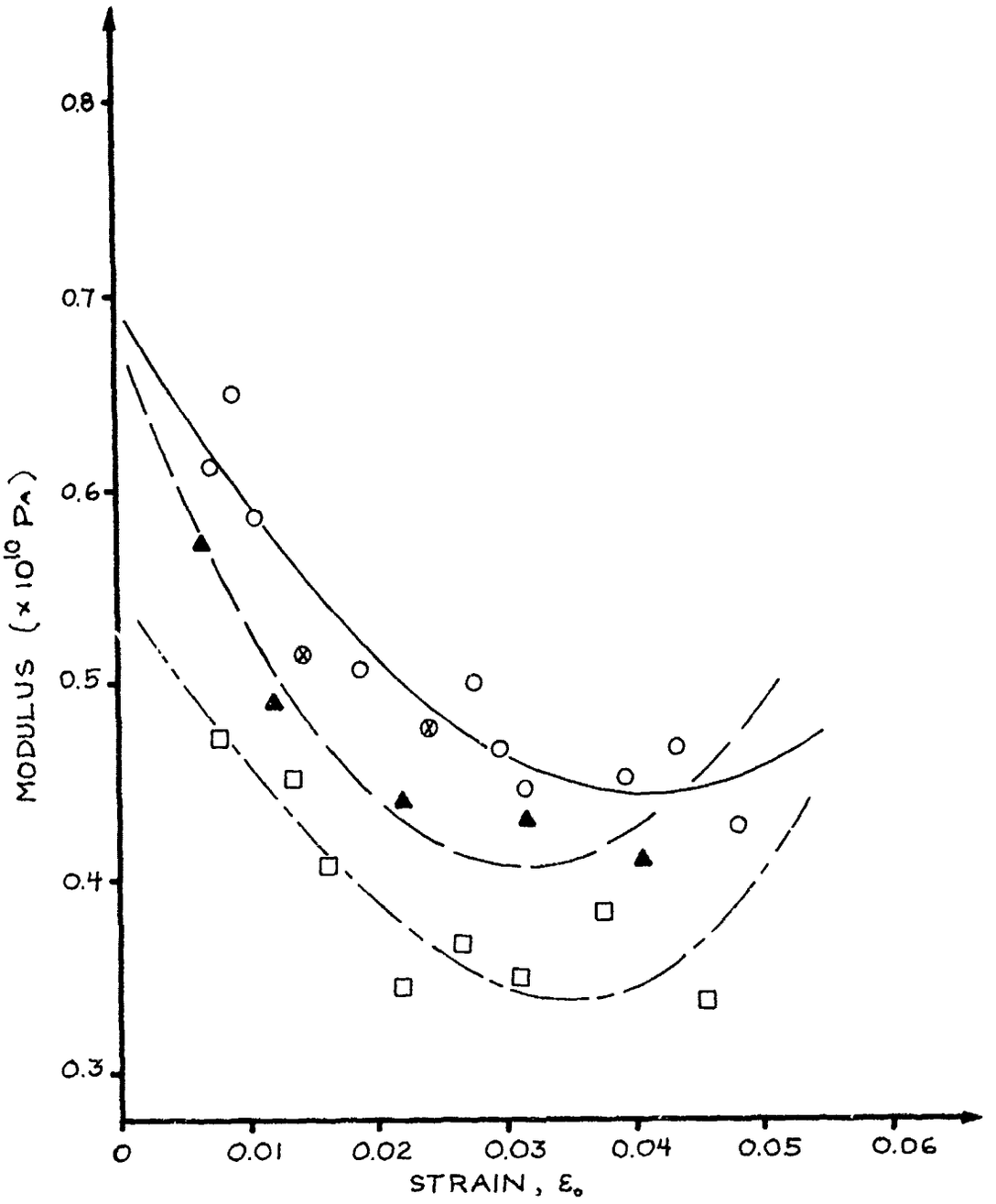

Figure 38: Stress Relaxation modulus at one minute vs. strain for unannealed, O, and annealed at 120°C, ▲, and 133°C, □. Curves are the least square regression fit to a five term Chebychev polynomial.

CONCLUSIONS

1) Highly oriented polypropylene films showed a nonlinear strain dependence of the stress relaxation modulus.

2) Shrinkage was necessary to have changes in modulus or structure due to annealing. The temperature of annealing increased the effect of annealing.

3) Sonic modulus is a better technique for monitoring amorphous orientation than is birefringence, because of its greater sensitivity and ease of use.

4) Stress relaxation modulus is a more sensitive indicator of changes in microstructure than orientation functions in highly oriented polypropylene. Other microstructural features control the stress relaxation modulus besides the overall orientation of the crystalline and amorphous regions.

5) Structural changes which were large enough to cause a decrease in modulus did not cause a change in the form of the stress relaxation modulus' dependence on strain, i.e., the shape of E (1 minute) vs. ε_o. Thus, either the structural components which control modulus and those which control the form of E vs. ε_o are different, or modulus is more sensitive to changes in structure than nonlinearity (the form of E vs. ε_o).

In the attempt to allow only one structural parameter, the amorphous orientation, to vary, we may have prevented the structural changes which were required to cause changes in the nonlinear behavior. It is possible that the crystallinity of crystalline orientation, or other structural features, must change before nonlinear behavior is changed. This is

suggested by the data of Hadley and Ward, and by our data.

6) The structural changes that occurred when films were annealed with shrinkage were not a simple relaxation or retraction of amorphous material. If they had been, amorphous orientation would be expected to decrease, whereas an increase was seen. Secondly, changes in crystallinity within the 1.6% scatter in crystallinity of unannealed film cannot account for the increase in sonic modulus.

A mechanism is proposed which is consistent with the shrinkage, the increase in sonic modulus, and the drop in stress relaxation modulus. This model suggests that annealing with shrinkage allowed microfibrils to move with respect to one another, resulting in the further development of the lamellar arrangement of crystallites in neighboring microfibrils. This decreased the amount of crystal-crystal connections along the draw direction. Consequently, more stress transfer must have occurred along crystal-amorphous connections, reducing the modulus along the draw direction. A small increase in amorphous orientation may occur during this rearrangement.

7) Fitting the multiple integral representation to the E (1 minute) vs. ε_o data, using Chebychev polynomial series, required at least four terms to fit the data. When convergence was tested the three-term solution was found to be convergent to $\varepsilon_o = 0.12$, the four-term solution to $\varepsilon_o = 0.002$, and the five-term solution to $\varepsilon_o = 0.05$. To the eye, the four- and five-term solutions were similar and "fit" the data up to strains of 0.025.

SUGGESTIONS FOR FUTURE WORK

There remain many interesting questions concerning the microstructural control of the nonlinearity observed in oriented polypropylenes. In this work the changes in structure were small, so that control of some aspects of structure could be maintained while other aspects were allowed to change. Because of this, little or no change was seen in the form of the stress relaxation modulus' dependence on strain. If larger changes were allowed by annealing under various dead loads, for example, to get larger and various shrinkages, a range of crystalline and amorphous orientations could be obtained. In this way, regions showing different types of strain dependence could be identified.

Another way to vary structure might be to draw the films further using a drawing procedure like Taylor and Clark's,[26] by drawing at 4%/min. at 130°C and getting a continuous crystal structure. An examination of the strain dependence of such a fiber's modulus would give insight into what features control nonlinear behavior.

Even more basic work could be done to understand nonlinear behavior, by varying crystallinity in an isotropic polypropylene and examining the effect on nonlinearity. If Buckley[49] is correct in his assertion that irregularities in structure give rise to nonlinearity, then probably the greater the crystallinity the greater the nonlinearity.

Another "next step" in this project might be to check the effect of annealing on the dynamic mechanical behavior in the 0°, 45° and 90° directions. If the mechanism hypothesized to explain the decrease in stress relaxation modulus is true, then the dynamic modulus and tanδ in the 45° and 90° directions should be affected and may give credence to or disprove the hypothesis.

APPENDIX A:

Measurement of Crystalline Orientation

Two techniques for measuring crystalline orientation, f_c, will be described in this Appendix. First, the use of a pole-figure goniometer (PFG) and associated theoretical considerations will be described. Results of the use of the PFG to measure f_c will be given. Finally, transmission X-ray photographs will be described and the photographs of annealed and unannealed film will be presented.

Theory of Crystalline Orientation

A quantitative measure of crystalline orientation can be obtained by using X-ray diffraction to determine the orientation of crystal planes in the specimen. This is done by measuring the average value of the angle, σ, between the draw direction and the chain helix axis. There are two functions which are used to express orientation quantitatively, $\langle\cos^2\sigma\rangle$ and f, called the orientation parameter and the orientation function, respectively. The orientation parameter, $\langle\cos^2\sigma\rangle$, takes values from +1.0 to 0.0. The orientation function, f, takes values from +1.0 to -0.5. A value of f = +1.0 indicates perfect orientation in the reference direction and a value of f = -0.5 indicates perfect orientation in the plane perpendicular to the reference direction. Random orientation yields a value of 0.33 for $\langle\cos^2\sigma\rangle$ and 0.0 for f.

In some polymers, polyethylene for example, the angle σ can be measured directly because there is a diffraction plane of type (00ℓ). However, in polypropylene no such plane exists. Wilchinsky has shown[1], however, that other planes containing the c-axis can be used to determine σ. The number of such planes required for the determination is dependent

on the crystal structure and the available diffracting planes.[2,3] Wilchinsky has shown that for monoclinic polypropylene only two diffraction planes are required to determine the orientation of the helix axis. The planes that are usually used are the (110) and (040) planes. Figure A-1 illustrates three major crystal planes in the monoclinic unit cell and their relation to the chain helices (indicated by triangular tubes). Note that all of these planes contain the helix axis. The unit cell dimensions for isotactic monoclinic polypropylene are:

	Wilchinsky[2]	Natta[55]	Turner-Jones et al.[57]
a	6.64 Å	6.65 Å	6.66 Å
b (monoclinic axis)	20.88	20.96	20.78
c	6.51	6.50	6.495
β	98.7°	99.3°	99.62°

Experimental determination of the orientation parameter is described by Wilchinsky and by Alexander.[4] An understanding of the geometry of the experimental setup is vital to the determination of $\langle \cos^2 \sigma \rangle$. Figure A-2 shows the important angles.

The first important angle is that between the beam and the plane that is being observed. The X-ray source and detector are set at 2θ degrees to one such that the (hkl) reflection that satisfied Bragg's law is detected. The crystals that are observed are those whose (hkl) plane normals are coincident with the bisector of the angle between the source and the detector. Another important angle is that between the sample draw direction and the crystal plane normal being detected. The conventional way to describe the orientation of a crystal is to describe the location of its (hkl) plane normal with respect to a reference direction. Figure

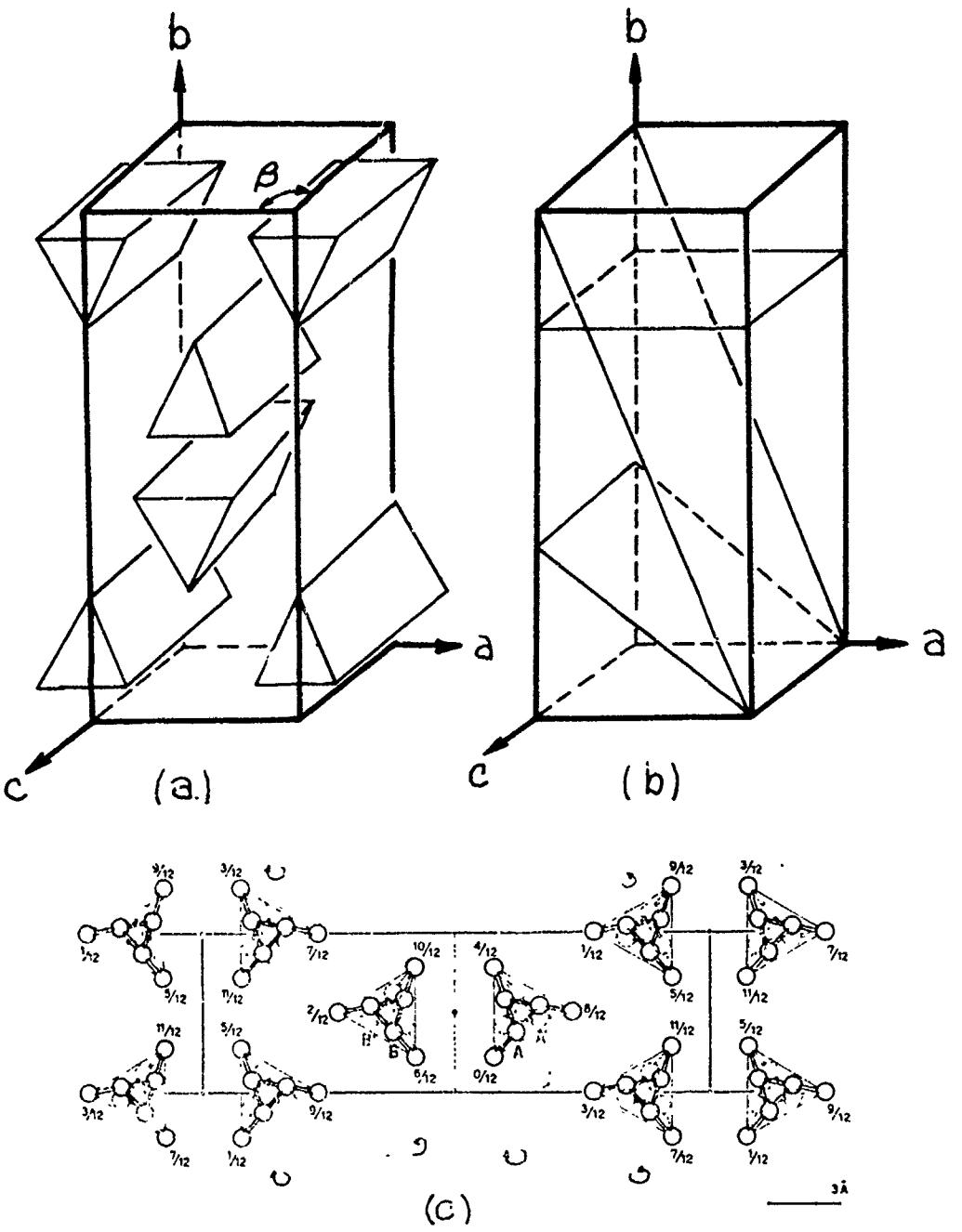

Figure A-1: The isotactic polypropylene monoclinic unit cell. (a) Unit cell with chain helices indicated; (b) Unit cell with the diffracting planes (040), (110), and (130) indicated; (c) Crystal structure of PP projected along the helix axis. (From Natta, Ref. 55)

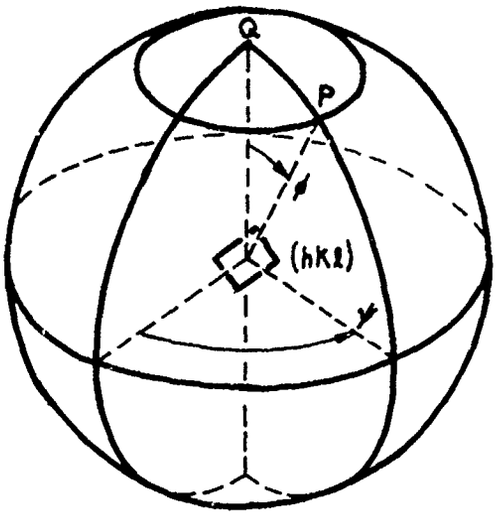

(a)

Figure A-2: Spherical coordinates (ϕ,ψ) of normal P, to plane (hkl), with respect to reference direction, Q.

A-2 shows this. The two angles ϕ and ψ allow us to describe the orientation in space of the plane normal. For example, consider a sample located at the center of the sphere in Figure A-2. If we specify some location on the sphere, P, we are indicating those crystals whose orientations are such that their (hkl) plane normals "point" at the position (ϕ_1, ψ_1). If we wish to observe the number of crystals whose (hkl) planes have their normals pointing at (ϕ_1, ψ_1), we must rotate the sample with respect to the X-ray source and detector so that the plane normals are coincident with the bisector of the X-ray beam. The rotation of the sample is of course a rotation of the reference direction in the sample away from the bisector of the X-ray beams by angles ϕ_1 and ψ_1.

If the concentration of planes oriented with their normals pointed at the equator (i.e., $\phi = 90°$), is to be measured, the film would be rotated in its own plane (i.e., rotation around the normal, Q), thereby varying ψ. To observe the concentrations over the whole range of ϕ and ψ the procedure is to set Q at some specific ϕ value, say 10°, from the bisector and then rotate the film in its plane, giving intensity as a function of ψ for a constant ϕ value. By varying ϕ from 0° to 90° by 10° intervals, the concentration of (040) planes at all orientations can be observed.

In actually carrying out the measure of orientation, the geometry used was the transmission geometry. In this case the setup of the specimen is shown in Figure A-3. This setup and a derivation of the absorption correction factor for this geometry was first presented by Decker[5]. The transmission geometry can theoretically be used to measure the concentration of crystals whose plane normals have locations in the range of ϕ from 90° to 30° and a full 360 range of ψ. At lower values of ϕ the X-ray beam enters the sample film at too small an angle and gives poor results.

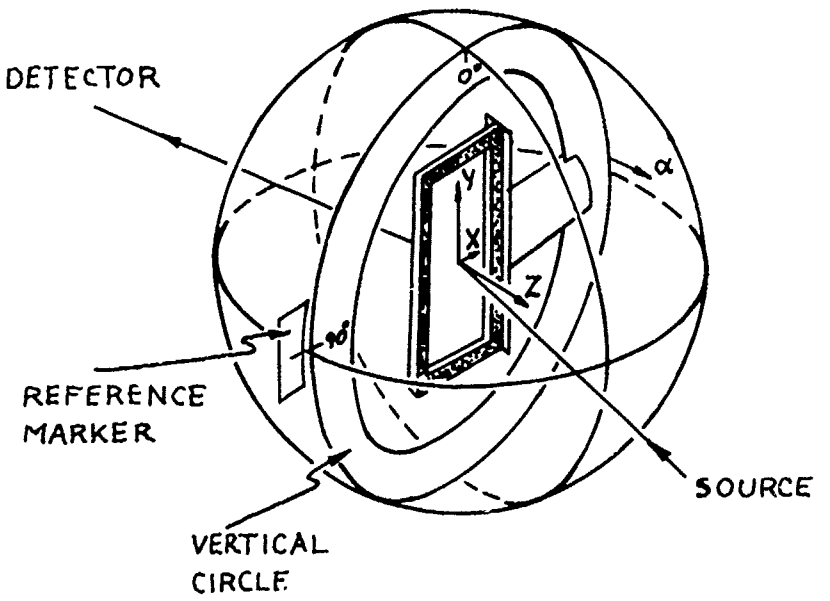

Figure A-3: Transmission holder from goniometer showing rotation angles.

In fact, the range of ϕ may be even further restricted due to the setup of the specimen holder. Again, a value of ϕ is set by fixing the plane of the film so that its normal is at an angle ϕ from the bisector of the beam. The sample is then rotated through the angle ψ as desired by rotating the vertical circle.

Decker's absorption correction factors[5] are required because as the film sample is rotated to varying ϕ values, the diffracting volume changes and consequently the diffracted beam intensity is varied. Decker describes an angle α which equals $90° - \phi$. See Figure A-4.

$$\frac{I_{\alpha=0}}{I_{\alpha}} = \frac{\mu t \cdot \exp[-\mu t/\cos\theta] \cdot \left\{[\cos(\theta-\alpha)/\cos(\theta+\alpha)]-1\right\}}{\cos\theta \cdot \left\{\exp[-\mu t/\cos(\theta-\alpha)]-\exp[-\mu t/\cos(\theta+\alpha)]\right\}} \qquad \text{(A1-1)}$$

From the orientations of the (110) and (040) planes, the orientation of the chain helix axis may be calculated. The value of $\langle \cos^2\sigma_c \rangle$ may be calculated from values of $\langle \cos^2\phi_{040} \rangle$ and $\langle \cos^2\phi_{110} \rangle$ using a relationship derived by Wilchinsky and discussed by Alexander. They are related as follows:

$$\langle \cos^2\sigma_c \rangle = 1-1.099 \langle \cos^2\phi_{110} \rangle - 0.901 \langle \cos^2\phi_{040} \rangle . \qquad \text{(A1-2)}$$

The value of $\langle \cos^2\sigma \rangle$ is defined as follows:

$$\langle \cos^2\sigma \rangle = \frac{\int_0^{\pi/2} I(\phi) \cdot \cos^2\phi \cdot \sin\phi \, d\phi}{\int_0^{\pi/2} I(\phi) \cdot \sin\phi \, d\phi} \qquad \text{(A1-3)}$$

where $$I(\phi) = \int_0^{\pi/2} I(\phi,\psi) d\psi.$$

Here $I(\phi,\psi)$ is the pole concentration which represents the relative amount of the crystals having their (hkl) plane normals in the direction ϕ,ψ.

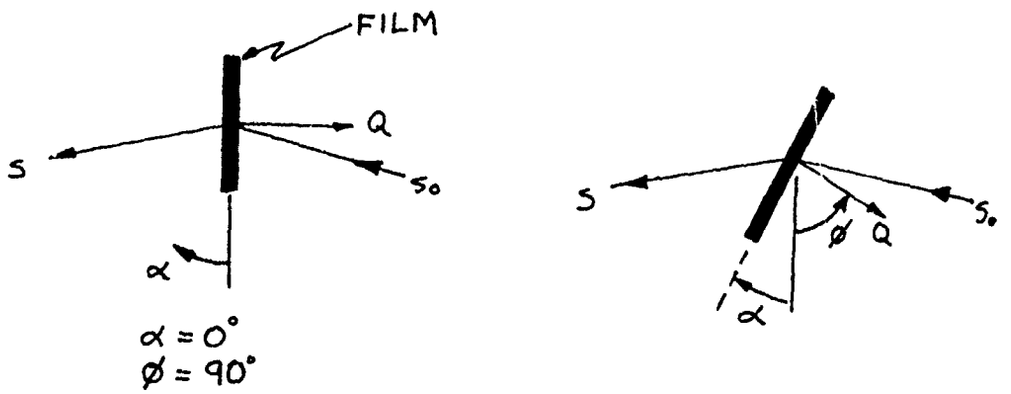

Figure A-4: Angles in transmission geometry.

The intensity, $I(\phi,\psi)$ is the diffraction peak intensity after background correction and absorption corrections. The assumption is that the corrected intensity is proportional to the pole concentration.

The orientation function, f, is defined as

$$f = \frac{1}{2}(3\langle\cos^2\sigma\rangle - 1). \qquad \text{(A1-4)}$$

Experimental Procedure: Pole figure goniometer

The equipment used to obtain X-ray data was the Siemens pole-figure goniometer with a transmission-specimen holder.[6] With this setup, shown in Figure A-5, the film sample is attached to a transmission-specimen holder which is mounted in a "vertical circle", shown in Figure A-3. The plane of the film is in the plane of the circle. The circle can be rotated by a drive motor in its plane, giving rotation in ψ when the reference direction is defined as the film normal. The circle can also be turned to specific α values by turning it with respect to the X-ray beam.

The draw direction, y, of the polypropylene film was designated as the reference direction. To determine $\langle\cos^2\alpha\rangle$, the intensity of the (040) and (110) planes would have to be measured over the range of ϕ and ψ. The usual procedure is to set ϕ to a specific value, ϕ_1, and rotate throughout ψ as shown in Figure A-6, and then integrate under the intensity vs. ψ data so obtained. This results in a value of $I(\phi_i)$. Next, the value of ϕ is changed by a specific amount, say 5°, and the procedure is repeated. These values of $I(\phi_i)$ are then used to calculate $\langle\cos^2\sigma\rangle$ according to:

$$\langle\cos^2\sigma\rangle = \frac{\Sigma I(\phi_i)\cos^2\phi_i \sin\phi_i}{\Sigma I(\phi_i)\sin\phi_i} \qquad \text{(A1-5)}$$

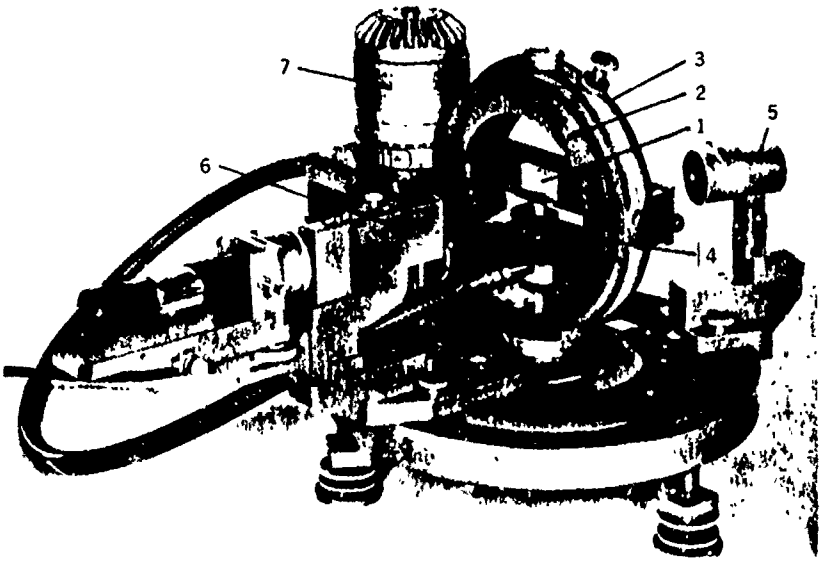

Siemens pole-figure goniometer with transmission-specimen holder 1 – transmission specimen holder, 2 – vertical (β) circle, 3 – toothed outer rim that houses vertical circle, 4 – azimuthal circle, 5 – direct-beam collimator, 6 – diffracted-beam collimator, 7 – drive motor. (Courtesy of Siemens Aktiengesellschaft)

Figure A-5: Pole figure goniometer used in orientation function measurement. (Ref. 4)

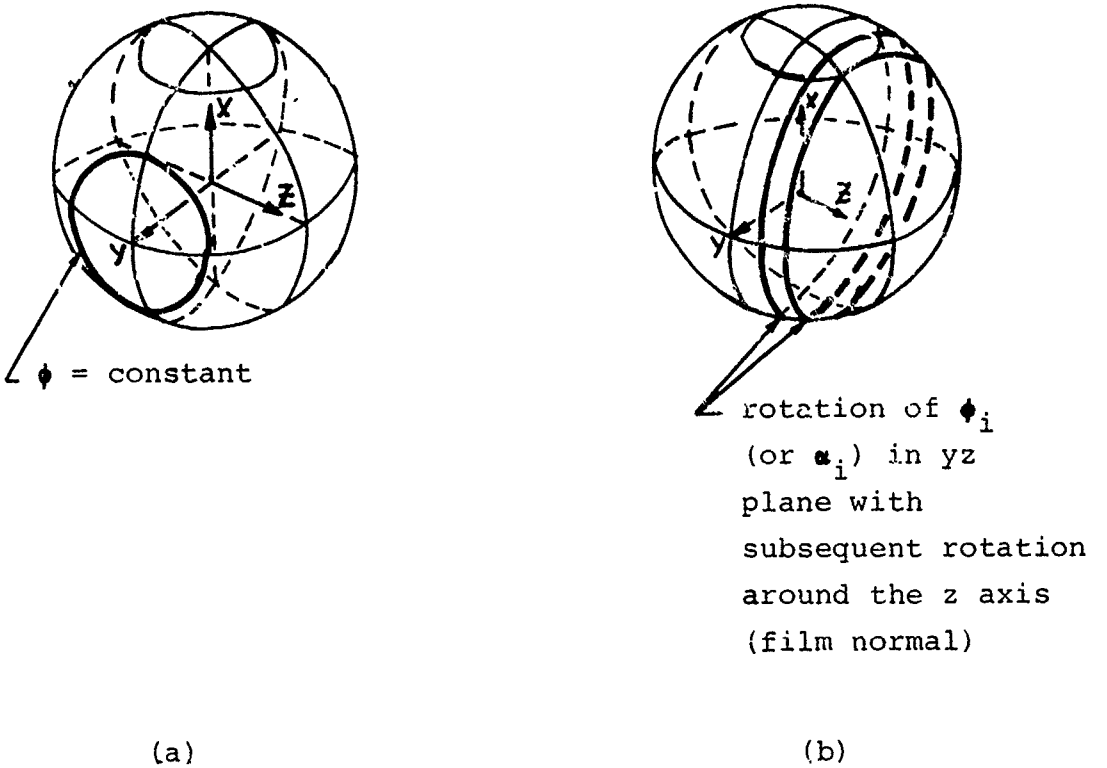

(a) (b)

Figure A-6: (a) Rotation around the stretch direction, y, corresponding to constant ϕ; (b) Rotation around the film normal, z. N.B.: This is not a constant ψ rotation.

Some simplifications of this procedure may be made if the films are transversely isotropic. This would mean that the crystals have no preferred direction in the plane perpendicular to the stretch direction, i.e., the x-z plane. To test this assumption, the intensity of the reflections for various values of ψ at the same ϕ were observed to see if they were constant. If the intensity after corrections is the same, then the values of $I(\phi)$ could be measured at one value of ψ, instead of integrating over a range of ψ. This $I(\phi)$ could then be used directly to calculate $\langle \cos^2\sigma \rangle$.

Results

Table 1-A shows the intensity at $\phi = 90°$, corresponding to the transverse direction of the film, for ψ values varying from 0° to 35° for the (110) reflection and for several values of ψ for the (040) reflection. Figure A-7 shows the scans in ϕ at $\psi = 0$. Using Decker's absorption correction, corrected values of intensity are obtained. As can be seen, these values both for the (110) and the (040) planes are constant. The intensity for the (110) planes shows a variation around an average value of 3.20, having a standard deviation in the intensity of 0.16 (5%). These values for the (040) plane are an average intensity of 1.87 with standard deviation in the intensity of 0.12 (7%).

Because these values are constant in ψ, the calculation of $\langle \cos^2\sigma \rangle$ can be made directly using the curve of intensity vs. ϕ for $\psi = 0°$. This data is shown in Figure A-7 for the (110) and (040) planes, along with a background scan at $2\theta = 11°$. From these scans, it is clear that the intensity of the (110) and (040) reflections are zero except in the regions around $\phi = 90°$. To carry out the evaluation of $\langle \cos^2 \phi_{hkl} \rangle$,

TABLE IA

Demonstration of Transverse Isotropy
of Polypropylene Films

ϕ	(hKℓ) & θ	I (ψ = 90)	$I\phi = 90° / I\phi_{exp.}$	I corrected
0	110 7.07°	3.18	1.00	3.18
5		2.98	1.007	3.00
10		3.11	1.006	3.13
13		3.39	1.003	3.40
15		3.33	0.998	3.32
20		3.47	0.983	3.41
25		3.11	0.959	2.98
30		3.45	0.929	3.21
35		3.55	0.892	3.17
				$I_{av.}$ = 3.20 s=0.16 (5%)
0	040 8.5°	1.85	1.00	1.85
10		1.98	1.011	2.00
25		1.99	0.970	1.93
-25		2.03	0.844	1.71
				$I_{av.}$ = 1.87 s = 0.12 (7%)

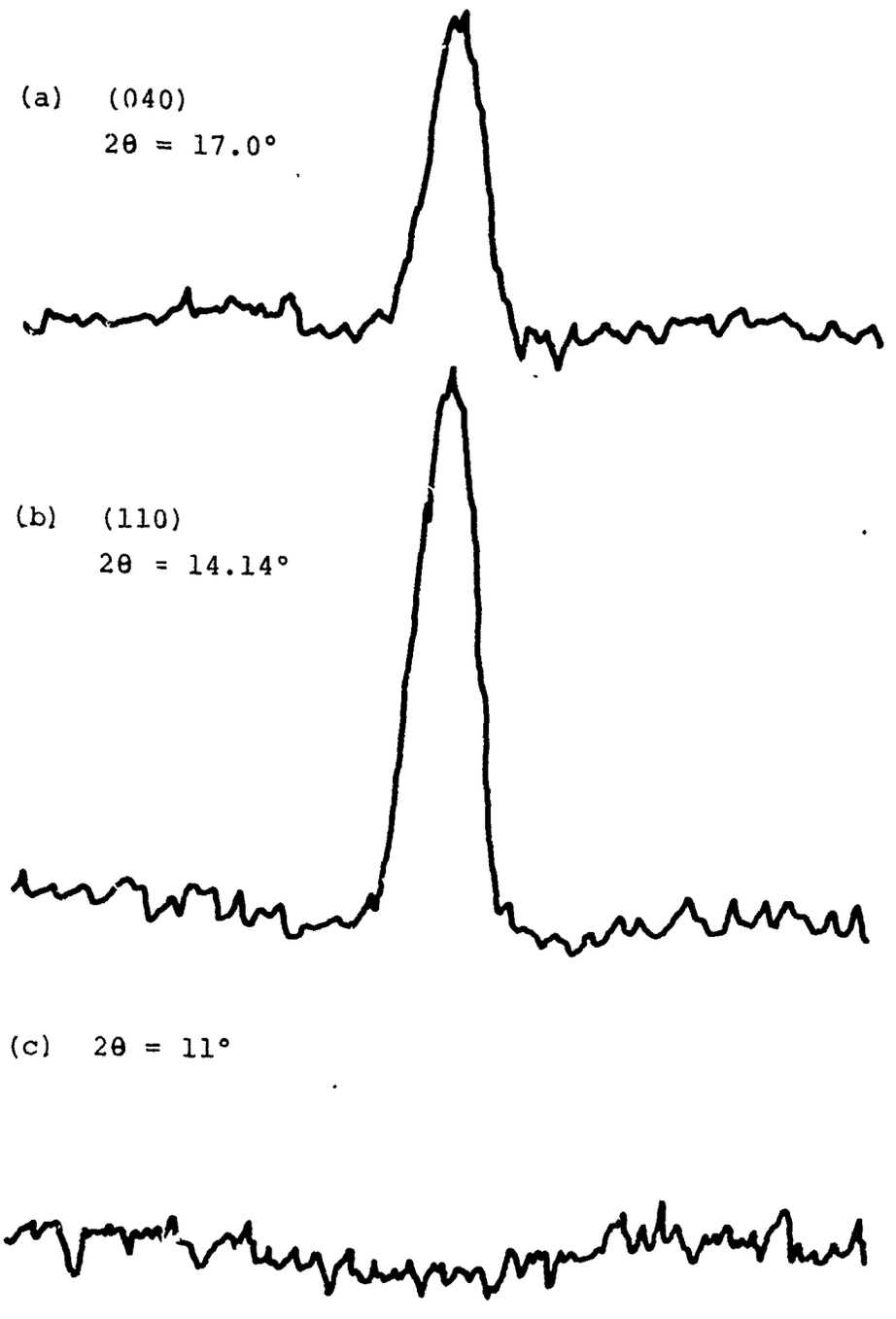

Figure A-7: Variation of intensity with azimuthal angle ψ at constant 2θ and $\alpha = 0$ (beam bisector coincident with plane of film): (a) for (040) plane; (b) for (110) plane; (c) background.

the intensity at intervals of $\phi = 1.44°$ was recorded and the summations were performed using an HP-25 program to calculate $\langle \cos^2\phi_{hkl} \rangle$ using equation (A1-5). The values of $\langle \cos^2\phi_{hkl} \rangle$ and f_{hkl} so obtained, and the value of $\langle \cos^2\phi_c \rangle$ obtained by using equation (A1-2), are tabulated below and are those reported in the thesis.

	$\langle \cos^2 \rangle$	f
(110)	0.0124	-0.481
(040)	0.0105	-0.484
c-axis	0.98	0.97

Experimental Procedure: Transmission X-ray Photographs

Another way to assess crystalline orientation besides the use of a goniometer, is by use of a transmission X-ray photograph. Figure A-8 shows the experimental setup.[4] Figure A-9 gives examples of such photographs for a series of drawn polypropylenes.[10] Photographs of this kind are useful for qualitative comparisons of crystalline orientation, and can be made quantitative by use of a densitometer.

This technique was used to compare unannealed polypropylene films with films which had been annealed at 121°C and 133°C with 1% shrinkage allowed. Pads of each type of film were made by cutting the tensile specimens into uniform pieces. The pieces were aligned between two pieces of aluminum which were the same size as the specimens. By clamping the aluminum pieces together, applying Duco cement on the sides and, once dry, cutting away the aluminum pieces, a sturdy pad of about 1 mm thick was made. By making the pad, the alignment of the films could be preserved. A pad of films about 1 mm thick was needed to optimize the intensity of the diffracted beam (see Ref. 4, p 68 for discussion) without causing a large geometrical broadening of the reflections.

The transmission photographs were taken using CrK_{α} radiation (λ = 2,29 Å) with exposures of 20 - 25 minutes. The sample was 6.8 cm from the photographic plate. Polaroid Type 57 High Speed film was used. Figure A-10 shows the photographs from an unannealed specimen and from specimens annealed at 121°C and 133°C with 1% shrinkage allowed. No broadening of the diffraction spots was seen, indicating that the orientation of the crystals was not altered by the annealing procedure.

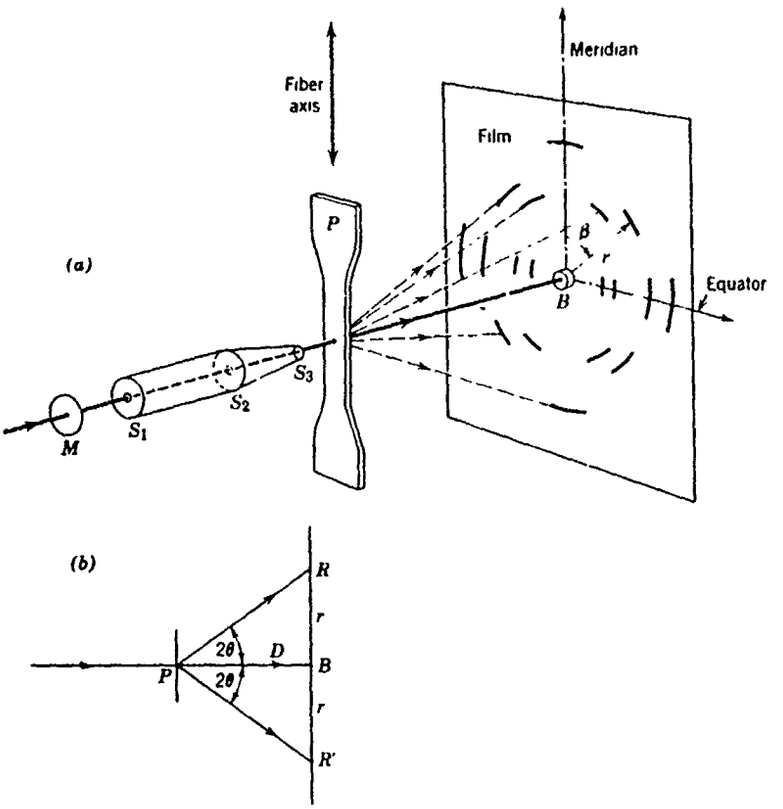

Geometry of diffraction by specimens with axial (fiber) orientation: (*a*) schematic perspective, (*b*) dimensional relationships

Figure A-8: Equipment for transmission X-ray photograph. (Ref. 4)

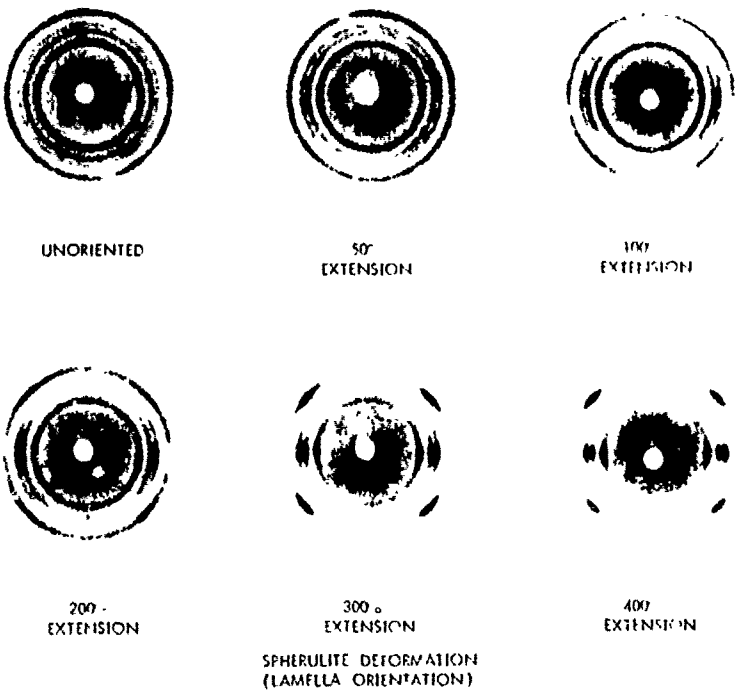

Effect of isotactic polypropylene film extension on the wide-angle x-ray diffraction pattern

Figure A-9: Examples of transmission X-ray photographs of PP. (Ref. 10)

(a) Annealed at 133°C for 1.5 hr. 1% shrinkage.

(b) Annealed at 121°C for 1.5 hr. 1% shrinkage.

(c) Unannealed.

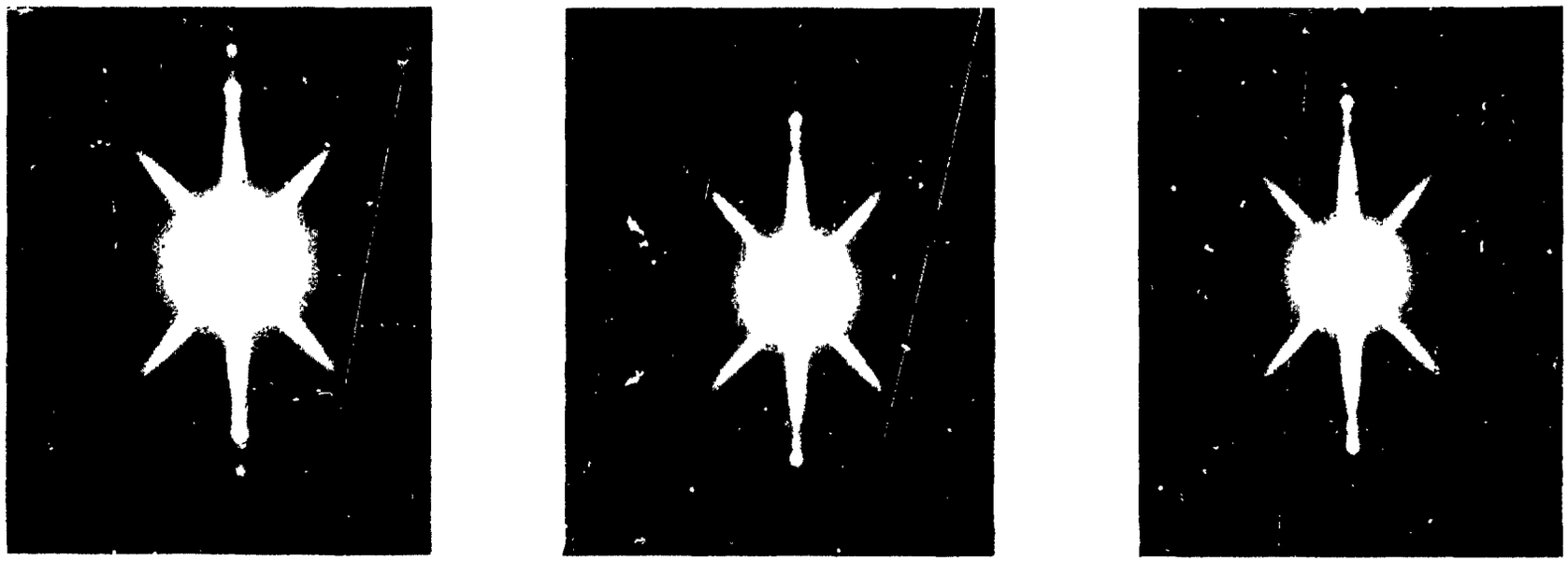

Figure A10: Transmission X-ray photographs: Cr K_α radiation (λ = 2.29 Å). Photographic film was 6.8 cm from PP specimen. Draw direction of specimens: ←——→

APPENDIX B:

Birefringence Measurement

The phenomenon of birefringence is observed when a material is anisotropic and there is a difference in the speed of light as it passes through the material in one direction compared with another direction. The definition of birefringence, Δ, is

$$\Delta = n_{\parallel} - n_{\perp}$$

$$\text{where} \quad n = C_{vacuum} / C_{medium}$$

Here $n_{\parallel}$ and $n_{\perp}$ are the refractive indices of the film parallel and perpendicular to the orientation direction respectively, and C is the speed of light. This phenomenon arises due to anisotropy in the polarizability of the units along the molecular chain and perpendicular to it. Several texts discuss this phenomenon in detail.[8,9] Also, several authors have treated the phenomenon of birefringence in oriented films.[10,11]

To measure the birefringence of the polypropylene film, a Berek compensator was used. The compensator measures the phase difference (retardation), Γ, between two mutually perpendicular, plane-polarized wave motions emerging from the sample. The retardation, Γ, is related to birefringence, Δ, through the thickness, t, by the relation

$$\Delta = \frac{\Gamma}{t} .$$

Figure B-1 shows the arrangement of polarizer, sample, compensator and analyzer. The compensator is placed in the microscope between the sample and the analyzer. The compensator consists of a calcite crystal which has a thickness that gives, when the crystal is level, an integer number of

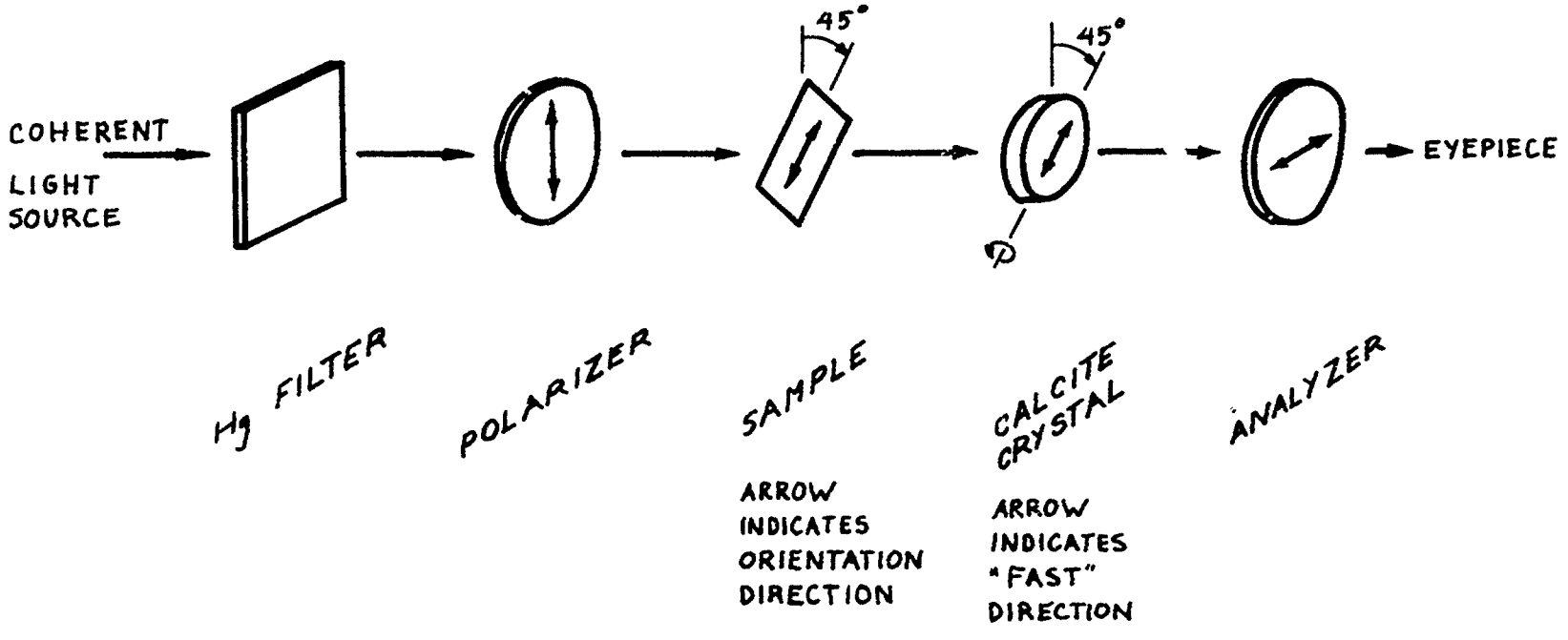

Figure B-1: Birefringence measurement

550 nm. retardations. This means that when the compensator is in place in the microscope and is set at its zero position (indicated by a red number 30 on its dial) it has no compensating effect, i.e., it does not alter the light passing through it if the light has a wave length of 550 nm. The retardation of the sample is measured by matching the sample's retardation with an equal and opposite retardation using a standard calibrated crystal.[10] Compensation occurs when the "fast" direction of the calcite crystal is placed parallel to the "slow" direction of the sample; this arrangement is known as the "compensating" position. In a Berek compensator the crystal is rotated, causing an increase in the apparent thickness for the light passing through it. Consequently, as the crystal is rotated, the phase difference between the light parallel and perpendicular to its fast direction increases.

This phenomenon is used to measure the birefringence of a sample by first aligning the sample with the compensator crystal in the "compensating" position. In polypropylene films, the compensating position occurs when the orientation direction of the film is perpendicular to the arrow on the compensator. The arrow is parallel to the axis of rotation of the crystal. Next the calcite crystal is rotated until there is no phase difference between the parallel and perpendicular waves.

The point at which there is no net retardation can be determined only with white light. White light must be used because fringes of all orders are black under monochromatic light. In white light only the zero-order fringe is black, with white fields on either side, while all other fringes are colored. Once the black, zero-order fringe is found, a monochromatic interference filter is placed in the light path to give a sharper extinction line. In this work a 550 nm (band width, 10 nm) green filter

was used (Oriel Co., Stamford, Conn.). The extinction line is then aligned with a crosshair, and the measurement taken from the compensator's vernier scale. Using tables, this measurement can be converted into a retardation in nanometers.

Another way to get a rough idea of the retardation in a uniformly oriented sample is to cut a wedge in the sample. When the wedge is observed in monochromatic cross-polarized light, and if more than one full wave length of retardation occurs, an extinction band will be observed for every 550 nm of phase difference caused by the specimen. Figure B-2 shows a photograph of the polypropylene film with such a wedge. The wedge was made by polishing. Two extinction bands can be seen, indicating 1100 nm retardation. Thus a rough idea of the retardation can be obtained using a wedge only. The function of the compensator is to give a more precise measurement of retardation.

The actual measurement of the retardation in the specimen is performed as follows. First, with no sample in the light path and with the compensator at its zero position (the red "30" on the dial), the analyzer is rotated with respect to the polarizer until extinction occurs. Next, the sample is placed in the field of view, focus adjusted, and the stage is rotated until maximum extinction again occurs. Here the orientation direction is parallel to the polarizer. This position is known as the extinction position. The stage is then rotated 45° so that the film's orientation direction is perpendicular to the fast direction of the calcite crystal (indicated by an arrow on the compensator holder). The filter should then be removed.

A crosshair or some kind of marked eyepiece is required for the subsequent measurements. The compensator is rotated from its zero position

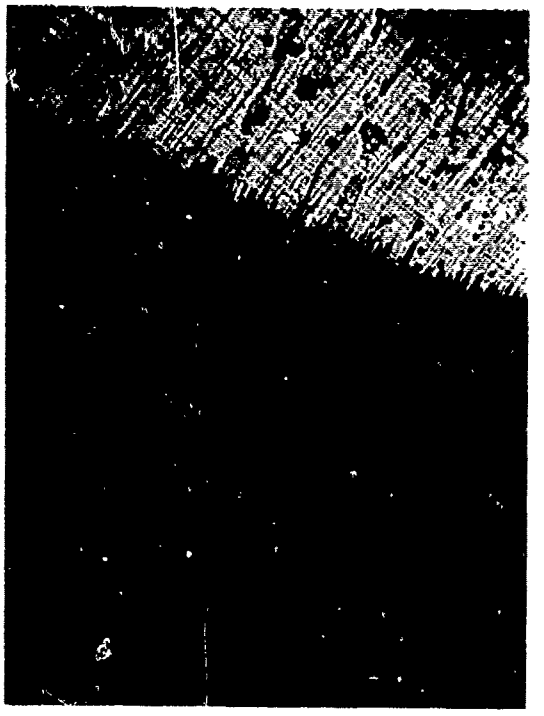

Figure B2: Wedge in PP film seen through crossed polarizers with monochromatic light (Hg filter: $\lambda_{min.}$ = 1100 Å - green). Top of photo is the full thickness. Dark bands in wedge indicate a full wavelength retardation

(the red 30) to higher numbers on the dial, until the zero-order black band, with white bands on either side, is seen moving in across the field of view. This band should be lined up with the crosshair. The filter is then replaced, and the band aligned with the crosshair. The position on the compensator dial is then returned to the 30 mark and this procedure is repeated, turning the knob to lower values. This position is known as b. The sample is then removed.

This procedure is followed with the filter in place and with no sample, to determine the relationship between the knob markings and the compensator effect. Because there is no sample, the first band that is observed is due to a retardation of one full wave length, and subsequent bands are due to integer numbers of wavelength retardation. This provides a calibration beween knob markings and the amount of retardation.

The calculations of retardation from the compensator readings proceed as follows: the angles of tilt for compensation, i , are found:

$$i = (a - b)/2$$

A function, f(i), related to thickness, but not directly so, is determined from tables found with the compensator. This value of f(i) is found both for the sample and for the compensator alone. Then the relationship for the retardation, Γ, in the sample is

$$\frac{\Gamma_{(nm)}}{f(i)_{sample}} = \frac{\lambda_{(nm)}}{f(i)_{compensator}} \qquad \text{(B-1)}$$

Birefringence is then determined from the retardation Γ and thickness, t:

$$\Delta = \frac{\Gamma}{t}$$

Experimental:

Birefringence was measured in several unannealed and annealed film specimens. All annealed specimens had been annealed for 1.5 hours at the indicated temperatures. Thickness was determined by measuring length, width and weight. These measurements, along with the measured density, were used to determine thickness. At one or more locations on each of the four films, the retardation was measured. These data were taken with the compensator fast direction perpendicular to the orientation direction. These data are presented graphically in Figure B-3 and in Table 1B.

Discussion of Birefringence Measurements:

In the initial use of birefringence as a measure of structural change due to annealing, the thickness of the film was measured by weighing and the retardation at one or two locations on the film was measured. The birefringence was calculated from this data. However, large variations were observed and the thought arose that perhaps the retardation should be measured at more locations on each film specimen. However, even when this was done, the variation in the birefringence between ostensibly similar film specimens was not eliminated. In fact, when the birefringences of unannealed films were compared, a standard deviation of 3.6% in the average birefringence of 0.0326 was found. This large a variation encompassed nearly all other measured values of birefringence for the annealed films. Also, there was no observable trend in the mean birefringences for a set of annealing treatments. For example, two films were annealed at 145°C. Both were cut from the same piece of film and were annealed at 145° for one and one-half hours, with 2.5% shrinkage. Despite the care taken to give these films very similar treatments, their average birefringences were quite dif-

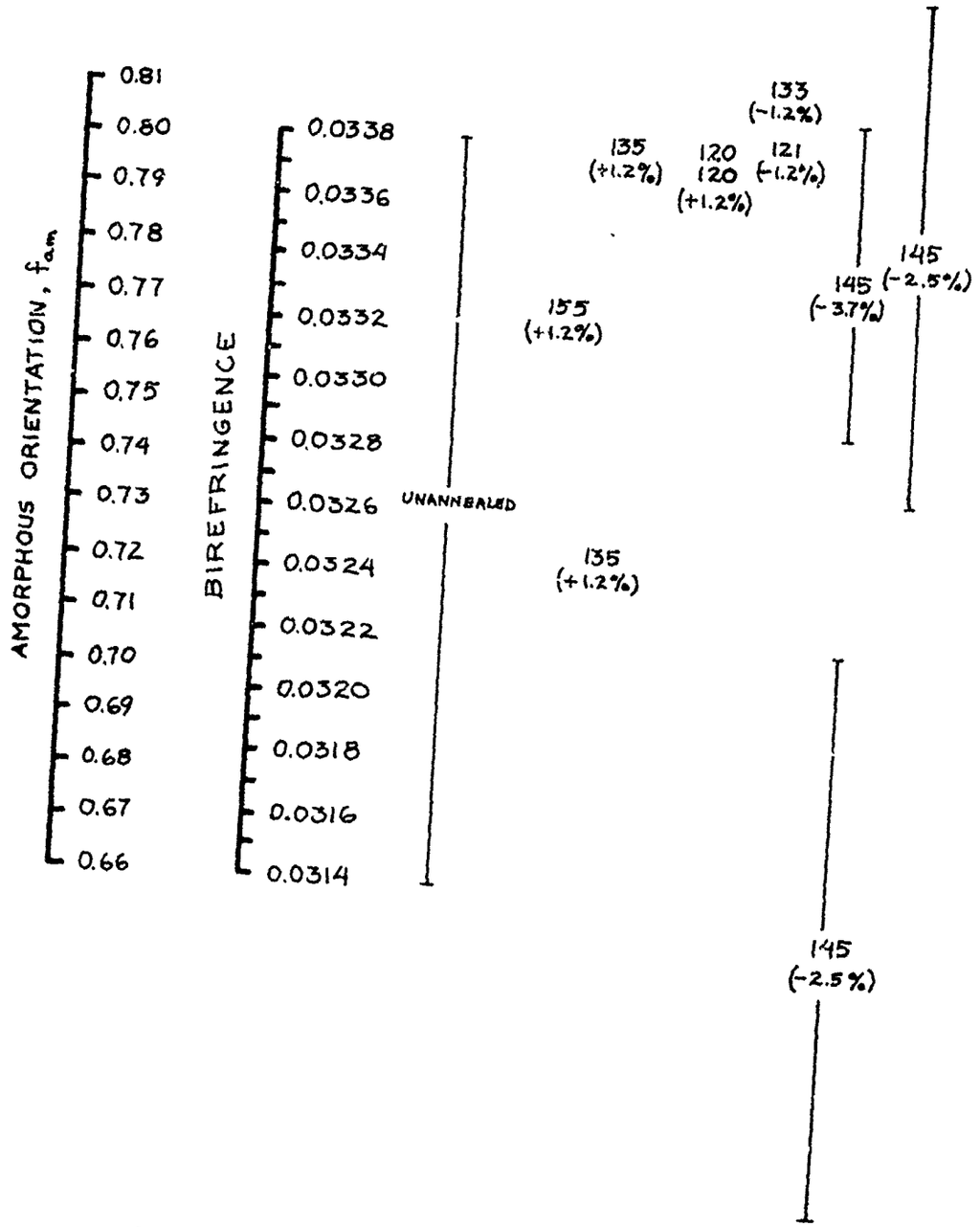

Figure B-3: Birefringence measurement.

TABLE 1B

Results from Birefringence Measurements						
film #	date of test	annealing temp. (°C)	shrinkage (-) or strain (+) %	t (mil)	Γ(nm)	Δ
1	7/9/80	-	-	1.621	1381	0.0335
	8/6/80	-	-	1.621	1343	0.0326
2	8/6/80	-	-	1.600	1394	0.0343
3	8/19/80	-	-	1.536	1257*	0.3?2
Average of all unannealed samples						0.0326 s = .0012 (3.6%)
1	7/9/80	155	+1.2	1.51	1277	0.0333
1	7/9/80	135	+1.2	1.487	1277	0.0338
2	7/23/80	135	+1.2	1.388	1149	0.0325
1	7/9/80	120	+1.2	1.467	1262	0.0338
2	7/23/80	120	+1.2	1.370	1178	0.0338
1	8/6/80	121	-1.2	1 653	1420	0.0338
1	8/6/80	133	-1.2	1.577	1362	0.0340
1(A)	8/19/80	145	-2.5	1.594	1359*	0.0335 (s=.0008)
2(B)	8/19/80	145	-2.5	1.726	1371*	0.0313 (s=.0009)
1	8/19/80	145	-3.7	1.459	1239*	0.0334 (s=.0005)

*Each of these retardations is the average value from measurements at 8 locations on the specimens.

ferent, being 0.0335 and 0.0313, one greater and one lower than the birefringence of the unannealed film. From this information, the conclusion must be drawn that if any changes in birefringence had occurred on annealing, it was not possible to detect them because of the large variation between the individual films' birefringences.

Orientation and Birefringence

The equation relating amorphous orientation, f_{am}, and measured birefringence, Δ_M, is:

$$\Delta_M = \beta\, fc\, \Delta_c^\circ + (1-\beta)\, f_{am}\, \Delta_{am}^\circ$$

or

$$f_{am} = \frac{\Delta_m - \beta\, fc\, \Delta_c^\circ}{(1-\beta)\Delta_{am}^\circ}$$

The value of crystalline orientation, f_c, is 0.97, and of crystallinity, β, it is 0.72. The constants Δ_c° and Δ_{am}°, the intrinsic birefringence of perfectly oriented crystal and amorphous regions, respectively, have values of 0.0291 and 0.0600 respectively,[10] in polypropylene.

APPENDIX C:

Density Measurement

Density measurements were made using the density gradient technique described in ASTM D1505. The density gradient column was a Techne Incorporated DC-1 Density Gradient Column consisting of a temperature controller, water bath, cooling coils, column tube, and filling device. The filling system is described in ASTM D1505 as Method C - continuous filling (liquid entering gradient tube becomes progressively more dense). Figure C-1 illustrates this system.

For measuring the density of isotactic polypropylene, the liquids used to form the density gradient were isopropanol and ethylene glycol. Floats having a range of densities determined by the manufacturer to four decimal places, were used to calibrate the column. Heights of objects in the column were measured using a cathetometer, which is a leveled telescope on a vertical stand, marked in 0.1 cm gradations and having a vernier enabling measurement to 0.005 cm.

Samples were introduced into the column after immersion in ethylene glycol and then placed in the column just below the surface of the liquid. The samples were then allowed to fall to their equilibrium position. At least 24 hours elapsed before the heights were measured. The height was taken by estimating the center of mass of the float or sample. Note was taken of the height of the top and bottom of each object in order to estimate the error in location. The height and density data for the calibration floats were then used to calculate a least square fit for these data points. From this, the density of the film was determined from the height measurements of the samples. Table 1C summarizes this data.

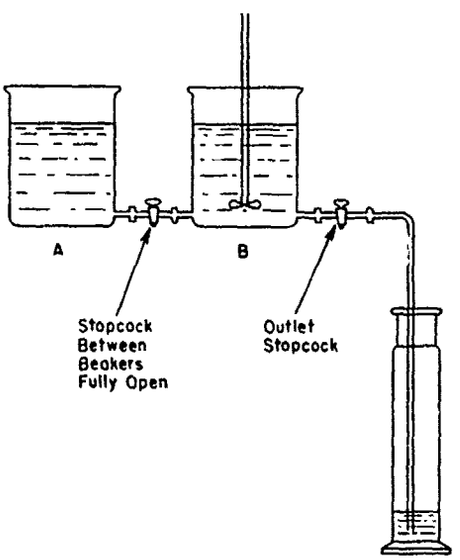

Apparatus for Gradient Tube Preparation
(Method C).

Figure C-1: Density Gradient Column (from ASTM D1505).

Table 1C: Density Measurement

Color of float	Density (g/cm^3)	Height
Lime green	0.9976	34.550
Clear	0.9800	40.850
Green	0.9326	56.545
Orange-red	0.9050	62.180
Blue	0.8823	68.235
Yellow	0.7968	97.195

Result of least square fit: height = $a_o \cdot$density + a_1

$a_o = -304.6$

$a_1 = 338.9$

Film sample heights
60.765
60.560
60.515
60.515
60.450
60.420
60.315
59.845

Average height = 60.42

s = 0.27

Density resulting from the average height is 0.914 ± 0.001 g/cm^3.

A density of 0.914 $\pm$ 0.001 g/cm^3 was found for a series of specimens. To determine the degree of crystallinity from density, the densities of the two phases were required. Samuels[25] and Desper[11] use values of amorphous density, ρ_{am}, of 0.858 g/cm^3 and crystal density, ρ_c, of 0.936 g/cm^3. These values were obtained from work of Ruland and Danusso, Maraglio and Natta. (See Ref. 25) The total density, ρ_T, is related to the degree of crystallinity, β, by:

$$\rho_T = \rho_c \beta + \rho_{am} (1-\beta)$$

$$\text{or} \qquad \beta = \frac{\rho - \rho_{am}}{\rho_c - \rho_{am}}$$

The density of 0.914 $\pm$ 0.001 g/cm^3 corresponds to a crystallinity of 0.72 with a variation of no more than 1.6%. Among the annealed samples studied in this thesis, no variations in density were found beyond the 0.1% scatter.

APPENDIX D:

Sonic Modulus

Relating Sonic Modulus to Orientation

Sonic velocity has been used to measure orientation for a number of years. Moseley[73,74] in 1959 and Ward[75,76] in 1960 and 1962 found by two different approaches that orientation and sonic velocity were related through the following:

$$E = \rho c^2$$

$$\frac{1}{E} = \frac{1 - \overline{\cos^2\theta}}{E_t^\circ}$$

where E = measured sonic modulus

ρ = density

c = sonic velocity

θ = angle between the symmetry axis of the molecular units and the direction of sound propagation

$\overline{\cos^2\theta}$ = orientation parameter, defined in Appendix A

E_t° = intrinsic lateral modulus of a fully oriented fiber

This relationship held true for those polymers whose glass transition temperatures, T_g, were well above the temperature at which the sonic modulus was measured. For such polymers the sonic modulus was found not to depend on crystallinity. Thus, the theories of Moseley and Ward were based on the overall orientation of one-phase systems. The relationship between modulus and velocity, $E = \rho c^2$, assumed a longitudinal sound wave travelling through a rod-like structure.

When the sonic modulus was affected by changes in crystallinity, as in the case of polypropylene, the two-phase character had to be considered in relating orientation to sonic modulus. R. J. Samuels[10] developed such a relationship in 1965 by using a mixing equation involving bulk compressibilities. Thus he wrote:

$$K = \beta K_c + (1-\beta)K_{am}$$

where K, K_c, K_{am} = bulk compressibility of the overall solid, the crystals, the amorphous regions

β = degree of crystallinity

The bulk compressibility was related to the bulk modulus, B, and Young's modulus, E, through Poisson's ratio, ν, by:

$$K = \frac{1}{B} = \frac{3(1 - 2\nu)}{E}$$

Samuels used a value of $\nu = 0.33$ found by Waterman for iostactic polypropylene at room temperature. The equation above then reduces to

$$K = \frac{1}{B} = \frac{1}{E} = \frac{1}{\rho c^2} \quad .$$

The equation that Moseley and Ward used to relate orientation and modulus was assumed to be true for each phase. The above equations combine to give:

$$\frac{1}{E_{OR}} = \left(\frac{\beta}{E^\circ_{t^c}}\right) (1-\overline{\cos^2\theta}) + \left(\frac{1-\beta}{E^\circ_{t_1{}^{am}}}\right) (1-\overline{\cos^2\theta})$$

This can be put in terms of the orientation function, f, which is related to the orientation parameter, $\overline{\cos^2\theta}$, by:

$$f = \frac{3\,\overline{\cos^2\theta} - 1}{2} \quad .$$

This gives:

$$\frac{3}{2} - \frac{1}{E_{OR}} = \left(\frac{\beta}{E^{\circ}_{t_1 c}}\right)(1-fc) + \left(\frac{1-\beta}{E^{\circ}_{t_1 am}}\right)(1-f_a) \ .$$

Experimental Technique:

A Series Five Pulse Propagation Meter (H.M. Morgan Co., Inc., Cambridge, MA) was used to measure sonic modulus. The instrument measured the transit time in microseconds of a 10 kHz longitudinal wave between transmitting and receiving transducers. The distance in millimeters between the transducers was varied. Thus the data was a collection of time-distance points. Using a least squares calculation, the velocity (slope of time-distance) was found. The 95% confidence of the slope was also calculated following the procedure described in Erwin Krysig's text, Advanced Engineering Mathematics, 3rd Edition, pp. 784-7.

Results:

The sonic modulus of six films was measured. For each film approximately fifty distance-time points were measured. The slope was determined and the 95% confidence limit was calculated. The results are listed in Table 1D and shown graphically in Figure D-1. The annealed specimens show an increase of up to 8% in sonic modulus as compared to the unannealed films. This increase is a real increase, as the changes are outside of the 95% confidence limits.

A comparison between birefringence and sonic modulus is made in Figure 30. The proportional change in sonic modulus and birefringence with changes in amorphous orientation at high crystalline orientation (f_c = 0.97)

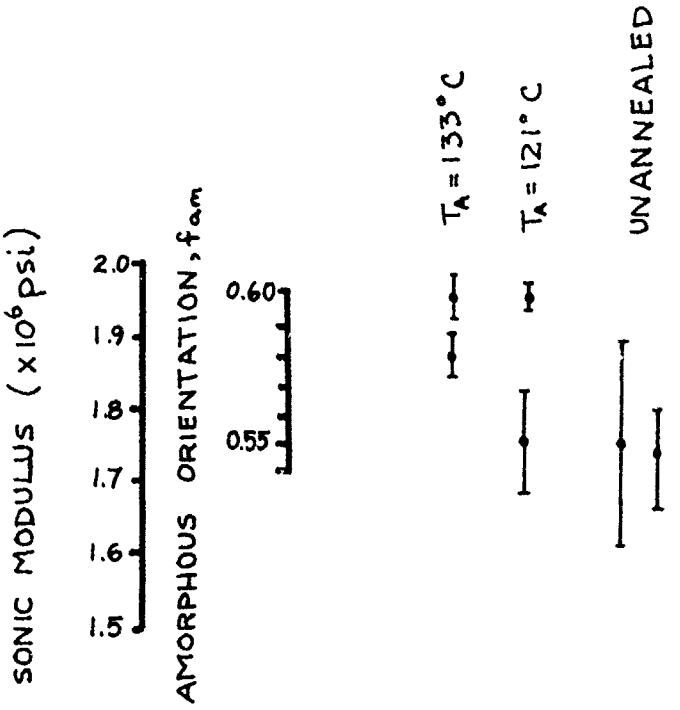

Figure D-1: Sonic Modulus measurement. Error bars are the 95% confidence limits calculated from the time-distance data used to calculate sonic velocity.

TABLE 1 D

Sonic Modulus Data

Sample ID.	* ^{1}/velocity ($\frac{\mu sec}{mm}$)	** $E_{OR} = \rho c^2$	† f_{am}	no. data points
unannealed	.274 (.011)	1.76 x 10^6 psi (8%) 1.213 x 10^{11} d/cm^2	.552	27
unannealed	.275 (2%)	1.75 x 10^6 psi (4%) 1.206 x 10^{11} d/cm^2	.550	30
121°C, 1% shrinkage	.274 (2%)	1.758 x 10^6 psi (4%) 1.212 x 10^{11} d/cm^2	.552	69
121°C, 1% shrinkage	.261 (0.4%)	1.950 x 10^6 psi (0.8%) 1.344 x 10^{11} d/cm^2	.598	54
133°C, 1% shrinkage	.261 (0.6%)	1.951 x 10^6 psi (1.2%) 1.345 x 10^{11} d/cm^2	.599	55
133°C, 1% shrinkage	.265 (0.6%)	1.883 x 10^6 psi (1.2%) 1.298 x 10^{11} d/cm^2	.583	54

* values in parentheses are the 95% confidence limits

** for $\rho = 0.914$ g/cm^3

† for $f_c = 0.97$, $X_c = \beta = 0.72$

and a crystallinity, X_c, of 0.72 are compared. The sonic modulus is more sensitive to the amorphous orientation than birefringence. For our case, a change in amorphous orientation from 0.55 to 0.60, as determined from sonic modulus, gave an 8% change in sonic modulus, whereas the resulting change in birefringence is only about 2%. Thus because of its superior sensitivity and ease of use, sonic modulus is the preferred method for measuring small changes in amorphous orientation in highly oriented polypropylene.

APPENDIX E:

Spring-Dashpot Models - Newtonian Dashpot - Eyring's Activated Dashpot

Spring-Dashpot Model: Newtonian Dashpot

As a first attempt to model the stress relaxation process in the 0° specimens, a simple standard linear solid with a Newtonian ($\sigma = \eta\dot{\varepsilon}$) dashpot was used. A value for η was chosen so that the time constant, τ, ($\tau = \eta/k_2$) was equal to the time at which half the relaxation had occurred. The spring constants, k_1 and k_2, were given by the modulus at the shortest and longest time, $k_1 + k_2 = E_{initial}$, and $k_1 = E_{final}$. Figure 33a shows the spring-dashpot arrangement. The stress resulting from a strain program of $\varepsilon(t) = \varepsilon_o$ is:

$$\sigma(t) = E_i\varepsilon_o + \varepsilon_o(E_i - E_f)\exp(-t/\tau)$$

so: $$E(t) = \sigma(t)/\varepsilon_o = E_f + (E_i - E_f)\exp(-t/\tau).$$

This is plotted with the experimental data on a E(t) vs. t plot. For comparison, a log E vs. log t plot is shown in Figure E-1. The log E vs. lot t plot shows the usual drop in modulus around the τ value from the initial modulus plateau at $t < \tau$ to the final modulus plateau at $t > \tau$. It is clear that the experimental data are not fit well by this formulation but instead show a much broader relaxation. This is not surprising since a spectrum of relaxation times is expected to govern the relaxation process. This could be modeled by adding additional arms to the model. This was not done because, though such a model could fit the curve, it could not handle the strain dependence of the modulus and because it gave no insight into physical sources of the nonlinearity. A method which promised to address the latter was Eyring's[44] approach. The model was introduced in

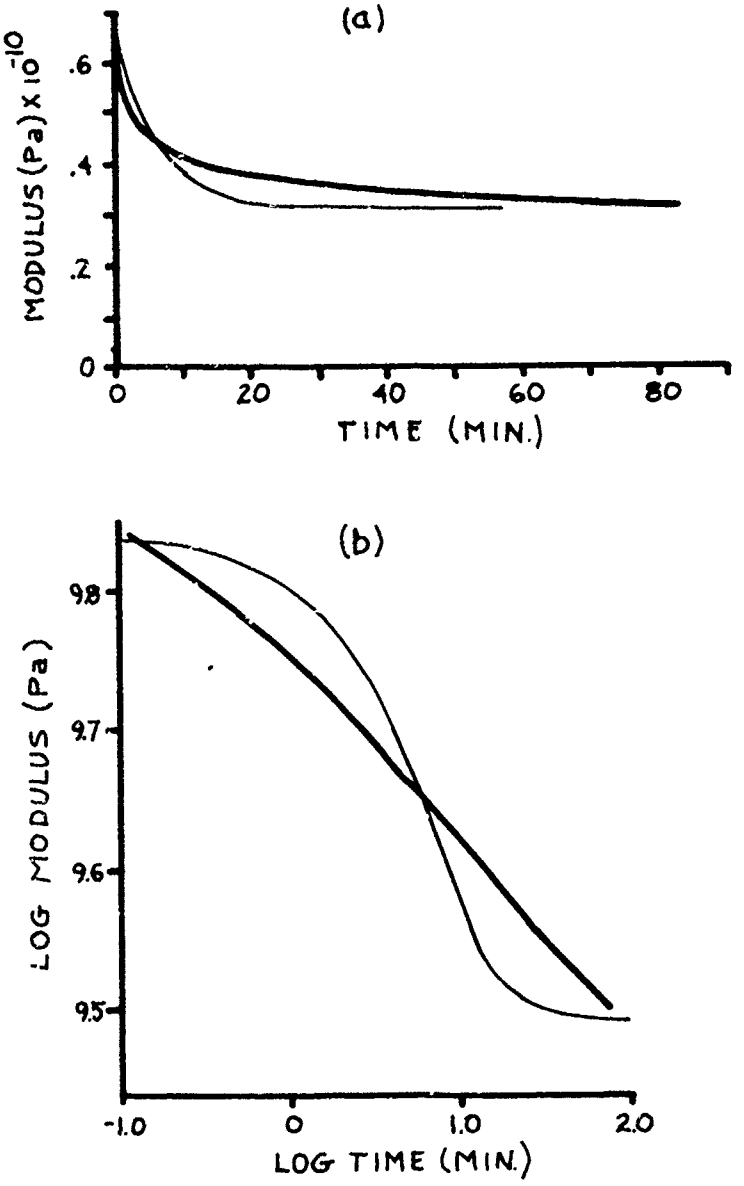

Figure E-1: Results from exponential model showing (a) linear, and (b) log-log plots. (Heavy lines are experimental data and fine lines are model results.)

che background section on nonlinear viscoelasticity. A discussion of the use of this model follows.

Standard Linear Solid: Eyring Dashpot

The predictions of the Eyring spring-dashpot model were examined. Figure 33(b) shows the spring-dashpot arrangement. The stress in a standard linear solid having an Eyring dashpot during stress relaxation is:

$$0 = \dot{\sigma}/k_2 + A \sinh (\alpha\sigma - \alpha k_1 \varepsilon_o).$$

The data, corresponding log $E(t_i)$ and log t_i values, from the stress relaxation experiments on the 0° specimens, were placed in computer files.

The spring constants, k_1 and k_2, were assigned values determined from the modulus at the shortest and longest times, $E_{initial}$ and E_{final}, respectively ($E_{initial} = k_1 + k_2$, and $E_{final} = k_1$). A value of α was chosen so the initial argument of the hyperbolic sine function was about 5 to 7, and a value of A was guessed. A finite difference technique was used to iterate from the initial modulus and time to the final modulus and time. The equation in finite difference form is:

$$\sigma^t = \sigma^{t-1} - Ak_2\Delta t \sinh(\alpha\sigma^{t-1} - \alpha k_1 \varepsilon_o).$$

The calculation took this form: in the first use of this relation, Δt was kept constant throughout the iteration, but since the change in stress with time is small at longer times, a decision was made to iterate in log time. This was done by dividing the log time range into 250 parts, each part having a value of $\Delta(\log t)$. The new time in the iteration, t_i, was found by adding $\Delta(\log t)$ to log t_{i-1}, i.e., log t_i = log t_{i-1} + $\Delta(\log t)$. The difference in time, Δt, between t_i and t_{i-1} was found by subtraction. Using this Δt and the stress calculated from the

previous iteration, σ^{t-1}, the new stress, σ^{t} at time, t_i, was calculated.

In order to find the correct value of A, the values of k_1, k_2, A and α were used to iterate until a test point, at $t = t_T$, was reached. The experimental value of stress at t_T was compared to the calculated value of $\sigma(t_T)$. If the value was not close enough, a new value of A was found by an estimation procedure. This was repeated until a satisfactory value of A was found. The whole curve was then calculated with the new A. The calculated stress relaxation modulus and the experimental data were plotted together. If the fit was poor then the α value was changed and the whole procedure begun again. In this way, it was possible to fit all the stress relaxation tests for strains of 0.0059 to 0.0664. An example is shown in Figure E-2. When the final values of k_1, k_2, A, and α were compared from the different tests, there was no discernable trend. This was not unexpected, since the ability to fit the curves with the two constants, A and α, does not provide unique values of A and α.

The simplest version of this model would be that in which the spring constants were constant and the dashpot parameters, A and α, were also constant. Since, according to Eyring, A and α are related to the chain segment volume and the hole volume, it seemed that they should be constant for a constant temperature. To test this, the best fit to the experimental data from an intermediate strain (0.0128) was determined and the A and α values from that fit were then used to calculate the stress relaxation data for other strain values. The k_1 and k_2 values were allowed to vary to get the best fit to the data at those strains. This worked well for tests at strains around 0.0128. However, for strains lower and higher than 0.0128, the fit was not good. Figures E-3 and E-4 show the best obtainable fits for a low strain (0.00678) and a high strain (0.0664) test.

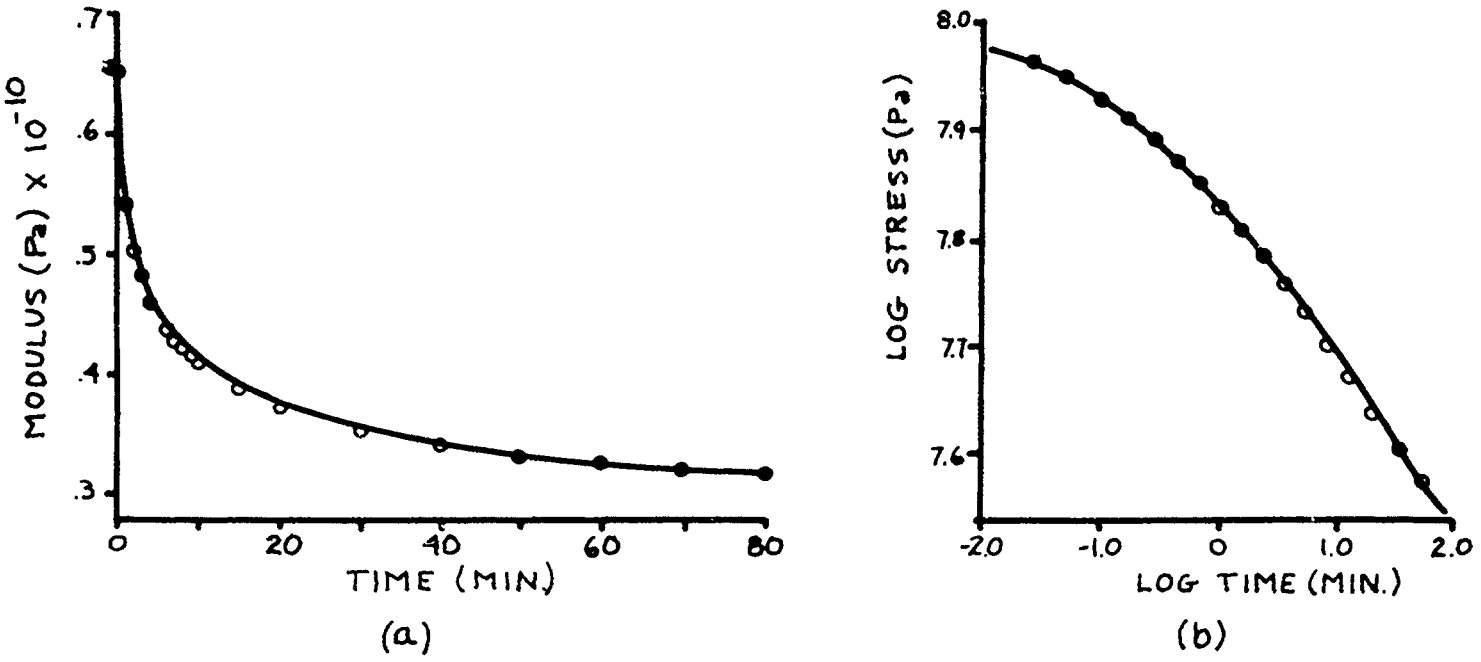

Figure E-2: Results from Eyring model (line is model value, symbols are experimental data).

(a). E(t) vs. t for $\varepsilon_o = 0.00594$

$A = 0.182 \times 10^{-4}$, $\alpha = 1555.4$, $k_1 = 0.45 \times 10^6$ psi, $k_2 = 0.55 \times 10^6$ psi

(b) $\log_{10}\sigma$ vs. $\log_{10}t$ for $\varepsilon_o = 0.0128$

$A = 0.451 \times 10^{-4}$, $\alpha = 884.4$, $k_1 = 0.38 \times 10^6$, $k_2 = 0.667 \times 10^6$ psi

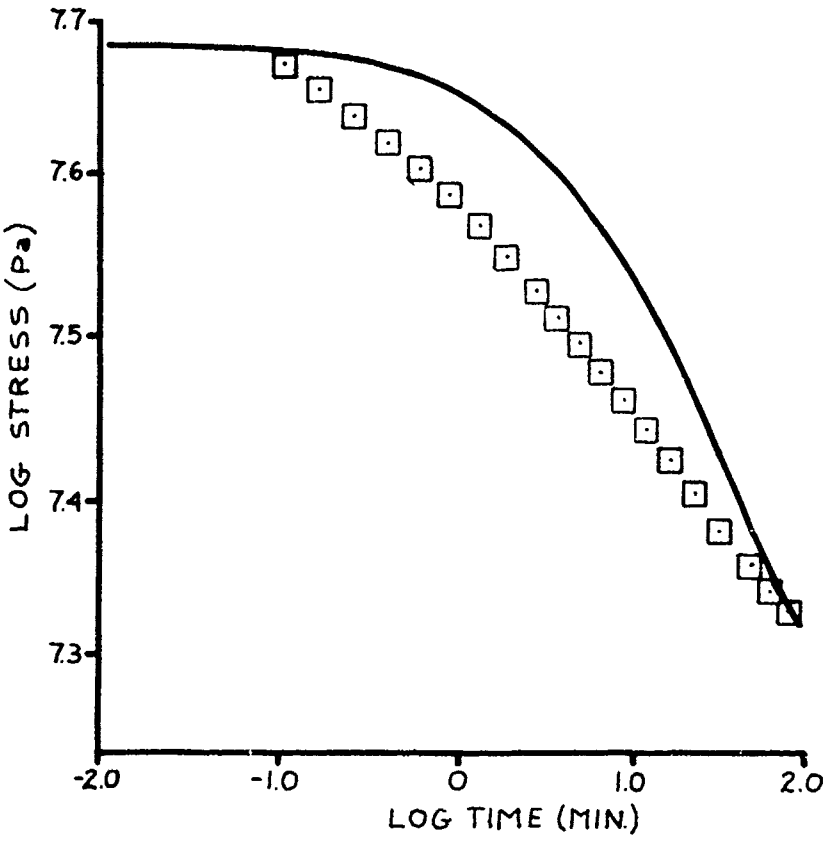

Figure E-3: Eyring model using A and α values from $\varepsilon_o = 0.0128$ for $\varepsilon_o = 0.00678$. This is the best fit obtainable by adjusting k_1 and k_2.

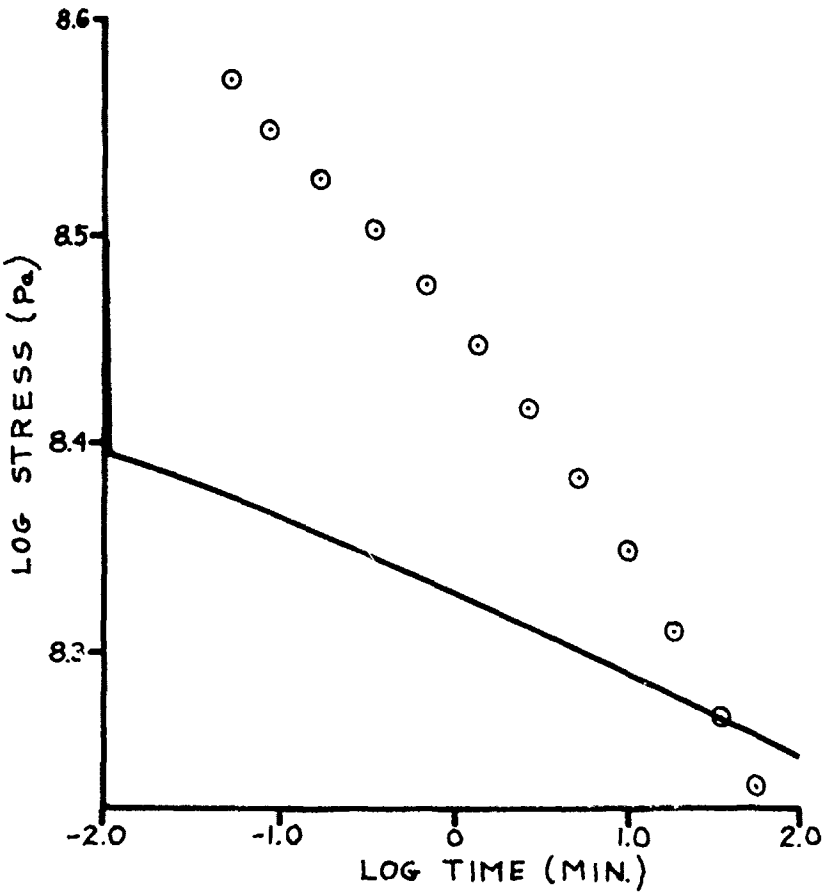

Figure E-4: Eyring model using A and α values from $\varepsilon_o = 0.0128$ for $\varepsilon_o = 0.0664$. This is the best fit obtainable by adjusting k_1 and k_2.

This indicates that the dashpot parameters are not constant with strain. Not only did constant dashpot parameters, A and α, prove unsatisfactory, but the spring constants had to be varied significantly from one strain to another.

Ward discussed the Eyring model (Ref. 37, pp. 205-7) and pointed out that it was attractive because it gives a form for creep of $\sigma = a' + b' \log t$. Even though the creep curves are sigmoidal when plotted over a large time range on a logarithmic time scale, over a middle region they approach a straight line. He concludes that this approach is simply a curve fitting procedure, rather than a valid molecular theory. He points out that since this model was proposed, the idea of a relaxation time spectrum has become accepted and is a more reasonable model than Eyring's model.

BIBLIOGRAPHY

1. Wilchinsky, Z.W., J. Appl. Phys., 30 792 (1959).
2. Wilchinsky, Z.W., J. Appl. Phys., 31(11) 1969 (1960).
3. Wilchinsky, Z.W., Advances in X-ray Analysis, 6, Plenum Press, 1963, p. 231.
4. Alexander, L.E., X-ray Diffraction Methods in Polymer Science, Wiley-Interscience, 1969, Ch. 4, p. 198.
5. Decker, B.F., Asp, E.T., Harder, D., J. Appl. Phys., 19 388 (1948).
6. Alexander, L.E., op cit, p. 230.
7. Durelli, A.J., Riley, W.F., Introduction to Photomechanics, Prentice-Hall, Inc., p. 95.
8. Wahlstrom, E.E., Optical Crystallography, 4th edition, John Wiley and Sons, Inc., 1969, p. 182.
9. Sweeting, O., ed., The Science and Technology of Polymer Films, Vol.I, Interscience Publishers, 1968, p. 182.
10. Samuels, R.J., Structured Polymer Properties, Wiley-Interscience, 1974, pp. 51-63.
11. Desper, C.R., J. Macromol. Sci.-Phys., B7(1) 105 (1973).
12. Arridge, R.G.C. and Barham, P.J., J. Polymer Sci: Polymer Physics, 16 1297 (1978).
13. Arridge, R.G.C. and Barham, P.J., Polymer, 19 654 (1978).
14. Bigg, D.M., Polym. Eng. and Sci., 16 725 (1976).
15. Datta, P.K. and Pethrick, R.A., Polymer, 19 145 (1978).
16. Garton, A., Carlsson, D.J., and Wiles, D.M., Text. Res. J., 48 115 (1978).
17. Garton, A., Sturgeon, P.Z., Carlsson, D.J., and Wiles, D.M., J. Mat. Sci., 13 2205 (1978).
18. Brydson, J.A., "The glass transition, melting point and structure", Ch. 3 of Polymer Science, ed. A.D. Jenkins, American Elsevier Publishing Co., Inc., 1972, pp. 231-238.
19. Nadella, H.P., Spruiell, J.E. and White, J.L., J. Appl. Polym. Sci., 22 3121 (1978).
20. North, A.M., Pethrick, R.A., and Phillips, D.W., Macromolecules, 10 992 (1977).
21. Peterlin., A., Colloid and Polymer Sci. 253 810 (1975).

22. Peterlin, A. and Balta-Calleja, F.J., J. Appl. Phys. 40 4238 (1969).
23. Samuels, R.J., J. Macromol. Sci. -Phys., B8 41 (1973).
24. Samuels, R.J., J. Pol. Sci.: A-2, 6 1101 (1968).
25. Samuels, R.J., J. Pol. Sci.: A, 3 1741 (1965).
26. Taylor, W.N. Jr., and Clark, E.S., Polym. Eng. Sci., 18 518 (1978).
27. Gibson, A.G., Davies, G.R. and Ward, I.M., Polymer 19 683 (1978).
28. Owen, A.J. and Ward, I.M., J. Macromol. Sci. -Phys., B7 417 (1973); see also ERRATA: B7 747 (1973).
29. Clements, J., Jakeways, R., Ward, I.M., and Longman, G.W., Polymer, 20 295 (1979).
30. Cansfield, D.L.M, Capaccio, G. and Ward, I.M., Polym. Eng. Sci., 16 721 (1976).
31. Samuels, R.J., see Ref. 10, p. 14.
32. Balta-Calleja, F.J., and Peterlin, A., J. Mat. Sci., 4 722 (1969).
33. Balta-Calleja, F.J., and Peterlin, A., J. Polym. Sci.: A2, 7 1275 (1969).
34. Peterlin, A., Text. Res. J., 42 20 (1972).
35. Yoon, D.Y., and Flory, P.J., Polymer, 18 509 (1977).
36. Retting, W., J. Polym. Sci.: Symposium No. 42 605 (1973).
37. Ward, I.M., Mechanical Properties of Solid Polymers, Wiley-Interscience, 1971, ch. 10, p. 225.
38. Gupta, V.B. and Ward, I.M., J. Macromol. Sci. -Phys., B1 373 (1967).
39. Ladizesky, N.H. and Ward, I.M., J. Macromol. Sci.-Phys., B5 745 (1971).
40. Ladizesky, N.H. and Ward, I.M., J. Macromol. Sci.-Phys., B5 661 (1971).
41. Arridge, R.G.C. and Folkes, M.J., Polymer, 17 495 (1976).
42. Hadley, D.W. and Ward, I.M., Rep. Prog. Phys., 38 1143 (1975).
43. Seferis, J.C., McCullough, R.L., and Samuels, R.J., J. Macromol Sci. -Phys., B13 357 (1977).
44. Halsey, G., White, H.J., Jr., and Eyring, H., Text. Res. J., 15(9) 295 (1945).
45. Findley, W.N., Lai, J.S., and Onaran, K., Creep and Relaxation of Nonlinear Viscoelastic Materials, North-Holland Publishing Co., 1976, p. 132.
46. Ferry, J.D., Viscoelastic Properties of Polymers, Wiley, 1970, p. 402.
47. Jenkins, A.D., ed., Polymer Science, American Elsevier Publishing Co., 1972, p. 231.

48. Brereton, M.G., Croll, S.G., Duckett, R.A., Ward, I.M., J. Mech. Phys. Solids, 22 97 (1974).
49. Buckley, C.P., J. Phys. D: Appl. Phys., 10 2135 (1977).
50. Ward, I.M., and Onat, E.T., J. Mech. Phys. Solids, 11 217 (1963).
51. Hadley, D.W. and Ward, I.M., J. Mech. Phys. Solids, 13 397 (1965).
52. Ward, I.M., and Wolfe, J.M., J. Mech. Phys. Solids, 14 131 (1966).
53. Retting, W. J. Polymer Sci. : Symposium No. 42 605 (1973).
54. McCrum, N.G., Read, B.E., Williams, G., Anelastic and Dielectric Effects in Polymeric Solids, John Wiley and Sons, 1967, p. 377.
55. Natta, G. and Corrandini, P., J. Polym. Sci., 39 29 (1959).
Natta, G., Corrandini, P., Cesari, M., Atti Accad. Naz. Lincei, 21 365 (1956).
Natta, G. and Corrandini, P., Nuovo Cimento 15 Suppl. 1, 40 (1960).
56. Prifti, Joseph J., DeLuca, E., Alesi, A.L., Report: "Hardened Tuned-Wall Plastic Radomes for Military Radars (Unclassified)", Army Materials and Mechanics Research Center, Watertown, Massachusetts 02172.
57. Arridge, R.G.C., Barham., P.J., Farrell, C.J., and Keller, A., J. Mat. Sci., 11 788 (1976).
58. Clements, J., Jakeways, R., and Ward, I.M., Polymer, 19 639 (1978).
59. Desper, C.R., Characterization of Materials In Research, Ceramics and Polymers, Syracuse University Press, Syracuse, N.Y., 1975, Ch. 16 "Characterization of Molecular and Crystalline Orientation of Anisotropic Solid Polymers" pp. 459-499.
60. Desper, C.R., Preprint from 23rd International Symposium on Macromolecules (IUPAC), Madrid, Sept. 15-20, 1974, Vol. 2, p. 581, "Structural Characterization of Isotactic Polypropylene Films of Ultrahigh Orientation".
61. Desper, C.R., Transcript from talk at A.C.S. Ch.E., August 1979, "Structural Characterization of Isotactic Polypropylene Films of Ultra High Orientation. II. Segmental Orientation and the Continuous Crystal Model".
62. Wills, A.J., Capaccio, G., Ward, I.M., J. Polym. Sci: -Phys. 18 493 (1980).
63. Peterlin, A., Polym. Eng. and Sci., 18 488 (1978).
64. Peterlin, A., Macromolecules, 13 777 (1980).

65. Popli, R., Sc.D. Thesis, 1980, M.I.T.
66. Kamezawa, M., Yamada, K., Takayanagi, M., J. Appl. Polym. Sci., 24 1227 (1979).
67. Arridge, R.G.C., Barham, P.J., Keller, A., J. Polym. Sci.:-Phys., 15 389 (1977).
68. Lifshitz, J.M. and Kolsky, H., Int. J. Solids Structures, 3 383 (1967).
69. Hall, I.H., J. Poly. Sci.: A2, 5 1119 (1967).
70. Yannas, I.V. and Haskell, V.C., J. Appl. Phys., 42 610 (1971).
71. Yannas, I.V., J. Polym. Sci., Macromol. Reviews, 9 163 (1974).
72. Soussou, J. and Moavenzadeh, F., J. Eng. Mech. Div. (Proc. ASCE), 98 (No. EM5)1205 (1972).
73. Moseley, W.W. Jr., J. Appl. Polym. Sci. 3 266 (1960).
74. Charch, W.H. and Moseley, W.W. Jr., Text. Res. J. 29 525 (1959).
75. Ward, I.M., Proc. Phys. Sco. London, 80 1176 (1962).
76. Ward, I.M., Text Res. J. 34 806 (1964).
77. Darlington, M.W. and Saunders, D.W., Polym. Eng. Sci. 14 616 (1974).
78. The computer program which performed the regression analysis was generously provided by Mark Nodine, doctoral candidate, Department of Chemistry, M.I.T.